University of New Mexico
UNM Digital Repository

Chemistry ETDs | Electronic Theses and Dissertations

Spring 4-15-2019

Nanostructuring Organic/Inorganic Multicomponent Composites for Solution Processable Solar Cells

Brad Watson
Univeristy of New Mexico

Follow this and additional works at: https://digitalrepository.unm.edu/chem_etds

 Part of the Chemistry Commons

Recommended Citation
Watson, Brad. "Nanostructuring Organic/Inorganic Multicomponent Composites for Solution Processable Solar Cells." (2019).
https://digitalrepository.unm.edu/chem_etds/149

This Dissertation is brought to you for free and open access by the Electronic Theses and Dissertations at UNM Digital Repository. It has been accepted for inclusion in Chemistry ETDs by an authorized administrator of UNM Digital Repository. For more information, please contact amywinter@unm.edu.

Brad W. Watson II

Candidate

Chemistry and Chemical Biology

Department

This dissertation is approved, and it is acceptable in quality and form for publication:

Approved by the Thesis Committee:

Prof. Yang Qin, Chairperson

Prof. Ramesh Giri

Prof. Yi He

Prof. Sang Eon Han

Nanostructuring Organic/Inorganic Multicomponent Composites

for Solution Processable Solar Cells

BY

Brad W. Watson II

B.S. Chemistry Lewis University, Romeoville, IL USA 2011

DISSERTATION

Submitted in Partial Fulfillment of the

Requirements of the Degree of

Doctor of Philosophy

Chemistry

The University of New Mexico

Albuquerque, New Mexico

May 2019

Dedication

To King Sisyphus, the patron saint of this project and chemistry grad school in general

Acknowledgments:

To my parents, who have been my rock throughout this process and without their constant support and advice none of this would be possible…

To Dr. Yang Qin- for his great expertise in the lab, teaching me the basics, his patience, his kindness and for the not only being a great Boss but a great teacher…

To the love of my life Roshan, for his insights into the finer nature of organic synthesis…

To the second love of my life Griffin, for all the personal support and countless hours of therapy…

To the actual love of my life, Yun for being the light in my darkest hour…

To Dr. The Prince for being there when I needed him and for being a good friend throughout…

To Dr. Suren Thapa for all his insights into organic synthesis and all the coffee breaks to the SUB…

To the rest of Team Nepal: Dr. Prakash, soon to be doctor Shekar, Vivek and Rajoo for all the help that they have been both in and out of the lab …

To Robert Leburn and David Baca for reasons that they know about …

To Ben Datko for his friendship and insights into the mystical word of P.Chem…

To my fellow group member both past and present (Dr. Fei, Dr. Wenhan, Dr. Keda, Dr. JZ, Dr. Zhen "the master", Roberto the lawyer, Sheela, Ellie, Lingyao, Jin, Yousef, Jillian, Michael and the assorted undergrads) for being a tremendous help in lab…

To Dr. Karen Ann Smith for keeping me employed …

To Terese Anderson for keeping the building safe and fighting for the students…

To Robert Ortiz Jr. for keeping the building from falling apart…

To "Sir Salty" for showing me my possible future and why that was a dark path to take …

To Doug for being Doug…

To Dr. Ying Bing for allowing me to use the TEM and helping me troubleshoot when it went down…

To Scooter and Kim for allowing me a chance to tutor them for a time in the arts of organic synthesis…

To the God Emperor for keeping the forces of chaos at bay …

To Michael Williams for taking me under his wing and showing me the campus and ABQ…

To Ken and Cynthia from the Grain Station for giving us a place to hang out and cooking some great food…

To my committee members: Dr. Ramesh Giri, Dr. Yi He, Dr. Sang Eon Han for their time and for being on my committee …

To the Department of Chemistry at University of New Mexico for giving me the opportunity to achieve this degree…

To the fine staff at UNM hospital that kept me alive to see today…

To Geneva Anderson for just being you…

To Raymond L. Buchanan Jr. for the years of friendship and his help with the confusing world of Microsoft Word…

Thank you I would not be here without any of you

Nanostructuring Organic/Inorganic Multicomponent Composites for Solution Processable Solar Cells

BY

Brad W. Watson II

B.S. Chemistry, Lewis University, Romeoville, IL USA, 2011

Ph.D. Chemistry, University of New Mexico, USA, 2019

Abstract

The current state of organic photovoltaics is centered on systems of polymeric donors and some type of acceptor molecule (i.e. fullerene) formed into an active layer that adopts a bulk-heterojunction morphology. Although these devices have come a far way from where they were when they were first discovered in the 1980's much work is still needed to make them a viable technology. Two of the limitations of this type of devices revolve around the relatively narrow absorption window of the components and lack of control over the morphology after the film is cast. To overcome these shortcomings there are several strategies that have been developed.

In this dissertation, the use of a complementary absorber will be used to try and overcome the narrow absorption window of the active layer. The complementary absorber that will be used is the quantum dot. This class of material was selected because of their simple synthesis, tunable absorption window and the ease of modification through alteration of the ligand shell. To gain better control over the morphology, the polymeric donor material P3HT and a P3HT based block copolymer will be formed into nanofibers. To achieve even more control over the morphology, a core-shell system will be introduced based on a core of polymeric nanofibers and a shell of quantum dots. Also, this core-shell architecture will promote a cascade type mechanism of charge transport among the three components of the active layer. To ensure this orthogonal non-covalent bonding will be introduced to tether the quantum dots and polymer together. To achieve this non-covalent bonding regime between quantum dot and polymer, both will need to be modified. The

ligand shell of the quantum dot will be engineered to introduce a moiety that will interact with a modification to the side chain of the P3HT base polymer. This interaction will be designed to be a pi-pi type of interaction. Although the application of this complementary absorbing species drastically affected the performance of OPV devices in a negative sense, this study did demonstrate that quantum dots can be coordinated to the nanofiber.

TABLE OF CONTENTS

LIST OF FIGURES

LIST OF SCHEMES

LIST OF TABLES

LIST OF ABBREVIATIONS

Ace	Acetone
APTC	Ammonium Phenyl Dithiocarbamate
ATR	Attenuated Total Reflection
ATRP	Atom transfer radical polymerization
BCP	Block copolymer
BHJ	Bulk heterojunction
CA	Complementary absorber
Ca.	circa or approximately
CB	Chlorobenzene
$CHCl_3$	Chloroform
$CDCl_3$	Deuterated Chloroform
CP	Conjugated polymer
Cm	centimeter

CV	Cyclic voltammetry
D_2O	deuterated water
DCM	Dichloromethane
DMSO	Dimethyl sulfoxide
DSC	Differential scanning calorimetry
DSSC	Dye-sensitized solar cell
EPA	Environmental Protection Agency
eV	Electron Volt
Fc	Ferrocene
FF	Fill factor
GRIM	Grignard metathesis
HOMO	Highest occupied molecular orbital
ITO	Indium Tin Oxide
J	Current Density
J_{max}	Maximum Current Density
Jsc	Short Circuit Current Density

KCTP	Kumada catalyst-transfer polycondensation
kWh	Kilo Watt Hour
LUMO	Lowest Unoccupied Molecular Orbital
MDMO-PPV	Poly [2-methoxy-5-(3', 7'-dimethyloxtyloxy)-1,4-Phenylenevinylene
MEH-PPV	Poly(2-methoxy-5-(2'-ethyl-hexyloxy)-1,4-Phenylenevinylene
M_n	Number average molecular weight
M_w	Weight average molecular weight
NF	Nanofiber
Nm	Nanometer
NMR	Nuclear Magnetic Resonance
OPV	Organic Photovoltaic Device
P3AT	Poly(3-alkylthiophene)
P3HT	Poly(3-hexylthiophene)
P3HT-b-P3OTBST	Poly(3-hexylthiophene)-block- poly (tert-butyldimethyl(6-Thiophen-3-yl)) hexyloxy) silane
P3HT-b-P3OHT	Poly(3-hexylthiophene)-block-poly(6-(thiophen-3-yl) hexan-1-ol
P3HY-b-P3NicoT	Poly(3-hexylthiophene)-block-poly 6-(thiophen-3-yl) hexyl

	Nicotinate
PCBM	[6,6]-Phenyl-C61-butyruc acid
PC70BM	[6,6]-Phenyl-C71-butyruc acid or C70 PCBM
PCDTBT	Poly [N-9′-heptadecanyl-2,7-carbazole-alt-5,5-(4′,7′-di-2-thienyl-2’,1’,3’-benzothiadiazole)
PCE	Power Conversion Efficiency
PDI	Polydipersity index
PDIs	Perylene diimide
PEDOT: PSS	Poly(3,4-ethylenedioxythiophene)-poly(styrenesulfonate)
P_{in}	Power Input
P_{max}	Power Maximum
PPP	Poly (2,5, -dihexyloxy-p-phenylene)
PPV	Phenylene Vinylene
PS	Polystyrene
PSC	Polymer Solar Cell
PV	Photovoltaic
QD	Quantum Dot
RPM	Revolution Per Minute
R_s	Series Resistance
r.t.	Room Temperature
SEC	Size Exclusion Chromatography
T2PyTC	Triethylammonium Pyridin-2-yl dithiocarbamate
TBAF	Tetrabutylammonium Fluoride
TBS/TBDMS	Tert-butyldimethylsilane

TEA	Triethylamine
TEM	Transmission Electron Microscopy
TMS	Trimethylsilane
TOPO	Trioctylphosphine Oxide
TW	Terawatt
UV-VIS	Ultraviolet-visible
V	Volt
V_{max}	Maximum Output Voltage
Voc	Open Circuit Voltage
Vol	Volume
Wt	Weight
XRD	X-Ray Diffraction
δ	Chemical Shift
λ	Wavelength
χ	Flory-Huggins Interaction Parameter
χc	Flory-Huggins Interaction Parameter at Crystallization
χODT	Flory-Huggins Interaction Parameter at the Order-Disorder Temperature

Chapter 1

Introduction

1.1 Overview

With the advancements of the last one hundred years, the demand for energy has increased exponential with a promise for that need to further increase. Studies have stated that by the year 2040 the global energy consumption will be around 27 TW annually, increasing from a yearly usage of about 17 TW in 2018.[1] To feed this ever-growing need, humanity has depended on the burning of traditional non-renewable fuels to generate the needed power. [2] Besides the limited reserves, the use of these "fossil fuels" have caused a large amount of environmental harm along the production chain. [3-5] With recent public attention given to the nature of global climate change; there has been a large push to find an alternative source of power to feed our needs as well as to better preserve the environment. According to a 2016 EPA study, renewable energy sources contribute about 13% of all energy generated. With 1% coming from of that coming from solar sources.

Despite the facts that solar is not limited by geographical restraints and the amount of solar radiation that hits the earth, solar is relatively not exploited than the other renewable energy sources. Using average values, an American roof receives 450 kWh in a day. Factor in the current efficiencies of industrial solar cells (~15%) that number falls to 67.5 kWh, which is still greater than the 30 kWh that the average American uses daily. [6] Although with recent advancements in processing, the silicon solar cell cost has become more economically viable to the masses. However, it does not solve all the problems with these devices such as weight or their inflexibility. In the search for a classification of materials that can be printed on lightweight and flexible substrates, we find organic photovoltaics (OPV), an umbrella term for dye-sensitized solar cells (DSSCs), small molecules, perovskite solar cells [7*8] and polymer solar cells (PSC). These materials have garnered much attention from both industrial and academic research establishments over the past 10 to 15 years. [9-13] Of these materials, the polymer and small molecule solar cells have amassed great attention due to advantages in synthetic and processing methods. Versatile synthetic methodology has allowed for these small molecules and polymeric material's electronic and physical properties to be tuned to whatever is desired. [14] Ink printing and roll to roll printing allows these materials to be applied to lightweight and flexible substrates.

1.2 Overview of Organic Photovoltaics

1.2.1 History and evolution of Organic Photovoltaics

The history of solar cells began with the discovery and explanation of the photoelectric effect by early influential scientists such as: Alexandre Becquerel, Heinrich Hertz, Albert Einstein and Robert Millikan. The story of commercial solar power generation starts with the pioneering works of the scientists working at Bell laboratories, when they created the world's first silicon based solar cell in 1954. [15] The first notable discovery in the field of organic photovoltaics came from the Tang group in 1985. The group was among the first to report the use of an electron donor layer (copper phthalocyanine) and an electron acceptor (a perylenetetracarboxylic derivative) layer in a bilayer structure sandwiched between a silver electrode and an Indium Tin Oxide (ITO) covered glass substrate. The then record setting PCE of this device was 1%.[16] The next milestone on the journey to the modern OPV was the discovery of the bulk heterojunction, which can be described as the mixing of the donor and acceptor materials. Because an organic semiconductor is used as the donor material in these devices, it is necessary to add in acceptor material to allow for the separation of the active charge species generated from the absorption of a photon. The Yu group in 1995 reported that the mixing of poly (2-methoxy-5-(2'-ethyl-hexyloxy)-1,4-phenylenevinylene)) (MEH-PPV) and C60 fullerene had enhanced performance over films of pure MEH-PPV and contemporary bilayer devices. [17] The BHJ morphology, 2.5% PCE, was used to overcome one of the biggest limitations of OPVs. The key to the success of the BHJ is the increase in interfacial area between the donor and acceptor material, allowing for more charge separation than bilayer architecture. However, the BHJ was limited by the fact that the fullerene has limited solubility in most organic solvents. The Wudl group solved this problem through the introduction of soluble fullerene derivatives, such as phenyl-C61-butyric acid methyl ester

(PCBM). [18] Since then the BHJ and the soluble fullerene derivatives have become the standard for laboratory research.

Although the acceptor material and architecture have been set, there has been a large investment of effort into finding a suitable donor material for these devices. Throughout the early history of BHJ OPVs, PPV and PPV derivates were the dominant donor materials used. Though the highest PCE that was achieved was 2.5% by the Shaheen group using poly[2-methoxy-5-(3′,7′-dimethyloctyloxy)-1,4-phenylenevinylene] (MDMO-PPV) in an optimized device.[19] Although these devices help the field understand the inner workings of OPVs, they did little to forward the goal of commercialization. There was a need for a better donor material, one that would address the problems of high amorphous character of PPV films and their poor electronic characteristics. Around the year of 2005, PPV was replaced as the laboratory standard with poly thiophene derivates. When employing the BHJ architecture and PCBM as electron acceptor, these poly thiophenes can get around 5% PCE. [20-22]

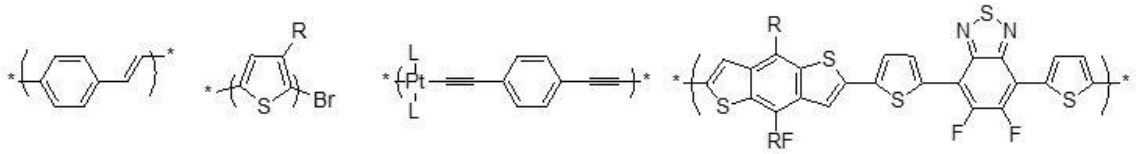

Figure 1.1 A representative look at the various electron donor materials throughout the history of the OPV (from left to right): PPV, P3AT, heavy metal containing polymer and push-pull type copolymer.

Yet even with this improvement in PCE, the OPV devices were still not commercially viable in the sense of completely replacing the inorganic solar cell. The Holy

Grail PCE that was set at 15% for this replacement to happen did not occur and other materials were needed. [23] This pushed research efforts away from simple polymeric: fullerene blends to a more complex donor materials as well as a possible abandonment of fullerene itself. Although the most recent developments in OPV technology are beyond the scope of this document, it should be noted to keep the reader up to date on this research topic. The most popular donor material in the current research environment are those that belong to the push pull design. These small molecules and polymers consist of two or more moieties within the backbone, one of these moieties is electron rich and the other is electron poor. This class of materials has pushed the band gap of donor materials to about 1.4 to 1.7 eV, lower than the 1.9 eV of the poly thiophenes and 2.3 eV of the PPV polymers. Briefly, the engineering of the band gap arises from the mixing of the molecular orbitals of the two components. Generally, the result of this is a HOMO that is slightly higher than

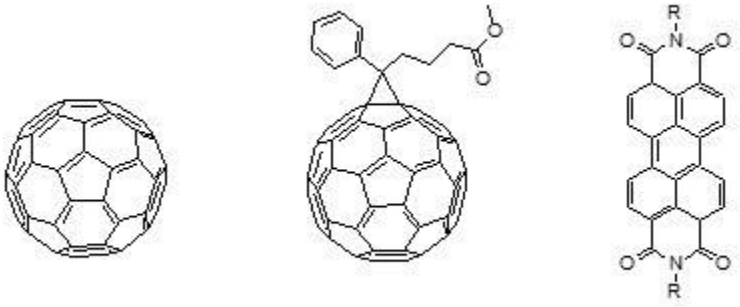

Figure 1.2 A representative look at the various electron acceptor materials throughout the history of the OPV (from left to right): fullerene C_{60}, $PC_{61}CM$ and perylene diimides (PDI)

either one of the two building blocks and a LUMO that is lower and overall a narrowing of the band gap. With careful considerations to which building blocks are used and how they are modified, the ability to easily modify the electronic properties of the material should be achieved.

Although, fullerene and its derivatives has been used as the work horse acceptor materials since its introduction from Tang in 1985 recent advancements in OPVs has pushed the demand for more versatile acceptors. The major drawbacks of fullerenes and their derivatives are that they are hard to chemically modify, difficulties in tuning their electronic characteristics, poor air stability, low harvesting capabilities of solar energy and have a high production cost. [24-26] Recent research efforts have fallen on the class of materials called perylene diimides (PDI). [27-30] PDIs generally are comparable to the fullerenes in the regards to it electron acceptor character and electron mobility but outmatch it in other categories. Depending on how the PDI is tuned, the absorption profile can be turned around the visible part of the solar spectrum, instead of being limited to the ultraviolet section like with fullerenes. The strongest point to PDIs becoming the future acceptor material in OPVs is their ease of functionalization. This would in theory lead to an acceptor material that can be tailored to various donor materials, opening this to a wider range of molecules and materials.[31-35]

1.2.2 Mechanisms of charge generation in Organic Photovoltaic

The physics behind the operation of an organic photovoltaic can be summarized as this. They are well known yet in a sense a complete mystery. The basics of the operation, the interplay between the energy levels of the donor and acceptor materials, the active mechanism of charge transport and what each layer in the device does are known and can be described in basic terms. The mystery comes in when there is a detailed look at the more specific terms that arise from the study of such devices.

The architecture of the common OPV device generally follows the form of an active layer sandwiched between two electrodes, where the cathode is a low work function metal (Ca or Al) and the anode is Indium Tin Oxide (ITO). More complex architectures can be built but they also follow this general form. The mechanism of charge generation within the active layer can be summed up in several steps.

Figure 1.3. Simplified illustrations of (left) bilayer structure where the donor and acceptor materials are atop of each other (middle) Bulk Heterojunction where the two materials are mixed together (right) Controlled morphology where the donor and acceptor material are patterned together

The first step is when photon is absorbed by the donor material-promoting an electron from the highest occupied molecular orbital (HOMO) of the donor to its lowest unoccupied molecular orbital (LUMO). The species formed from this promotion is called an exciton, a bound electron/hole pair. This exciton takes the form of Frenkel type. Meaning that paired electron and hole are strongly bound to each other, having a binding energy of 0.1 eV to 1eV. This is a result of the organic semiconductor having a relatively small dielectric constant. In contrast, the excitons generated in an inorganic semiconductor, whose relatively large dielectric constant weakens this bound pair, into a binding energy less than 0.01 eV. This large binding energy is also much larger than the thermal activation energy required for an exciton to split, thus facilitating the need for the acceptor phase.[40-42] Based on the materials used the exciton diffusion is generally thought to be between 10 and 20 nm, although it should be noted that if the donor material is highly crystalline this

length can drastically increase. In the second step the exciton diffuses randomly in the donor phase. If the exciton reaches the interface between the donor and acceptor phase, it splits into separate free charges. Although the exact mechanism of the charge splitting is still debated a simplified picture can be used to explain what happens. When the bound pair reaches the interface, it enters a transition state where it can either dissociate or recombine to the ground state. If it dissociates successfully, the now free electron falls into

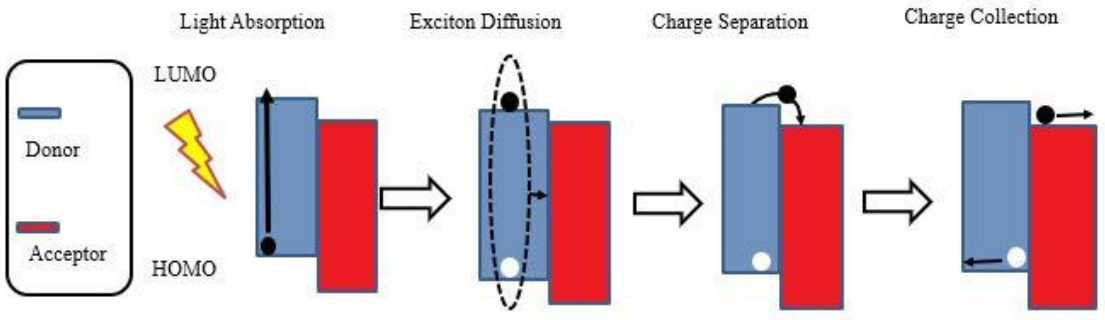

Figure 1.4 Illustration showing the working mechanism of an organic photovoltaic

the LUMO of the acceptor and hole remains in the HOMO of the donor phase. Finally, the free charges travel through their respective domains to the corresponding electrodes.[36-39]

Throughout this process either the exciton or the free charges can recombine. There are two major mechanisms for the charge species to recombine: germinate or non-germinate. Germinate recombination arises from excitons that recombine along their journey through the donor phase. Germinate recombination is the recombination of nascent charge pair that recombines soon after the exciton dissociates. Germinate recombination may be affected by the electric field within the active layer. Non-germinate or bimolecular recombination occurs after the exciton is separated into independent charges.[43-47] This occurs when opposite charges met and quench themselves either from the OPV having low charge mobilities or the lack of interpenetration of the donor and acceptor phases. In either

case the energy used to generate that species is lost, either through the emission of a low energy photon or heat. [48]

1.2.3 Measuring Organic Photovoltaics

The ability of the active layer to generate charge can be quantized in a value known as the power conversion efficiency (PCE), which is derived from a current-voltage (J-V) measurement of the device while it is under illumination. Like with all semiconducting materials this measurement generates a curve from which we can find the important parameters of the short circuit current (Jsc) and the open circuit voltage (Voc). Open circuit voltage is the maximum voltage that a device can generate and is influenced by the offset of the HOMO of the donor material and the LUMO of the acceptor material.[52] Short circuit

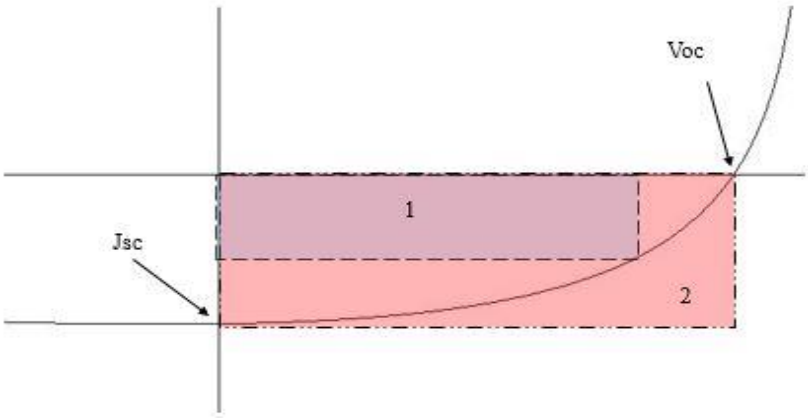

Figure 1.5. Illustration of a typical J-V curve generated by an organic solar cell under the illumination from a simulated solar spectrum

current is the maximum current that can pass through the device. This value is influenced by how efficiently the active layer generates and transports charge carriers. Mathematically the PCE is defined as $PCE = \frac{Voc*Jsc*FF}{P_{in}}$, where FF and P_{in} are the fill factor and the power

put into the device respectfully. Fill factor is defined as the ratio of actual maximum power output of the device to the theoretical power output of the device. As an example, in figure 1.5, it would be the ratio the area of the pink square to the area of the light purple square.

Of the three terms in the above equation, Jsc is the simplest to describe. The term itself is related to several processes that occur within the active layer. These include the flux of photons coming into the active layer, the number of photons absorbed, the ability of the material to efficiently generate and transport charge carries and the amount of recombination of charge carries.[51] Voc is generally explained through the energy off sets of the donor's HOMO and the acceptor's LUMO.[52] However, research has shown that there are several other factors that possibly influence this parameter. The effects of these various factors can be seen in the equation $Voc = \frac{nkT}{q}\ln(\frac{I_L}{I_0} + 1)$. Where n is the ideality factor, T is temperature, k is the Boltzmann constant, q is the fundamental charge I_L is the light generated current and I_o is the dark saturation current. It can be summarized that the intensity of light will have a logarithmic effect on the Voc and that temperature will have more linear effect.[53-54] FF is probably the most complex term to define in the sense that there are multiple components that go into its determination.[55] The easiest definition of FF is that it is the squareness of the J-V curve. As defined above, it is the simple ratio between the maximum power given by device and the theoretical maximum power. However, FF is not just defined by the Voc and the Jsc of the device. It is directly affected by the device's shunt resistance (R_{sh}) and the series resistances (R_s). Series resistance can arise from three possible sources: 1) movement of current through the emitter and base of the solar cell, 2) the contact resistance between the metal contact and the rest of the device, and 3) the

resistance of the metal contact.[56] Shunt resistance arises from manufacturing defects rather than in poor design of solar cell and is which in terms of solar performance the voltage that is usually built up within the device is siphoned off by an alternative current channel.[56] The difficultly in optimizing all these terms is the interplay that they have and often the contradictory nature of their interactions. For example, the engineering of the band gap of a material has a desired effect on the Voc but an opposite effect on the Jsc. Meaning that one of the largest challenges in designing an OPV is to find the optimal condition that maximizes all of the parameters, instead of trying to maximize just one over the other.

1.2.4 Optimizing Organic Photovoltaics

1.2.4.1 Interfacial layers

Although most of the research efforts have gone into optimizing the donor and acceptor materials of the active layer, a dedicated effort has been made to further refine the interfacial layer. Interfacial layers are implemented when the energy level of the active layer electrode need fine tuning,[58-60] to add in something that will allow the building of an electrical field within the active layer,[61] when the surface energy of the corresponding layer needs modification,[64] improve the charge selectivity[62-63] and increase the interfacial stability between layers most notable between the active layer and electrodes.[66,67] Of the interfacial layers, the two that have garnered the most attention are the cathode and anode interfacial layer. The most common materials for the cathode interfacial layer are metal oxides, water/soluble conjugated polyelectrolytes, low work function metals and metal salts. It is important for these materials to have work functions that overlap with the LUMO

of the acceptor material, to possess good electron transporting character while having good hole blocking character and to be chemical stable and compatible with both components of the active layer and cathode. The latter is important to reduce the interfacial defects between the two layers as well as lessen the energy loss. The world of cathode interfacial layers is currently dominated by the metal oxide materials, both the binary oxides (ZnO, TiOx and Nb_2O_5) and the newer ternary oxides (Al, Cs or Mg doped ZnO).[68-70] Of these materials Zinc Oxide is considered one of the best choices. It owes this status to the fact that is relatively low cost, easy to produce, non-toxic nature, stability to air and moisture, good electron transport character and a work function that match up well with various common fullerene-based acceptors.[71]

In contrast, the anode interfacial layer needs to have a high work function, one that ideally matches with the HOMO of the donor material. It is important for the hole transporting capabilities of this material to be high, as a side effect of this it will lower the series resistance in the overall device. Anode interfacial layers fall into several categories: conductive polymers, inorganic metals, metal oxides, metal sulfides or graphene oxides. Amongst these materials, conductive polymers and metal oxides are widely used and examples of them are poly (3,4-ethylenedioxythiophene) polystyrene sulfonate (PEDOT: PSS) and Molybdenum (VI) oxide (MoO_3) respectfully. PEDOT: PSS has a high enough work function to form a good Ohmic contact with most polymeric donors, smooths the otherwise rough surface of ITO, high electrical conductivity and a high resistivity to the common solvents used to cast the active layer.[72] Unfortunately, this material has several drawbacks that affect the long-term stability of devices with this interfacial layer, due to its acidic nature, the presence of sodium counter ions, hydrophilic nature and high moisture

sensitivity. There has been a lot of effort to replace PEDOT: PSS but most of those conductive polymers have the same shortcomings of PEDOT: PSS. Over the past couple of years, there has been a large interest in metal oxides, mostly Molybdenum and Vanadium based.[73] Where the Molybdenum based materials has the lion share of attention due to the cost of other metal oxides. More importantly, metal oxides seem to solve the drawbacks of the conductive polymers. [74-78]

1.2.4.2 Morphological concerns

The morphology of the active layer is important in facilitating the efficient transport of the charges to the electrodes. The morphology of the active layer has been a series of evolutionary steps over the history of the OPVs, which culminated in the bulk heterojunction. The bulk heterojunction is a simple mixing of the donor and acceptor material. This allows for an increase in interfacial area between the two materials, which decreases the distance the exciton needs to diffuse to the interface. Yet since it is a simple mixing of the two components, control over domain connectivity is lost. Where it is important to have a well-established network of pure domains to facilitate charge transport. There has be considerable effort in finding techniques and optimization conditions to fine tune the morphology of the active layer to facilitate both a large interfacial area and large connected domains of pure component.[80-82] These techniques are varied and include the initial choice of casting solvent, the use of additives and various forms of annealing.

When choosing an initial solvent for casting it is important to choose one that both the donor and acceptor material is soluble in. The speed of evaporation is also an important criterion to consider.[79] Fast evaporating solvents, low boiling point solvents, are good for

making a morphology that is well-mixed. Slow evaporating solvents, high boiling point solvents, will give larger domain size of each components. The slow evaporation rate gives longer time for each component to crystallize and aggregate. When working with a small molecule or highly crystalline donor, a fast evaporating solvent should be used to get a good morphology.[83] If your donor has more amorphous character, slower evaporating solvents should be the first pick. [81]

The interest in additives has grown with the growth of interest in polymer and fullerene blends. This methodology has the advantages over the use of annealing; including the fact that it is easy to implement and does not involve additional fabrication steps.[84] General considerations must be made when choosing an additive, it must have a higher boiling point than the casting solvent and that one component of the active layer must have significantly higher solubility in the additive than another component. The higher boiling point is needed to maximize the working time between the additive and the component during film formation.[85,86] The most prolific additive used with polymeric and fullerene systems is 1,8-diiodoocatane (DIO), since it afforded the highest PCE enhancement to polymeric: PCBM systems.[87-90] It is believed that DIO acts as a good solvent for the fullerene derivatives and is non-solvent for polymer domains. It is believed that the dipole of the terminal iodide of the DIO interacts with the fullerene derivative, causing a strong integration between the two. Thus, allowing for an enhancement in solubility of the fullerene derivative. In effect, the fullerene stays solubilized throughout the film formation allowing it to form smaller domains and giving a better degree of interpenetration. As the film forms, the solvent mixture becomes worst for the polymer, as the good solvent

evaporates and DIO becomes the majority solvent. As this process happens the polymer begins to aggregate and crystallize.[91]

Annealing is the use of either heat or solvent vapor to promote the growth of one of the domains in the active layer. When the film is cast, they have poor crystallinity and orientation due to the thermodynamics and kinetics of the casting process.[92-94] The application of heat promotes the crystallization of both domains, removes residue solvent that was trapped in the film, promotes the creation of interconnected networks of pure domains and increases the contact between the active layer and the electrodes.[95-97] For the increase in domain size, thermal annealing takes advantage of the immiscible nature of the donor and the acceptor. When talking about polythiophenes (P3AT) donor domains, thermal annealing promotes the growth of nanodomains along the stacking direction of the side chains and the face-on orientation of the domains increase.[98] Usually, this process is done after the deposition of the metal electrode. Solvent annealing is exposing the as-cast filmed to either solvent or solvent vapor for a given time while sealed or partly sealed in a container. It is used when either the materials or the substrate that the device is cast upon is thermal unstable or when an increase in nanoscale phase separation is not wanted.[99-101] The chosen solvent used must be a good solvent for one of the domains.

1.2.5 Overcoming the Limitations

The limitations of using organic semiconductors have been well documented and trying to overcome them to make a working solar cell has forced the field to evolve over the years. In summary, the weak dielectric constant spurred the use of two components in the active layer. The small excitation diffusion length found in these materials forces the

evolution of the BHJ. The BHJ's random nature mandated the use of additives and annealing to try and control the domain size. The race for smaller and smaller band gaps has pushed the benchmark donor materials from simple polymers, such as phenylenevinylenes, to other simple polymers, to P3AT and finally to push-pull polymers. The small excitation diffusion length has also spurred the development of heavy metal containing polymers with the hopes of generating long living triplets. When trying to capture the generated triplet, conventional acceptor materials may not have a low enough LUMO, giving rise to more exotic acceptor materials. The laborious effort needed to modify fullerene and its derivatives gave us the PDI class of acceptors. Yet, with all this change more is needed. When one parameter is optimized, another degrades resulting in the need for a new technique or material to try and overcome this new problem.

1.2.5.1 Fixing the Bulk Heterojunction

The BHJ morphology has several major drawbacks. Chiefly among them is the lack of long-term stability and control over the domain size of each component. Although, annealing and the use of additives can help control the domain size they do little for the long-term stability. Given the immiscible nature of the two components, they will spontaneously undergo phase separation. This in turn will cause the active layer to lose interfacial area and resemble the bilayer morphology. Overall, this will cause the device to lose efficiency as a function of time. Another, drawback of the BJH is that there is no control over the exact size of either of the domains. There have been numerous methods developed to try and overcome these drawbacks.

The lion's share of this attention has been in the form of tethering the acceptor to the donor. The first class of materials to emerge were called "double cable" polymers,

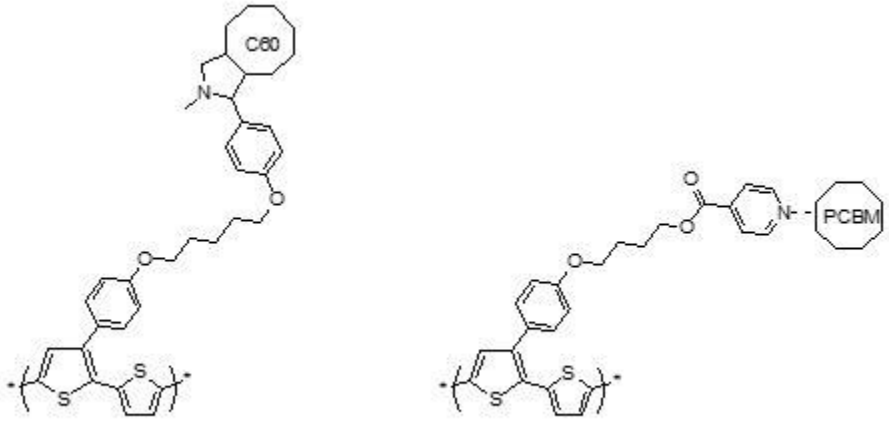

Figure 1.6 Examples of (right) tethered fullerene systems and (left) non-covalently bound fullerene systems

where they had a fullerene covalently bonded to the polymeric donor. The first example of this type of polymer was from the Janssen group in 2001.[102] Where they grafted a fullerene on the PPV monomer unit before polymerization. The results were less than impressive as the fullerene limited the polymerization to significant degrees when compared to the non-tethered polymerization. The next development was the use of post-polymerization modification to tether the fullerene to the polymer. This was done in hopes to eliminate the effect that the fullerene had on the solubility during the polymerization process. Although this fixed the problems that the BHJ had in regard to phase separation, the performance of the devices did not improve. This could have been caused by the lack of continuous charge transport pathways as well as an increase in charge recombination rates within the double cable complex.[103,104]

1.2.5.2 Controlling Morphology within BHJ

It is important to gain precise control of morphology in an active layer. However, the BHJ by nature has a total random distribution of components throughout the active layer. With methods outlined above, use of annealing and additives, individual domains can be grown but they still lack control over size and location within the active layer. With the limited exciton diffusion length, any donor domain that is larger than this will lose some of its ability to generate free charges. Any domain that is not attached to their respected electrode will form an isolation trap, resulting in the loss of possible charge migration through that area and the generation of trap sites that could cause a rise in non-germinate recombination. Numerous methods have been tried to increase the order in the active layer, including the use of nanoscale templating and the inclusion of Titania nanowires and other well-ordered inorganic nano-materials into the active layer. [105-109] Sadly, these methods have not provided an answer to the problem posed; as the implementation of these methods would prove too costly for mass production or result in a significant drop in power conversion efficiency.

A method utilizing the unique properties of block copolymers (BCPs) has been developed.[110] Block copolymers are polymers made up of two to more chemically distinct segments that are covalently linked. These materials can be grouped into three categories: coil-coil, rod-coil or rod-rod BCPs. Coil and rod denote the nature of the polymer's backbone. Coil polymers are made of flexible backbones, aliphatic in nature that take on an amorphous morphology. Rods polymers on the other hand are made of rigid subunits, conjugated in nature, which take on a more crystalline morphology. Based on the nature of the two blocks used in its synthesis, well-ordered domains can be achieved through relatively easy to apply methods.[111] There has been considerable effort that has gone into

understanding this class of material's properties and how to self-assemble them into ordered nanostructures. Different nanostructures can arise from varying two parameters: the volume fraction of each block and the Flory-Higgins interaction parameter χ. Where

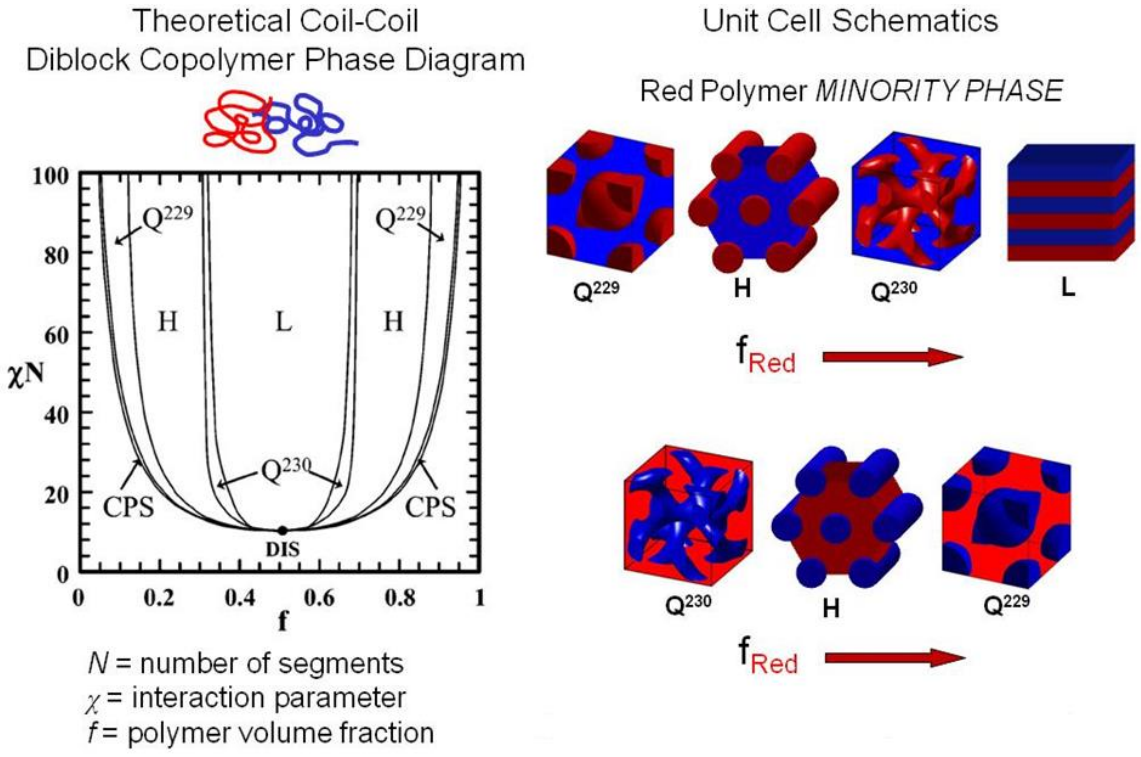

Figure 1.7 (Right) theoretical coil-coil diblock copolymer phase diagram (Left) various nanostructures of coil-coil based off that phase diagram. Copyright ACS 2006.

χ represents the incompatibility of the two blocks and their degree of polymerization. Figure 1.7 is a graphical representation of how varying these parameters will change the resulting nanostructure.[112]

All three categories of BCPs have made their way into solar cell applications, with rod-rod type being the most prolific. Coils in their very nature are not electronically active and act as insulators.[113] The coil is useful when acting as an opposing block to the rod portion, giving rise to the ability to form complex morphologies such as spheres and

gyroids. The more inflexible rod-like polymers favor linear, liquid crystalline type of morphologies.[114] This directs the rod to align with the electrodes, giving rise to high degree of donor-acceptor interface while allowing for ample charge transport pathways.[115] Since the nature of coil-coil BCPs are well explained by the traditional Flory-Higgins parameters, description of their morphologies will be skipped. For Rod-Coil type BCPs, interesting

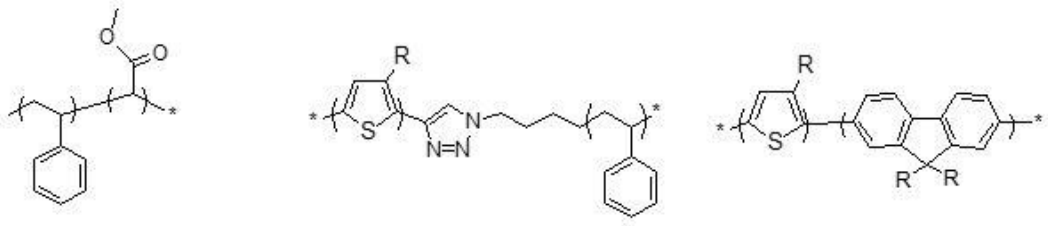

Figure 1.8 Representative structures of (right) coil-coil (middle) rod-coil (right) rod-rod diblock copolymer

morphologies arise from the fact that the two blocks are opposites. Since the fully conjugated rod polymer has the ability to form liquid crystalline domains a new interaction is introduced. This Marier-Saupe interaction describes the strength that the liquid crystal character has in the block copolymer.[117] If the Marier-Saupe interaction dominates, then the morphology will resemble a more lamella type structure. If the Flory-Higgins interaction dominates, then the morphology will resemble a non-lamella type structure.[116] Another consideration arises from the flexible nature of the coil block and that is the geometrical asymmetry parameter. When including these new parameters, the well-known phase behavior becomes progressively complex.

In terms of their photovoltaic performance, much is still needed from these two systems. Coil-Coil BCPs intrinsically lack any conjugation and chromophore behavior, meaning that they rely on chromophoric species to be graphed on their side-chains. As one would expect, the charge transport within such a polymer system is poor with systems

being able to reach sub-1% PCEs. Even with the addition of a chromophore on the main chain, Rod-Coil, PCEs are still only able to sub-1%. Again, possible retardation of charge transport that arises from the inclusion of the coil block is to blame.

The implementation of various synthetic methods has made obtaining Rod-Rod all conjugated BCP systems possible. Grignard metathesis (GRIM), nickel catalyzed Kumada catalyst-transfer polycondensation (KCTP) and other methods based off of noble metal cross coupling reactions have made obtaining these polymers in good yield with a narrow polydispersion possible.[118-125] The mechanism of GRIM and KCTP are reported to follow the quasi-living chain growth polymerization.[126] This method has allowed the explosion of interest in BCP donors based off of polythiophenes. Morphologically speaking these materials are pretty unremarkable, in the sense both blocks are crystalline, and their respective morphology will be crystalline in nature. Yet the picture is more complex when we account for the parameters that govern the crystallization of these BCPs. When defining the segregation strength of these systems, we must look at the Flory-Higgins parameters at the crystallization (χ_c) and order-disorder temperatures (χ_{ODT}). When χ_c/χ_{ODT} is less than three, crystallization is the dominating force. Crystallization is such a dominating force that any microphase separation is either distorted or completely destroyed. The general term of this is break out crystallization. If the system is more strongly segregated, χ_c/χ_{ODT} is greater than three, microphase separation dominates. In this regime two cases exist. In the case where T_{ODT} is lower than T_C, crystallization directs the formation of microphase separation and the formation of lamella structures are favored. In the opposite case crystallization only occurs within domains created by the phase separation and is denoted

as confined crystallization. There is a rare case called templated crystallization which only occurs in systems where the segregation strength is moderate, the guideline is that χ_c/χ_{ODT} is greater than one but less than three. In this regime, the microphase separation directs but does not fully contain the crystallization.[127,128] Yu *et al* gives a great example of the first two crystallization regimes, with his study of poly (2,5 -dihexyloxy-p-phenylene)-b-poly(3-hexylthiophene) (PPP-b-P3HT). In brief, after the thermal annealing of thin films with majority P3HT block copolymer gave rise to breakout crystallization, destroying any microphase separation that the film had before this treatment. However, if PPP was the majority block, the crystallization of P3HT was restricted to the lamellar domains.[129]

1.2.5.3 Ordering Polythiophene donor materials

Over the recent 10 years, polythiophene and its derivatives have been the work horse donor material in OPVs. As a result of this attention numerous methods have been developed to better order these materials in the active layer. Where the main driving force behind this has been to increase the charge transport throughout the polymer domain. There are two approaches when it comes to fixing polythiophenes: chemical and aggregation. Chemical means are generally involve cross linking two polymer chains together. Whereas aggregation is the controlled creation of nanoscale ordered domains through the use of polythiophenes natural crystallization pathways. Commonly these ordered domains take the form of long nanowires/nanofibers structures but can also take the form of spherical nanoparticles.

Chemical cross-linking involves modification of the polymers side chain to allow for instillation of a conjugated bridge group. When one thinks of hole transport, one probably will think of the intra-chain transport along the conjugated polymer backbone. However, since it rare to find a polymer chain long enough to span the entire active layer, hole transport is needed from chain to chain. The primary mechanism of charge transport follows a Dexter type process.[132] There are two requirements for Dexter transport to occur: the two molecules are with 10 Angstrom of each other and that there is significant wavefunction overlap between the excited state of the donor and the group state of the acceptor. The rate of this transfer is generally slower in materials of non-crosslinked polymer when compared to the same polymer with conjugated bridge groups. In a paper published by Zhou *et al*, a series of polythiophenes based block copolymers were created.[130] These block copolymers were constituted from a pure polythiophene chain

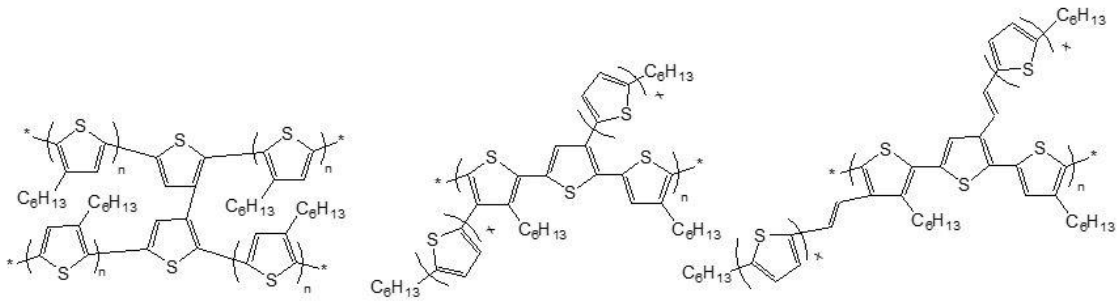

Figure 1.9 Representative structures of polythiophenes system that are fused together by use of a conjugated bridge group

attached to a chain that contained thiophene subunits with a pendent vinylene group on it. A thiophene was inserted as a bridge group via these vinylene moieties through Stille coupling. It was found that at 2% loading, the hole transport was on the order of a thousand higher than that of neat polythiophene, 4.7×10^{-3} cm^2/Vs vs 5.23×10^{-5} cm^2/Vs. When the loading of the bridging group is increased to 4% and 8%, it is found the hole mobility

values decrease from 2% value. This arises from lost in main chain planarity and the steric hindrance between polymer chains. The distortion of the main chain can also be seen in blue shift in absorption. The Bilge group developed an array of swivel-cruciform oligothiophenes dimers for the use in organic field-effect transistors.[131] This led them to use a 3-3' bithiophene monomer as a conjugated bridge group inserted into a polythiophene backbone. Inclusion of this monomer into the polymer was done through McCullough-type GRIM process resulting in a random copolymer. At 2% loading, the hole mobility did not increase in a significant manner, staying around the unmodified P3HT value of ~$4x10^{-4}$ cm^2/Vs. This coupled with the distortion of chain planarity (suggested by the blue shift in absorption) and the disruption of the order of the P3HT domains resulted in a decrease in PSC performance. When the loading was increased to 8%, the hole mobility decreased to 6.4×10^{-6} cm^2/Vs and the PCE of 0.13%. Although not in classical sense of cross-linking, there is an example by the Chen group that should be noted. In this approach, regioregular thiophene side chains where directly added to a pure polythiophene polymer. In this method, the vinylene bridge group was eliminated in hopes to remove the conformational disorder that were introduced from the cis/trans conformations. Although the library of compounds was limited to either a single pendent thiophene or an oligomer or two thiophene. It was discovered that as the conjugated length of the side chain increased, the degree of electronic communication increased, and the band gap lowered. From X-ray crystallography it was discovered that the side chains were nearly planar. Because of this these polymeric systems had excellent hole mobilities ($3.5x10^{-4}$ for the single thiophene and $5.3x10^{-3}$ for the double thiophene) and low HOMO levels (-5.46 eV and -5.62 eV respectfully). This contributed to impressive photoelectronic properties of a VOC of 0.91

V and a 2.5% PCE for the single thiophene. Unfortunately, the system with a double thiophene side chains exhibited poor solubility in their chosen solvent and thusly no solar cell performance could be found.

Cross-linking can be used to help stabilize the polymeric domains within the active layer. Instead of cross-linking directly on the polymer backbone, cross-linking that is done for morphological concerns is done at the termini of the side chain; in some cases, it should be noted that the side chains are only functionalized on a portion of the polymer. These side chains are commonly functionalized with several types of groups: oxetane, halogen (bromine is most common), vinyl and azides.[133-136] Where the cross-linking of these groups can be activated with either thermal or photochemical means. Photochemical is generally the preferred method as it does not disrupt the donor/acceptor blend morphologies. The process of cross-linking is usually done with a common handheld UV-lamp over a given period of time, anywhere from a few seconds to days. This process is usually accompanied

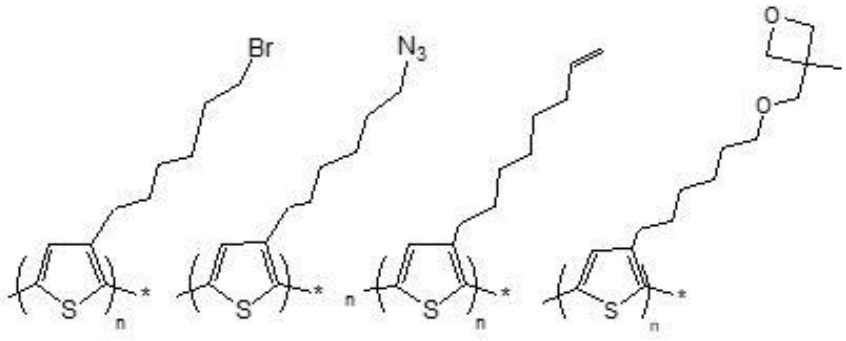

Figure 1.10. Common polythiophenes that can be crosslinked though the functional group on their sidechains (from right to left): bromide (halide), azide, vinyl and oxetane

by the "soft-curing" technique, a low temperature thermal annealing. Each of the various functional groups have benefits or drawbacks. The oxetane functional group readily undergoes UV cross-linking through a ring opening mechanism but produces cationic

species that may harm the overall performance of the device and the requirement of a polyalkylene glycols (PAG) additive that may disrupt the device morphology.[137] Halogen cross-linking operating mechanism is based off the generation of a halogen radical, which is unsurprisingly detrimental to the device's long-term stability as well as the performance. Vinyl and azide functional groups undergo a [2+2] type of cycloaddition. Although vinyl cycloaddition does not generate any charged species, which may act as charge traps throughout the active layer, the resulting cyclobutane moiety is not thermally stable. The azide reaction generates a highly reactive nitrene and nitrogen gas. In the sense of polythiophene based polymers, the bromine functionalized side chains are the most common. It has been reported that devices up to a functionalization loading of 20% do not suffer from significant photovoltaic performance degradation when compared to devices made of non-functionalized polymer. It should be noted that after cross-linking, these devices did see a decrease in PCE. However, after thermal aging, 48 hours at 150^{o}C, these devices were able to maintain ~90% of their initial PCE. This implies that the polymer domain was stabilized through the action of the cross-linking. Twenty-four hours into the thermal annealing process, there were no large PCBM domains in the active layer; in contrast the non-crosslinked films had PCBM domains on the micrometer size. Polymeric systems were also created with the vinyl and azide functional groups added to the side chain. The vinyl crosslinked polythiophene generally performed worse than the bromo functionalized analog, only retaining ~60% of the initial PCE value. This was attributed to the vinyl's incompatibility with the thermal aging method that was used. The azide polymer retained about ~65% of their initial PCE but this was offset by a significant decline in performance from the reference devices. It has been theorized that this was because of a

disruption in the polymeric packing caused by the inclusion of nitrogen bearing side chains or through a photo-degeneration which occurred during the cross-linking process. It should also be noted that the oxetane polymer has not been employed in the cross-linking studies, although several analogs of this polymer have been made with complete side-chain functionalization.

1.2.5.4 Overlapping with solar spectrum

Another weakness of the OPV is the small overlap between its absorption spectra and the solar emission spectra.[138] A method to try and overcome this is by the addition of

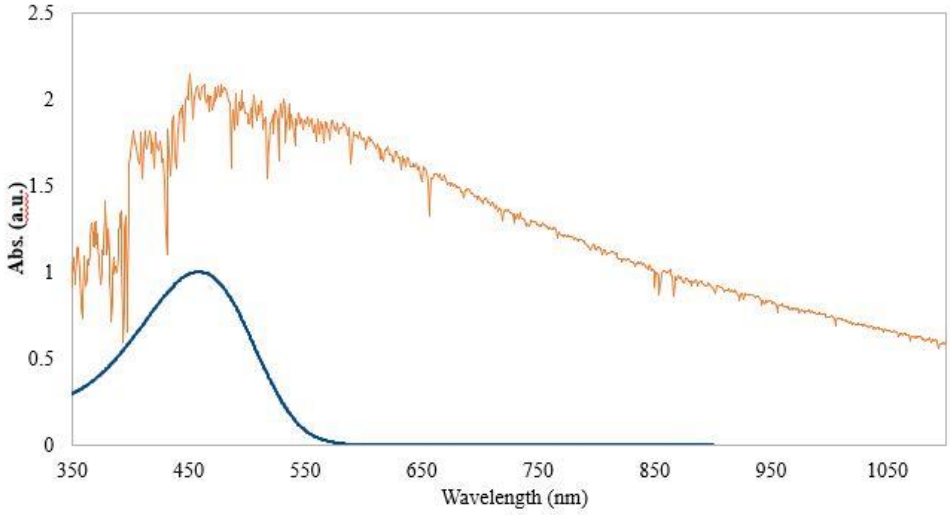

Figure 1.11 Normalized UV-VIS traces of the solar spectrum (orange) and P3HT (blue). Solar spectrum data was obtained from National Renewable Energy laboratories (NREL)

a complementary absorber to the blend. These can be either a small molecule (dye), an inorganic nanoparticle or another polymer.[139-149] Since PCBM is a weak absorber of light and takes up significant area within the active layer; the strategy is to replace it with a complementary absorber.[150] The charge transport mechanism for this process is the same as mentioned before except the CA acts as the electron acceptor. These devices have lower

performance than traditional polymer/fullerene systems, due to the poor electron transfer capabilities of these materials.[151]

To surmount this problem, the ternary blend has been developed.[152] Since the complementary absorber is a poor electron transporter, a fullerene derivative is added back

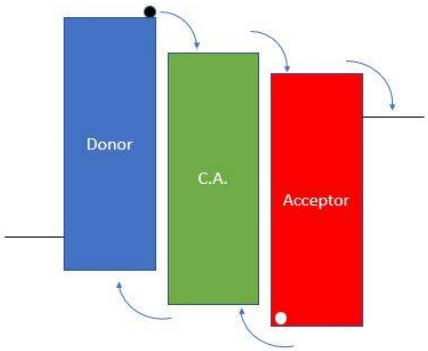

Figure 1.12 Illustration representing the cascade mechanism of charge transport between the components of a ternary blend solar cell. C.A. denotes the complementary absorber.

into the blend. This allows the device to have good absorbance characteristics while maintaining good charge transport through the active layer. Detailed in figure 1.12 is the charge generation mechanism within a three-part system, which is similar to the mechanism of a binary blend with the exception that charges can be generated and flow through the complementary absorber.

1.2.5.4.1 Ternary Polymeric Systems

The study of the inclusion of another low bandgap polymer into the active layer of an OPV device was started off by the Korpee group in 2010.[153] Where they included up to 20 wt % of a near IR absorbing polymer into a blend of P3HT and PCBM. The result of the addition was to increase the external quantum efficiency of the device in the wavelength range of 650 nm to 800 nm by 15%. This was significant because native P3HT and PCBM

blends do not absorb in this region. For peak PCE to come out of this device thermal annealing was needed. This highlighted a problem that most ternary blends have, that the addition of the ternary component to the active layer would disrupt the normally pristine morphology of the blend. This drove the study into the Hansen solubility, parameters that describe the solubility of each component in each other. The Hansen solubility parameters can describe as three different terms: the atomic dispersive interaction, the permanent

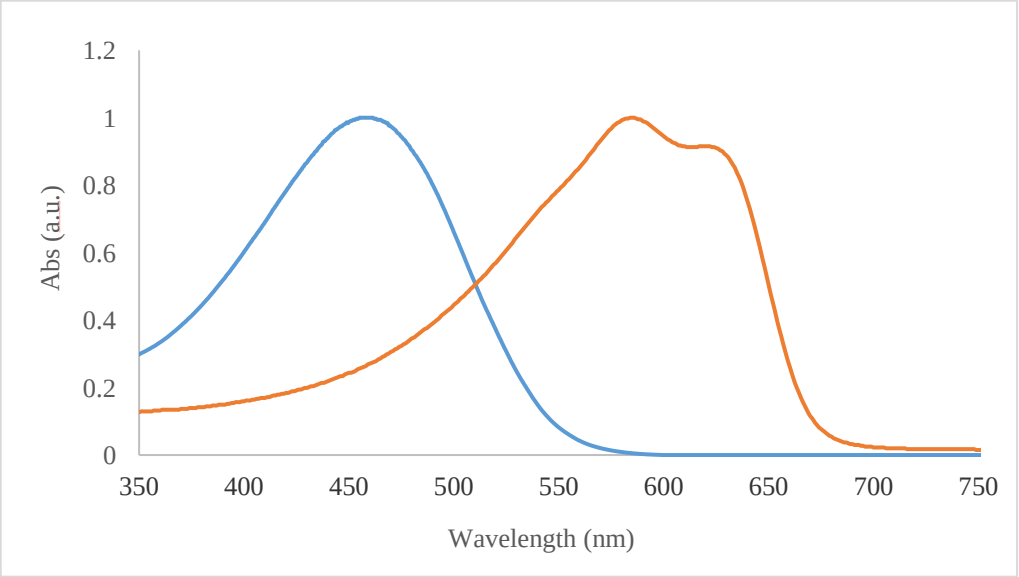

Figure 1.13 Normalized UV-VIS traces of two polymeric systems P3HT (blue) PTV (orange) where their absorption profiles are complementary to each other.

dipole-permanent dipole interaction and the molecular hydrogen bonding interaction. Where the method used to calculate these parameters is way beyond the scope of this paper, but the detailed method is in Ref 154. Since there is a small body of research work that has been done on the P3HT: PCPDTB: PCBM system it will be used as an example. All three compounds have shared solubilities in common solvents, making them compatible materials to be blended together. Yet, this compatibility does not ensure a good working device. The composition of the blend must be controlled to maximize the contribution of

each component and limiting its disruption to the blend. When the wt. % of the PCPDTB polymer is increased the device performance would decrease. Through the application of DSC, it was discovered that the blended film would become more and more amorphous in nature as the PCPDTB wt% would increase. When the polymer-polymer interactions are studied, it is found that the normally amorphous PCPDTB does not mix well with the crystalline domains of the P3HT but instead mixes with the more amorphous domains of P3HT. When the PCPDTB: PCBM interactions are studied a more surprising result was found. That above a certain wt.% the PCPDTB interferes with the PCBM's capability of crystallization. This effect can be counted by either the application of thermal annealing or through the use of an additive. Hu *et al*, used DIO to enhance the crystallization ability of the PCBM domains thus allowing them to reconstruct their domains otherwise disrupted by the inclusion of PCPDTB. [155-157]

1.2.5.4.2 Small Molecules and Dye Systems

Small molecules and dye photosensitizers have some benefits over their polymeric cousins. In general, these classes of materials have a well-defined chemical structure with no batch-to-batch variation while retaining an ease of production and modification. Where these materials fail, is the fact that they a high tenacity to self-aggregate, forming large domains that retard charge mobility throughout the active layer as well as reducing the overall absorption efficiency of the film. The history of the use of these materials as a complementary absorber can be traced back to the paper published by Huang *et al* in the year of 2010.[158] In summary, a small molecule was incorporated into the active layer consisting of P3HT and PC70BM. This gave the film an absorption profile along the

wavelengths of 300 nm to 650 nm, with a maximum at 420 nm. The device of a blend of 1:0.25:1 P3HT: SM: PC70BM gave the highest PCE value that was about 13% higher than devices using the binary P3HT:PC70BM blend. Higher dye loading lead to degradation of device performance as the added dye disrupted the morphology of the blend, which could be seen in a lessening of Jsc. The 2011 paper from the Che group shows work on tetramethyl copper (II) phthalocyanine dye in a blend with P3HT and PCBM.[159] This paper demonstrates the use of the aggregation of these small molecules to assist in facilitating charge transport throughout the active layer. Using the tendency of the dye to favor a nanorod structure, driven by the strong pi-pi interactions between molecules, Che *et al*

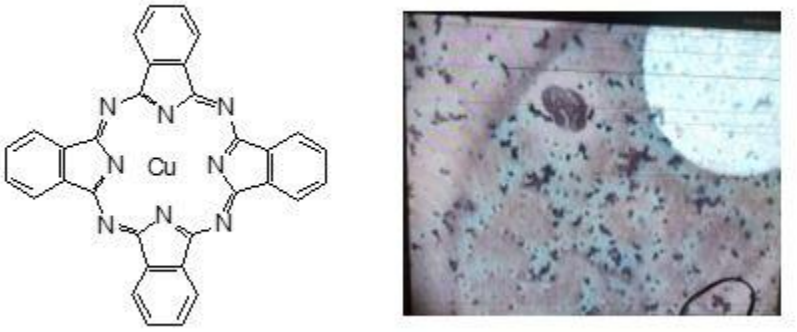

Figure 1.14 (right) The structure of copper (II) phthalocyanine(left) a picture showing the aggregation nature of a dye molecule (blue domain) from the polymer/PCBM domain (purple domain) after thermally annealing.

created a hole channel for the device. This can be seen when the hole mobilities of the film are tested under differing loadings of dye. Where the native P3HT films have a hole mobility of 7.3 x 10^{-2} Cm^2/Vs, films with an equal mixture (w:w) have a higher hole mobility of 2.5 x 10^{-2} Cm^2/Vs. When incorporated into the film the copper (II) dye nanorods formed tight bundles surrounded by P3HT; where these tight bundles did not

disrupt the packing of the P3HT. These two factors give rise to the ability of the film to efficiently move holes throughout.

1.2.5.4.3 Quantum dots

Quantum dots are nanosized crystals made from semiconducting materials of the diameter of around 2-10 nm. Cadmium selenide, cadmium sulfide and lead sulfide are among the most common binary systems used.[160] Since these materials are smaller than the effective Bohr radius, the average distance of the exciton in a given material, they exhibit strange properties somewhere between that of the bulk material and an individual atom.[161] Because of the Pauli Exclusion Principle, their band gaps undergo a quantization.[162] Giving rise to the tunable nature of these material's band gaps. The energy of which is inversely

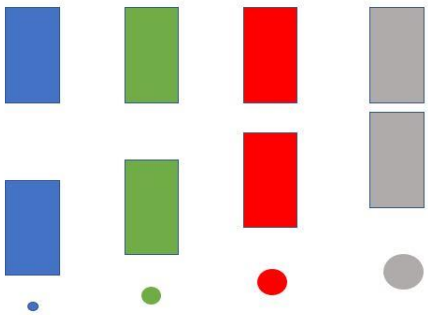

Figure 1.15 Illustration depicting the widening of the band gap of a semiconductor material as the size shrinks. (Grey depicts bulk band gap)

related to the size of the particle. As in when the particle grows, the band gap shrinks until it resembles the bulk materials band gap and all quantum mechanical effects are lost. This fact makes quantum dots an attractive complementary absorber in organic solar cells, as the band gap can be tuned to fit between those of the traditional components. Another benefit arises in the tunable nature of the absorption of these materials, allowing a filling

in of the areas of the device absorption spectra that the original components could not reach.[163]

As a result of the synthesis procedure, quantum dots are traditionally coated in a long alkyl surfactant ligand shell and is done to stabilize growing particles during synthesis and to keep the nanoparticles from aggregating in solution after.[164] Electronically these

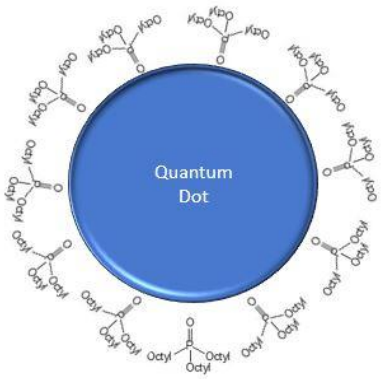

Figure 1.16 Illustration showing a spherical quantum dot with long alkyl ligands (Triocytlphosphene oxide (TOPO)).

long alkyl ligands form an insulating shell around the nanoparticle, generally isolating it from the rest of the system. To unlock efficient transport from the qd to the rest of the system, it becomes necessary to replace the native ligands with a shorter or aromatic ligand.[165] The most common ligand to exchange to is pyridine because of its small size and the relative ease of the ligand exchange process. Pyridine suffers from a weak coordination with the surface of the qd, resulting in an incomplete exchange and the possibility that it will fall off during future use. Another common set of ligands used for exchange fall into the classification of thiol and dithiocarbamate. These ligands have stronger binding interaction than pyridine and the native ligands. [166] This should lead to a more complete exchange when these systems are implemented while decreasing the likelihood that these

ligands will fall off in future use. Thiols and dithiocarbamates have the added benefit of introducing a wide range of functional groups to the ligand shell. This would allow certain possible non-covalent or covalent interactions to be built into the ligand shell.

1.3 Motivation of my project

The current paradigm of polythiophene based organic photovoltaics is limited by several factors. One of the largest of these factors is the relatively fixed absorption window of this class of materials. Where the number of photons that a given system can absorb is important, as this amount effects the Jsc and device performance.

In hopes of widening the active layer absorption window, semiconducting nanoparticle complementary absorbers will be added to the blend. However, these nanoparticles are covered in an insulating ligand shell. To increase the electronical communication between the nanoparticles and the rest of the active layer, a series of shorter and more aromatic ligands will be used. To better control the morphology of the active layer by the application of strong supramolecular orthogonal non-covalent interactions between components, i.e. pi-pi interactions and hydrogen bonding. To accomplish this a polythiophene block copolymer will be synthesized and functionalized to add in the possibility of these interactions. The ligand shell on the quantum dot were further modified to allow for these types of interactions. Within the morphology of the active layer, the quantum dots would be decorated along the long nanofibers made of the polythiophene block copolymer. The choice of the nanofiber structure was made to help increase the hole transport capability of the polythiophene, allowing for the more efficient splitting of the excitonic species as well as give a small degree of control over the morphology of the

active layer. Furthermore, having the nanoparticle fixed to the outside of the nanofiber allows for a cascade-type charge transport to occur throughout the active layer.

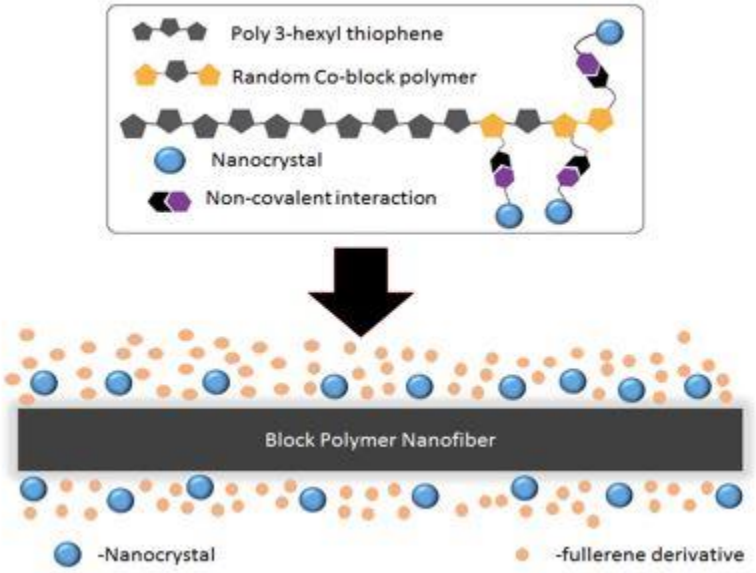

Figure 1.17 Graphical illustration of building a copolymer that is capable of non-covalently attaching to quantum dots then what the ideal structure with a nanofiber based active layer.

Chapter 2

Synthesis and Characterization of Polythiophene based Block Copolymer, their Formation into Nanofiber and its Application in Bulk-Heterojunction Solar Cells

2.1 Introduction

Over the past couple of decades, the best performing organic solar cells have been on conjugated polymers and fullerene derivatives. The architecture of these devices active layer takes the form of a bulk heterojunction or an interpenetrating network of the donor and acceptor materials with nanometer scale domains. The size, orientation and cohesiveness of these domains are random, since by the nature of the bulk heterojunction is a simple mixing of the constituting materials. There have been many strategies developed to try to overcome these limitations including the modification of the polymeric donor material into a block copolymer, the bonding of components to each other through covalent and non-covalent means, the nano-templementing of inorganic acceptor materials and usage of additive materials. When working with poly (3-alkylthiophene) (P3AT) systems a common approach is to self-assemble them into nanowires or nanofibers. Nanowires has

received a great deal of attention within the P3AT community due to unique electronic properties achieved through their formation. There are two methods used to generate nanowires: whisker and mixed solvent. The whisker method involves the controlled cooling of a dilute P3AT solution. The key for this methodology is the use of a marginal solvent, such as xylene. The mixed solvent methodology begins with a well dissolved solution of P3AT in a good solvent, such as chlorobenzene, while a bad solvent, such as methanol or acetone, is added slowly. The driving forces of the formation of nanowires is the interweaving of the side chain and the pi-pi interactions between P3AT backbones. Where the side chain interactions occur first, bringing the polymer chains together to allow for them to pi-pi stack. When devices made from nanowire's PCE are compared to the devices created from well dissolved solutions, these devices will exhibit higher PCE. This is because the nanowire has higher crystallinity and better charge mobility when compared to non-aggregated polymer.

2.2 Synthesis and Characterization of Block Copolymer

Chemical synthesis of the nicotinyl functioned block copolymer **P4** is summarized in scheme 2.1. The monomeric species were created using typical GRIM protocols, with the notable exception being the substitution of an iodine at the 5 position instead of the traditional bromine. This is done to drive the preferential substitution of the active magnesium species to the 5 position of the thiophene ring, allowing for a greater control over the regioregularity of the resulting polymer. To prove that this polymerization follows a quasi-living type of mechanism, a detailed kinetic study of polymerization was carried

out as summarized in Figure 2.1. The linear nature of the Ln ([M_0]/ [M] vs time and number average molecular weight (Mn) against monomer conversion proves the quasi-living nature of the polymerization method. The logarithmic nature of the plots of conversion of monomer to reaction time as well as the Mn vs the reaction time further prove this quasi-living nature of polymerization.

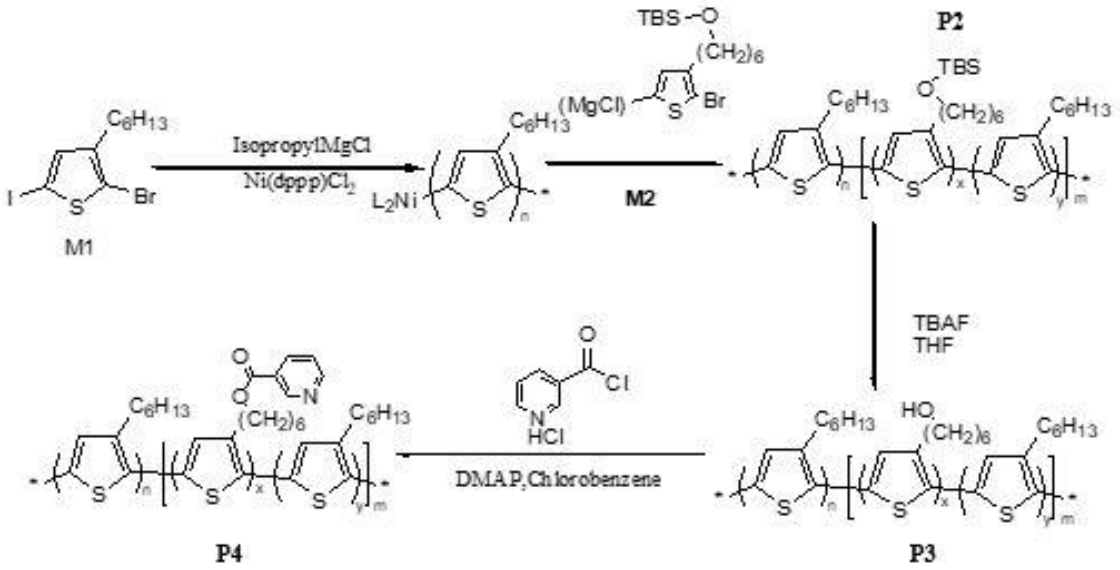

Scheme 2.1 Synthesis of polymers P2-P4

For the ratio of **M1**/**M2,** 10% functionalized was chosen, where the second monomer would be added at about 70 to 80% conversion. This was done to ensure complete chain extension as well as to give a large enough pure P3HT block to allow for formation of nanofibers. The block copolymer would consist of a pure P3HT domain, the longer of the two blocks, and a shorter random polymer block made of both **M1** and **M2.** During the polymerization reaction, prior to the addition of the activated **M2** species, a small aliquot of reaction solution was taken and quenched with acidic methanol. This was done to freeze the chain length of the first block, so we can further prove that chain extension occurred.

Although there is a small variation in each polymer, the typical functionalization fell around 7% of the total polymer, calculated as a ratio of functionalized methylene peak and the thiophene proton peak taken from the integration of 1H NMR peaks. Size Exclusion Chromatography (SEC) gave the following data: 42860 Da Mn, 47690 Da Mw and 1.11 PDI for the first block and 46620 Da Mn, 52550 Da Mw and 1.13 PDI for the total block polymer. The overall block length ratio is ca. 14/1 and the ratio of the 2nd block is ca. 12/19. The SEC plots in figure 2.2 shows relative narrow peaks giving rise to narrow PDI values.

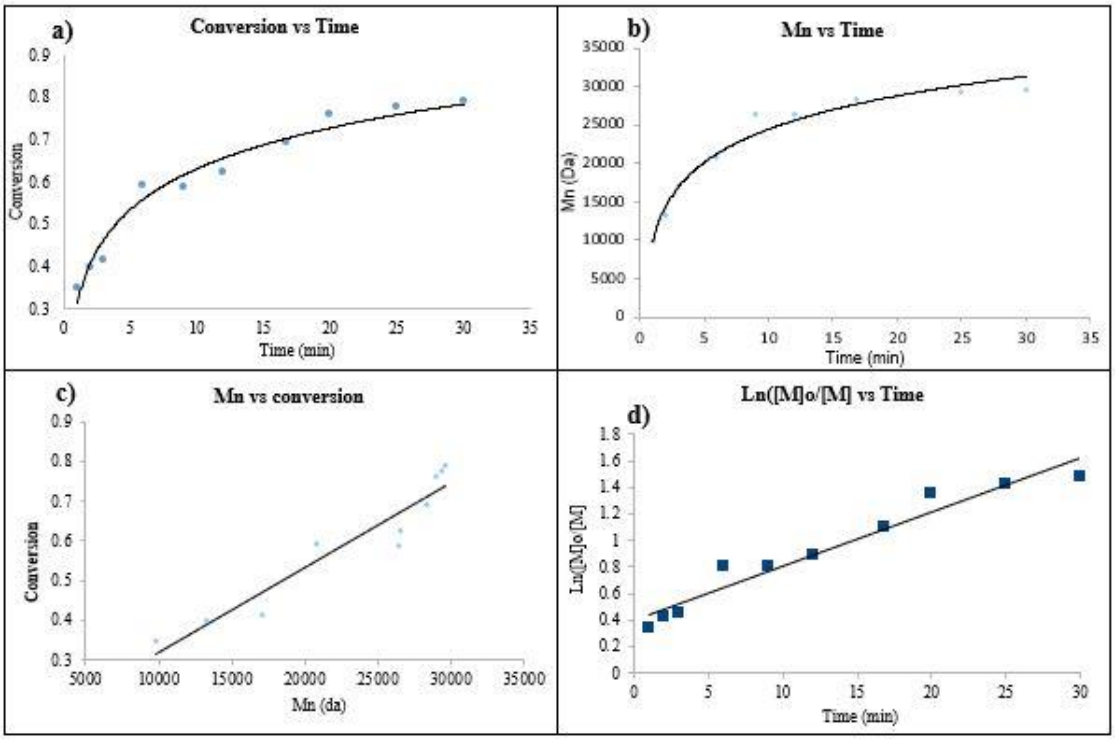

Figure 2.1. Kinetic plots of Turbo-GRIM polymerization of **M1** in THF (0.05M) using $NidpppCl_2$ (0.5%mol) at 35ºC. (a) monomer conversion vs reaction time (b) number average molecular mass (Mn) vs reaction time (c) Mn vs monomer conversion (d) Ln([Mo])/[M] vs reaction time.

The silyl ether functionalized co-block polymer was deprotected using tetrabutylammoinium fluoride giving rise to the hydroxyl functionalized polymer **P2**. This

deprotecting was confirmed by 1H NMR as the shift of the methylene signal from 3.61 ppm to 3.66 ppm as well as the disappearance silyl groups signals at 0.04 ppm and 0.89 ppm. The integrity of the polymer was confirmed by SEC. However, the hydroxyl polymer shows a lower molecular weight as the SEC trace shows a longer elution time with a somewhat longer tail. This would be indicative of the destruction of polymer but can be explained through the interaction of the polar hydroxyl group and the column packing

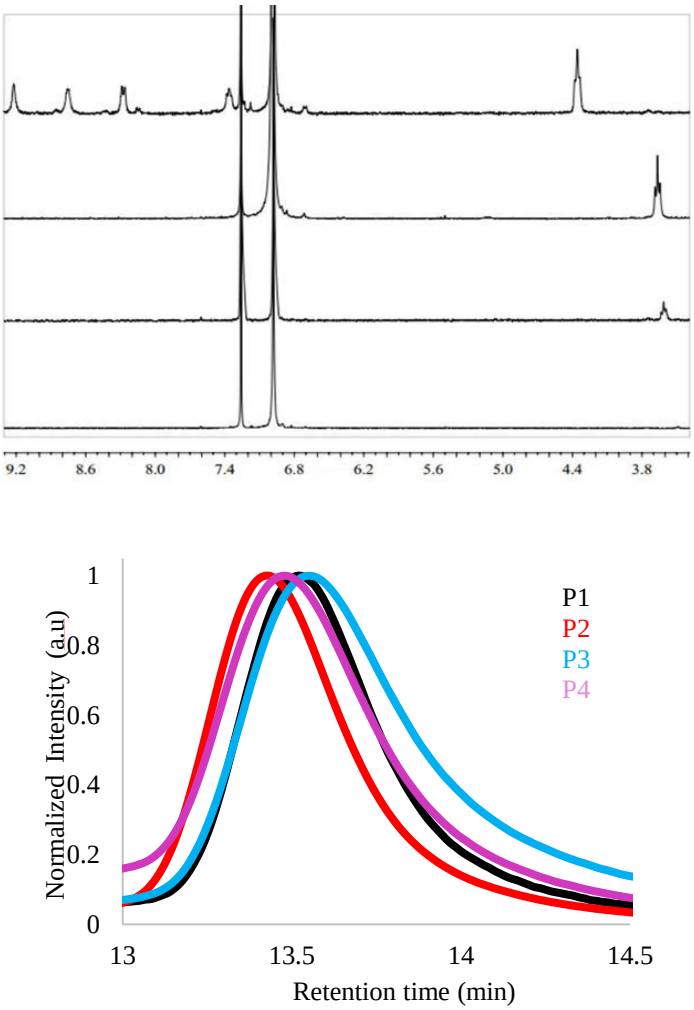

Figure 2.2 (Top) ^{1}H NMR spectra of **P3HT, P2,P3** and **P4**. Alkyl region and thiophene regions removed for clarity. (Bottom) Size Exclusion Chromatography traces of **P1-P4** using chloroform (0.5% TEA) as the eluent (1mL/min, 35^{o}C)

material. The final step is achieved through an esterification reaction between a base activated hydroxyl group and nicotinyl chloride, denoted as **P4**. The success of the reaction was confirmed through 1H NMR where the addition of the new peaks in the aromatic region have been attributed to the nicotinyl group (ppm) and the shift of the methylene peak from 3.66 pm to 4.16 ppm. The SEC trace confirms that the polymer was not destroyed through this modification process. The SEC trace shows the molecular mass of the polymer recover to nearly original non-modified polymer's molecular mass. Although this value is slightly lower than the non-modified polymer, this can be attributed to the fact that there might be an interaction between the slightly polar pyridine pendent group and the column packing material. To further test this material's properties, a model molecule (**M1)** and a random copolymer (**P4r**) were also created. Though as a note, the random copolymer had a slightly higher percent of functionalization than the average block copolymer.

2.2.1 XRD analysis

The thin film XRD traces corresponding to both the P3HT and **P4** polymeric systems are shown in figure 2.3. Both samples were drop cast from chlorobenzene solutions and then thermally annealed for 15 min. It can be seen in both samples have the characteristic three diffraction peaks that P3HT based systems normally has. These peaks correspond to the (1,0,0), (2,0,0) and (3,0,0) planes produced by the stacking of crystalline P3HT domains. There is also a broad peak located around 22^{o} which either corresponds to the glass substrate or the amorphous areas of the thin film, as not all of the P3HT crystallizes when the film is cast. The d spacings of the two samples are pretty close, with

the P3HT having slightly smaller d spacings. Where they differ by 0.23 Å for the (1,0,0), 0.12 Å for the (2,0,0) and 0.03 Å for the (3,0,0). The smaller d spacing as well as the sharper peak nature of the P3HT leads to the conclusion that the P3HT system exhibits more crystalline nature than that of the **P4** system.

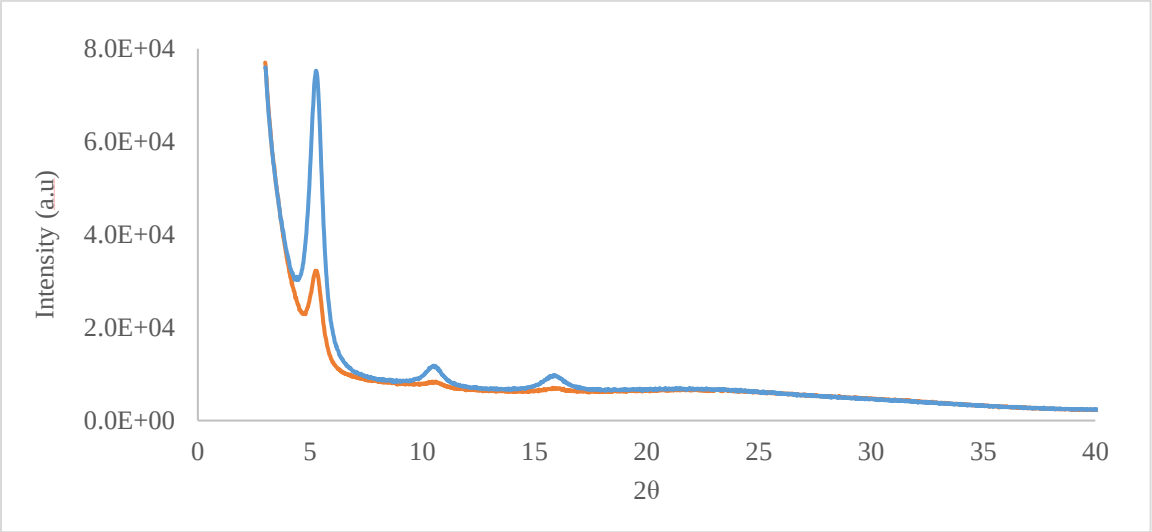

Figure 2.3 Thin film X-ray scattering pattern for P3HT (blue) and **P4** (orange)

2.3 Formation of Nanofibers

2.3.1 Determining the Bad Solvent

Of the two methods used to create polythiophene nanofibers, mixed solvent was chosen over the whisker method. This choice was made because of the high concentration of the polymer needed to create solar devices. The good solvent was selected to be either chloroform or chlorobenzene, proven good solvent for high molecular weight polythiophenes. Of these two solvents, chlorobenzene was chosen. This was done for two reasons: the solvent had a boiling point and the evaporation rate promoted better formed polymer domains in the finished solar device. The choice for bad solvent was a little more

difficult, as there are so many bad solvents for polythiophene based materials. This choice was narrowed down the additional requirement of being a decent solvent for the semi-polar pendent group on the second block; as the architecture of the active layer requires the functionalized side chain to be unaggregated. With this requirement in place, the choice of bad solvent was limited to acetone, methanol, ethanol or pyridine. Where the alcohols would cause the polythiophene backbone to aggregate, force the interpenetration of the alkyl side chains of the non-functionalized subunits as well as enable hydrogen bonding interactions with the pyridine pendant group- stabilizing it within the solution and allowing it to stay unaggregated. If this class of solvent was chosen, the defining attribute would be boiling point needed for the application. Acetone would serve as a slightly less polar option, which would in principle serve the same role as the alcohols. Acetone has been known to force the aggregation of polythiophenes with the same effect on the alkyl side chain. However, this would bring up the question of the solubility of the pendant group in this solvent system. The least polar solvent that was considered was pyridine. Again, polar solvents are all considered either bad solvents or non-solvents for the polythiophene backbone. Pyridine was thought to have interacted with polymer backbone in the same nature as the other polar solvents, the solvability of pendent group should be guaranteed by either a dipole-dipole interaction or through pi-pi interactions between the aromatic species. The starting ratio for the nanofiber formation trials was based off of studies that were initially ran by Dr. Fei Li.[167] His system was close to the system that was employed in this project and thusly serves as a sort of test model for the ensuing study. The initial ratio of good solvent was 4:1 good solvent: bad solvent, with UV-VIS spectroscopy ran at regular intervals to monitor the formation of nanofibers. The individual solutions were also

visually monitored through the process to see if visible aggregation, either the formation thick films on the wall of the vial or small spherical particles in the solution, was detected. Although aggregation was the result that was sought, too much aggregation would be detrimental to the final performance of the device. It was found that at this solvent ratio that the alcohols would form large aggregation within three hours of the start of the study. The polarity of these solvents forced the nanofibers to begin to aggregate themselves in an uncontrollable manner forming spherical "nanoblobs" of polymers. On the other hand, pyridine is a bad choice when it comes to aggregating polythiophene. Even at a high ratio of pyridine to chlorobenzene there is little evidence of nanofiber formation in the UV-VIS spectra. This might be because either the pi-pi interactions between the pyridine and thiophene backbone might disrupt the formation of nanofibers or the solvent itself is not polar enough to induce the formation of nanofibers. The latter might be true since the pyridine has only slightly more polarity than the good solvent of chloroform. Acetone can be seen as a good middle road solvent, where it is not as polar as the alcohols and is significantly more polar than the pseudo good solvent pyridine. As figure 2.4 shows, the kinetics of nanofiber formation when acetone is used as the bad solvent was acceptable, if not outstanding. The UV-VIS graphs show that as the time increases the maximum wavelength of absorption undergoes a noticeable redshift, indicative of the increase in conjugation seen from the formation of well-ordered domains of P3HT. Also, as a function of time, vibrionic features also arise from the single peak assisted with the amorphous well-dissolved solutions of P3HT. The ratio of the A0-1 (552 nm) and the A0-0 (603 nm)

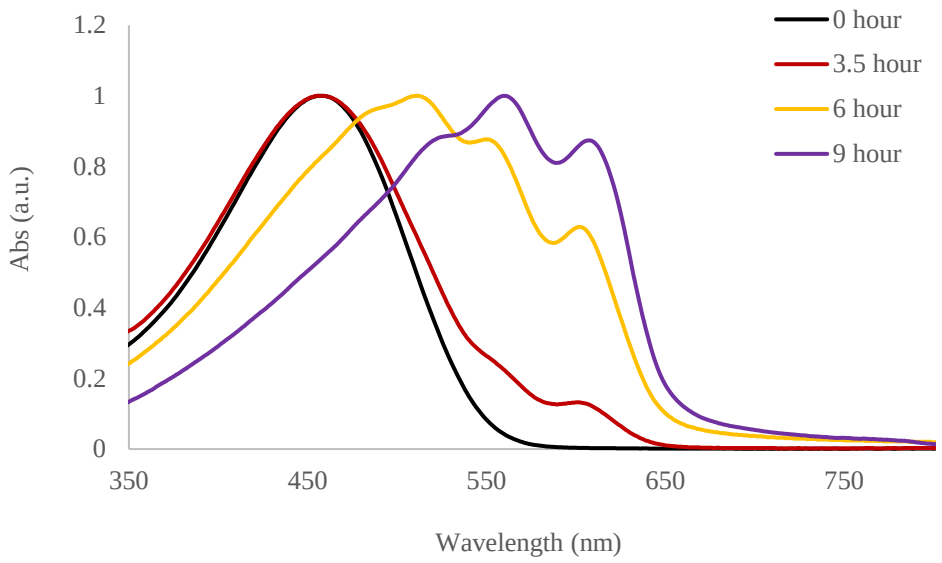

Figure 2.4 Kinetics of nanofiber formation using the normalized UV-VIS traces of **P4** solution after the addition of acetone. (dilutions of 100:1) 4:1 chlorobenzene: acetone ratio used

absorption peaks gives information into what type of aggregation is formed. The ratios that arise from the acetone formed nanofibers, as well as the red shift in the spectra, indicate that J-type aggregation was formed. Within the solution, the minimum time of formation of nanofibers was about 9 hours after the addition of the bad solvent, where the stability of the nanofibers after their formation was more than 48 hours. There are three signs that the nanofibers have aggregated further: the lost in the vibrionic structure in the absorption spectra, the return of the amorphous shoulder in the spectra and the fact that there were visible aggregates observed in the solution. There was further work done to fine tune the best performing, where less bad solvent would either take too long to nanofibers or not form nanofibers at all and too much bad solvent would lead to uncontrollable aggregation and the loss of the well-ordered domains of polymers.

2.3.2 Side chain solubility study

With the nanofibers formed, the question of whether the pendant group on the second block stayed soluble in solution was still not answered. Since it is thought that the acetone will act as a relatively good solvent for the second block and will remain as a bad solvent for the first block, the suggested structure of the nanofiber of the block copolymer will be a polythiophene core with the nictonyl functionalized side chains extending out from this core. Since the pure P3HT block is much larger than the second block, the hexyl groups on the P3HT will pack in an interdigitated way with the acetone acting as a driving force for this to occur.

To answer this question, a series of 1H NMR were taken while the polymer underwent aggregate. In order to undertake this study, block copolymer was dissolved in deuterated chloroform and deuterated acetone was added in the proper solvent ratio. The ratios of the methylene closest to the thiophene (**My1**) and the methylene closest to the ester (**My2**) were studied, where the **My1** would represent the non-functionalized side chains. That the ratio of **My1** and **My2** changes as a function of time after the addition of acetone-d6. Where the peak intensity of **My2** increases compared to **My1**. This is because of the effect that aggregation has on the relaxation time of the nuclei, protons in this case, within an NMR experiment. As something becomes more aggregated, the relaxation time increases, even to times possible longer than the scan rate of the given experiment. This will give rise to the signal given off by these nuclei present being diminished in the overall spectra. So, the fact that **My1**'s signal decreases while functionized **My2**'s signal does not,

indicates that the pendent group on the functionalized side chain keeps its solubility even though the rest of the polymer undergoes aggregation.

2.3.3 TEM analysis

Although the UV-VIS measurements are a good but secondary evidence of nanofiber formation, however these traces do not lend direct evidence of their formation. For this direct evidence to be observed transmission electron microscope (TEM) was needed. TEM samples were created from the UV-VIS solutions, diluted from the stock

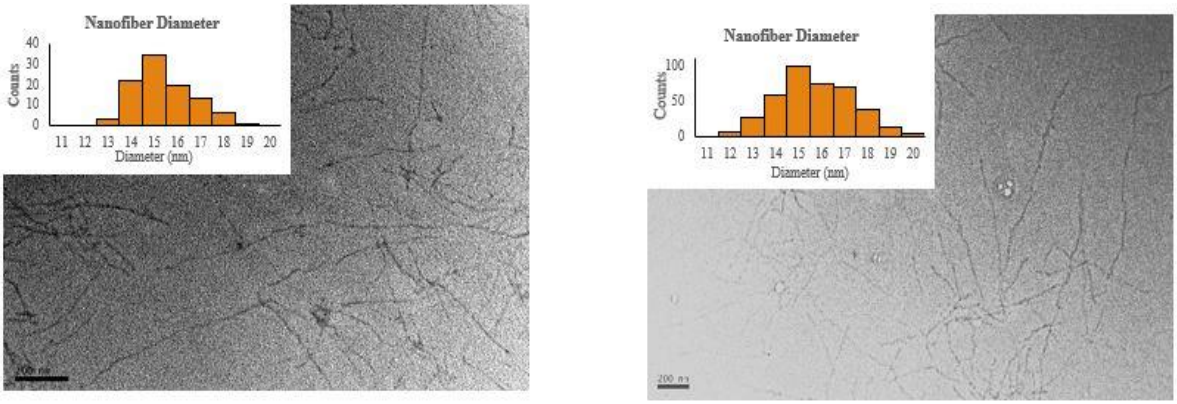

Figure 2.5 TEM images of P3HT nanofibers (right) and **P4** nanofibers (left) inserts are the side distribution of the nanofibers.

solutions by a hundred-fold. Ten microliters of this solution were dropped onto a carbon coated copper TEM grid, the excess solution being drawn away from by the filter paper support. Figures 2.5 show that both polymeric systems create nanofibers. Statistical analysis of these samples generates an average nanofiber width of 14.90 nm ± 1.267 nm and for pure P3HT systems and 15.16 nm ± 1.657 nm of block-polymer systems. This is within the parameters of 10 nm domain size needed for our pseudo-controlled morphology as well to allow for an efficient splitting of exciton.

2.4 Solar Cells

Table 2.1 shows the average solar cell performance of devices cast from the various polymeric systems. We can see that the P3HT: PCBM devices are comparable to record high values found in the literature at about 5% PCE. Nanofibers seem to detrimentally effect the PCE of devices, where the Jsc value drops by 14%. This drop is indicative of a loss of morphology within the active layer and the resulting loss in effective charge transport throughout. Even though the nanofiber itself has been proven to enhance the charge transport along the fiber itself, it might not help the charge transport over the entirety of the active layer. The way nanofibers stack within the polymer domain may limit the intra-chain charge transport to a few points, where ever the fibers overlay. The Voc figures do not suffer from such a significant drop in performance, meaning that the electronics of the active layer do not change in any significant manner. When the unmodified polymer and **P4**, the results are a little more shocking. Between the two systems, non-nanofiber, there is a ca. 48% drop in PCE. The value that takes the largest drop is the Jsc. Showing that the inclusion of the slightly polar nicotinyl group may significantly disrupt the morphology of the polymeric domain of the active layer. There have been no reported effects of this moiety or related moieties (pyridines based) acting as a charge trap, basically eliminating this as a possibility of the loss of Jsc. The loss of PCE can also be seen in when the nanofiber devices are compared, suffering a ca. 40% loss. Again, with non-nanofiber case and without the pyridine charge trap, the possible cause being the disruption of morphology resulting from the nicotinyl group. There is also a large increase in Voc values between P3HT and **P4**, where solar devices that have **P4** donor materials have the higher values.

Table 2.1 Table summarizing the solar cell performance of devices made from 1:1 wt:wt polymer: PCBM. N.f. denotes devices that use nanofibers.

Composition	Power Conversion Efficiency [%]	Short Circuit current [mA]	Open Circuit Voltage [mV]	Fill Factor	Series Resistance	Shunt Resistance
P3HT	4.97% (±0.240)	14.10 (±0.692)	0.570 (±0.004)	0.618 (±0.003)	1.572 (±0.222)	946.211 (±109.30)
P3HT nf	3.97% (±0.430)	10.60 (±1.181)	0.580 (±0.000)	0.644 (±0.016)	2.523 (±0.252)	996.487 (±136.6)
P4	1.75% (±0.48)	5.640 (±1.713)	0.64 (±0.000)	0.489 (±0.016)	4.660 (±1.044)	704.750 (±137.18)
P4 nf	1.70% (±0.24)	6.880 (±1.167)	0.63 (±0.013)	0.394 (±0.029)	6.794 (±2.220)	454.830 (±83.354)

There has been some evidence presented that the lesser the crystallinity a donor material in an active layer the higher the resulting Voc is. [168] Although the paper that reports this phenomenon does not go into any detail about the specific reasons behind this, but it appears that the degree of crystallinity of the polymer directly affects its HOMO level. When comparing the two **P4** systems, the nanofiber case sees a small decrease in PCE, about 1% and close to the standard deviation of the systems. The lesser effect of the disruption might be from a directing effect that the nicotinyl groups have, one would imagine a pi-pi type interaction between the aromatic systems directing the lining up of nanofibers in a parallel manner.

To further probe the possible disruption to the morphology caused by the nicotinyl group, a random copolymer was made. The synthesis methodology was the same as the previous block copolymer with the exception that the second monomer was in the same flask as the first monomer from the start of polymerization. There was an attempt to make

nanofibers out of this material but under standard conditions no nanofiber formation was observed. Formation was still not observed even when the solvent mixture was changed have a higher percentage of acetone or when the solvent was changed to the more polar methanol. Furthermore, TEM confirmed the lack of nanofibers within the solutions, where the polymer takes on the appearance of unordered "nanoblob" structures. This can be attributed to the effect that even this low loading of nicotinyl has on the long-term order of polythiophenes. It appears that it is either the polar nature of the ester linkage, the lone pair of electrons on the nicotinyl group or a mixture of the two that is causing this disruption. It can be said that the block copolymer **P4** is not pure rod-rod type but a mixture of rod-rod and rod-coil types. Although it is not a coil in the classical sense that it has a conjugated backbone. This second block would be more cable in nature, not as soft as a coil but not as rigid as a rod. To put this a second way, the polar nature of the functional group would form a sort of pearl within the active layer, the way that a grain of sand forms a real pearl in an oyster. The morphology of the polymer domain has to in a small way to accommodate this group.

2.5 Conclusion

It was found that to form good quality nanofibers from both P3HT and **P4**, acetone was required as a bad solvent in 1:4 (v: v) solvent mixture. The UV-Vis traces reveal that the polymers form a j-type aggregate and the lack of the 458 nm shoulder indicates that most of the polymer is in this crystalline form. The dimensions of both the P3HT and **P4** nanofibers are within the limits needed for the pseudo-controlled morphology that was

being engineered into the active layer. Solar cell performance for the P3HT devices were within acceptable parameters, the non-nanofibers devices are around the published average value for such cases. The cause for the nanofiber case decreases in performance is uncertain at this time but can be tentatively attributed to either the loss of efficient charge transport through the polymer domain or through some unforeseen device processing error. The significant decrease in the performance of devices containing **P4** can mostly likely be contributed to the disruption of the polymer stacking caused by the inclusion of the semi-polar ester group. We can see this from the lack of formation of nanofibers from the random copolymer as well as the fact that there is a fairly large increase in Voc between P3HT and **P4** devices.

Although the inclusion of the nicotinyl functional group to the block copolymer caused significant degradation of device performance, this material would serve as a test system to prove that through the usage of non-covalent means could be used to graph quantum dots to the polymeric donor. The nanofibers, at least in this case, caused a small decrease in device performance. Though through the use of these nanofibers, we can better quantify the adhesion or lack of adhesion of the nanocrystal to the polymer through the usage of TEM imaging.

2.6 Future Work

With the limitation of the current block copolymer being made apparent through poor performance compared to devices created from pure P3HT, modification is needed to

make this system viable. The largest problem with the current system seems to be with the ester group, although the effect of the lone pair on the pyridine has on the morphology of the active layer should not be discounted. To lessen the polar nature of the connecting group, the ester should be changed to something smaller like an ether functionality. Although they contain oxygen atoms, ether functional groups can be considered non-polar. The only concern would then be the lone pair of electrons on the oxygen. However, since this group is smaller than the previous ester the effect on morphology should be lessened. Another tactic could be directly attaching the pyridine group to the polymer side chain. Any of the carbon-carbon bond forming reaction that are capable with pyridine can be considered. This would eliminate any possible concerns over the oxygen's lone pair and their effects on the morphology. The last modification that could be made to the system would be the elimination of the pyridine, although there are a couple of directions that it could take. The only limitation to the new chosen function group is that it would have some type of non-covalent interaction with the ligand shell of the quantum dot. This could take the form of either pi-pi type that could be generated from the addition of two aromatic species, hydrogen bonding type generated from A-B pairing or have the side chain itself act as the ligand itself through installation of the strongly binding thiol functional group. Each of these interactions have their benefits and downsides: aromatic groups are generally non-polar so the possible disruptions to the morphology caused from the "pearl" group. However, these interactions can be weak, or they are not selective enough as there is nothing stopping the aromatic group from burying itself into the pi system of the polymer. Hydrogen bonding requires a dipole, sometimes a strong one at that, which again would cause possible significant disruption to the morphology although you can tailor the

corresponding groups to only interact with each other. The thiol or any other strong quantum dot binding groups would eliminate the need for a corresponding ligand but might disrupt the morphology the same way that an alcohol, ether or ester functional group does. Although, this last point would depend on whether the lone pairs are coordinated to the nanoparticle thus being masked.

Another direction that this project can go is the modification of the block copolymers into polyelectrolytes. Polyelectrolytes being a polymeric system that incorporates either positive or negative groups within the main or side chain. Within the solar cell application these materials have garnered attention due to their use of relatively environmentally safe solvents that can be used in their processing. Three systems can be developed off the block copolymers already used in this project. A polycationic system can be achieved through the simple methylation of **P4**, a polyanionic system can be achieved through the reaction of **P3** and class of reagents known as sultones. The final class being polyampholytes, bearing both cationic and anionic groups, and can be created from **P4** and sultones. Methylation of **P4** is a relatively simple reaction, were the methylation agent would be dropped into a well solvated solution of polymer. The only concern with this material is the limited solubility of the resulting polymer. Although primarily work has been done on this material, the amount of work done is limited to the fact that once the polymer is drying to a solid it becomes impossible to solvate. Numerous solvent mixtures, heating to high temperatures, sonication and combinations of these have been tried and yielded no fruitful results. The possible solution to this problem is changing the installed methyl group to a longer alkyl group. Although if the solubility issue is solved then that would bring up another problem that would need to be addressed, the problem with counter

ion. As mentioned in the cross-linking portion of the introduction, the introduction of impurity will negatively affect the device performance. The proposed strategy to get around this will be further discussed in chapter 3's future plan section. Another strategy to create the polycationic material based of the previous block copolymers would involve the modification of the terminal group into a halide (bromine). This would allow for the installation of a cationic nitrogen species through a relatively simple substitution reaction. This synthesis has already been reported by numerous groups and is confirmed to be soluble in numerous common solvents, i.e. chloroform, methanol, water, etc. The polyanionic material would possibly suffer from the problems that the polycation would suffer from, where the solubility is not guaranteed and the counterion's presence would probably hurt the device performance. The final class would at least solve the problem of the counterion, where in the polyampholyte would serve as its own counterion. But for the proposed usage, again more details in chapter 3, it might not be as useful as the other two species. The final challenge that would have to be overcome in order to use the polyelectrolyte as a donor material is with the very nature of the charged pendent group on the polymer. It has been reported that this group could act as a charge trap site, which is immensely bad for the performance of any solar cell.

2.7 Experimental Section

2.7.1 Materials and General Methods

All reagents and solvents were used as received from either Sigma Adrich, Alfa Aeisa or TGI unless otherwise noted. Cadmium Selenide quantum dots were purchased from Ocean Nanotech and was produced in house according to reported literature procedure. Dry Tetrahydrofuran was distilled over sodium using benzophenone as an indicator and was collected in a flame-dried, air free storage flask. Other solvents were dried by first exposing it to CaH and then through the application of a freeze/pump/throw cycle. Hexanes and dodcane were dried via bubbling a dry stream of nitrogen through the solvent overnight. All NMR spectra were recorded on one of two Bruker Avance III 300 MHz using standard proton experimental protocols, unless otherwise noted. All NMR spectra are referenced internally to the solvent signals or referenced by an internal standard such as Trimethylsilane (TMS). Size exclusion chromatography was performed on a Waters 1515 series equipped with a 2414 refractive index detector and 2707 auto sampler. The mobile phase was chloroform with 0.5% (v/v) triethylamine passing through two styragel columns (Polymer Laboratories, 5 m Mix-C) at a flow of 1 mL/min, kept in a column heater at 35^{o}C. SEC trials were calibrated by external polystyrene standards (Varian). Ultraviolet-visible (UV-VIS) absorption was recorded on a Shimadzu UV-2401 PX spectrometer over a range of 300-900 nm using quartz cuvettes. Infrared spectra were generated by a Bruker Alpha-P spectrometer, using a powder sample in ATR mode. TEM imaging was performed with a JEOL 2010 microscope with a lanthanum hexaboride beam source and Gatan camera while in bright field mode. Samples were prepared by drop casting a diluted sample onto a carbon coated copper grid.

2.7.2 Procedure for nanofiber preparation

In a dry scintillation vial 5 mg of polymer and a magnetic stir bar were added. The vial was transferred to a nitrogen glovebox. This polymer was dissolved in 0.4 mL chlorobenzene and was heated at 90^{o} C for 1 hour while undergoing stirring at 400 RPM. The solution was allowed to cool down to room temperature and allowed to stir for another 1 hour. At this time, 0.1 mL of acetone was added dropwise via a microsyringe. The solution was allowed to age for an amount of time, 9 hours seems like the minimum time for good nanofiber formation to about 72 hours when the nanofibers start to aggregate. The color of the solution is also a good indicator of the progress of nanofiber formation. The solution needed to be violet and any hints at a red color shows that the process is yet to be completed. For nanofiber solutions that required the inclusion of PCBM two methods were used. The first method involved preforming the nanofiber in the method outlined above then adding solid PCBM powder to the solution. The solution was allowed to stir at room temperature for an additional 6 hours before further analysis was undertook. It should be noted that this method was not preferred as PCBM was not well dispersed throughout the solution. The second method involved co-dissolving the polymer and PCBM in chlorobenzene before the addition of the bad solvent. The only difference from the before mentioned method is that the initial time of heating was increased to at least 6 hours.

2.7.3 Solar Cell preparation and testing

Blend solutions were prepared by dissolving predetermined weight ratios of polymer and PCBM in chlorobenzene and heating it for 1 hr at 90^{o}C in a nitrogen glovebox. The solution was then taken off the heat and stirred for 1 hr, when a predetermined amount of “bad” solvent (usually acetone) was added dropwise via a micropipette. This solution was stirred

at 400 RPM for 9 hr. ITO-coated glass substrates (China Shenzhen Southern Glass Display Ltd, 8/) were cut into 1 in^2 squares and then underwent a cleaning procedure: 15 min ultrasonic sequentially in detergent, DI water, acetone and isopropyl alcohol, finally undergoing an UV Ozone (Novascan PSD series) treatment for 45 min. These sides were then stored in nitrogen glovebox until MoO_3 coating. 10 nm of MoO_3 was deposited using an Angstrom Engineering Amond deposition system with a vacuum level of $<7x10^{-8}$ Torr. The blend solution was spin coated on to the MoO_3 surface at "500" RPM for 30 sec. Aluminum electrodes were then added to the device via thermal evaporation through patterned masks. Some devices were then annealed through the application of heat (150^oC) for a set amount of time. Current-voltage measurements were taken by a Keithley 2400 source while the device was under irradiation (100 mW/cm^2) generated by a Xe arc lamp-based Newport 67005 150 W solar stimulator equipped with an AM1.5 filter. The light intensity was calibrated on wavelength 576 nm by a Newport thermopile detector (model 818-010-12) equipped with a Newport 1916-C Optical Power Meter.

2.7.4 Synthetic detail

3-bromothiophene 10.74 g of Magnesium metal (0.4417 mol), 0.95 mL of 1,2 dibromoethane and ca. 400 mL of anhydrous THF were added to a clean 1000 mL 3 neck round bottom flask. Mixture was allowed to stir at room temperature for ca 1 hour. 28 mL of 1-bromohexane (0.193 mol), diluted in 15 mL of anhydrous THF with .15 mL of 1, 2-dibromoethane, was added to the mixture dropwise. This reaction was allowed to cool back to room temperature when it underwent a cycle of reheating and cooling. After the solution cooled to room temperature, it was transferred to a 1000 mL three neck flask containing

17.34 mL of 3-bromothiophene (0.184 mol) and 2.99 g of $NidpppCl_2$. The reaction mixture was cooled down to 0°C and allowed to warm to room temperature overnight. The product was extracted via diethyl ether and finally fractional distillation. 1H NMR (300.13 MHz, $CDCl_3$): δ (ppm) = thiophene H (multi):7.25-6.91, methylene-thioiphene: 2.62 alkyl chain (multi):1.56-1.04

2-bromo-3hexylthiophene In a darkened 100 mL single neck round bottom flask, ca. 60 mL of DMF was added to 6.677 g of 3-hexylthiophene. (0.040 mol) Mixture was stirred at 0°C, when 7.061 g of N-bromosuccinimide (0.040 mol) was slowly added. Reaction was allowed to warm overnight. Product was extracted via dichloromethane. (8.380 g) 1H NMR (300.13 MHz, $CDCl_3$): δ (ppm) = thiophene (doublets): 7.19 and 6.78, methylene-thiophene: 2.57 alkyl chain (multi): 1.55 and 1.36

2-bromo-3-hexyl-5-iodothiophene In a darkened 250 mL single neck round bottom flask ca. 85 mL of dichloromethane was added to 8.377 g of 2-bromo-3-hexylthiophene (0.034 mol). Mixture was stirred at 0°C, when first 6.002 g of (Diacetoxyiodo) benzene (0.019 mol) and then 8.601 g iodine (0.034 mol) were added. Reaction was allowed to warm for ca 4 hours. Product was extracted using diethyl ether and purified via fractional distillation. (11.302 g) 1H NMR (300.13 MHz, $CDCl_3$): δ (ppm) = thiophene (singlet): 6.96, methylene- thiophene: 2.52, alkyl chain (multi): 1.51, 1.34 and 0.8

Poly 3-hexylthiophene 0.5 g of 2-bromo-3-hexyl-5-iodothiophene (1.34 mmol), 0.032 g lithium chloride (0.755 mmol) and a stir bar was pumped overnight in a 100 mL 3 neck round bottom flask. 24 mL of anhydrous tetrahydrofuran was added to the round bottom flask. The solution was cooled down to 0°C when 0.67 mL of 2 M isopropylmagnesium

chloride was added via deoxygenated syringes. The mixture was allowed to react for ca. 30 minutes, completeness of reaction was tested via NMR. The solution was warmed to 35ºC and 0.0075 g of Dichloro(1, 3bis(diphenylphosphino)propane) nickel (0.0134 mmol), suspended in 2.3 mL of anhydrous tetrahydrofuran, and was injected into the grignard solution via a deoxygenated syringe. This was allowed to react for 10 minutes when it was quenched with an excess of methanol. The polymer underwent soxhlet purification: first with methanol, then with acetone/hexanes, tetrahydrofuran and chloroform. The chloroform solution was concentrated and precipitated into methanol. (101.8 mg, 19480 Mn PDI: 1.21) 1H NMR (300.13 MHz, $CDCl_3$): δ (ppm) = thiophene (s) 6.98, methylene-thiophene (t) 2.80, alkyl chain (m) 1.71. Alkyl chain (m) 1.40, alkyl chain (m) 0.93

(6-(2-bromo-5-iodothiophen-3yl) hexyloxy)(tert-butyl) dimethylsilane

Same procedure as the synthesis for 2-bromo-3-hexyl-5-iodothiophene except the substitution of 3-bromohexane for [(6-bromohexyl) oxy] (tert-butyl) dimethylsilane. 1H NMR (300.13 MHz, $CDCl_3$): δ (ppm) = thiophene (singlet): 6.96, methylene- OTBS: 3.62, methylene- thiophene: 2.52, alkyl chain (multi): 1.51 and 1.34, methyl- TBS (singlet):0.89, tert-butyl-TBS (singlet):0.06

Poly 3-hexylthiophene-b-poly tert-butyldimethyl(6-(tiophene-3-yl)hexyloxy)silane

1.00 g of 2-bromo-3-hexyl-5-iodothiophene (2.68 mmol), 0.576 g lithium chloride (1.34 mmol) and a stir bar was pumped overnight in a 100 mL 3 neck round bottom flask. In a 25 mL two neck RBF flask (flask two), 0.134 g of **M_2** (.268 mmol) was combined with 0.058 g of lithium chloride (0.134 mmol) and a stir bar and was pumped overnight at the

same time. Anhydrous tetrahydrofuran was added to both the round bottom flask and flask two: ca. 50 mL and 5 mL respectfully. Both solutions were cooled down to 0ºC when a total of 1.98 mL of 2.11 M isopropylmagnesium chloride was added to the RBF and .137 mL was added to flask two via deoxygenated syringes. The mixtures were allowed to react for ca. 30 minutes, completeness of reaction was tested via NMR. The RBF solution was warmed to 35ºC and 0.0076 g of Dichloro (1, 3-bis (diphenylphosphino) propane) nickel (0.0134 mmol) was suspended in 2.30 mL of anhydrous tetrahydrofuran and injected into the Grignard solution via a deoxygenated syringe. After 30 minutes a .3 mL aliquot was taken and quenched into an excess of ethylmagnesium bromide and pumped down. Immediately the contents of flask two were transferred into the RBF via cannula transfer. This was allowed to react for 45 minutes when it was quenched with an excess of ethylmagnesium chloride. 1H NMR (300.13 MHz, $CDCl_3$): δ (ppm) = thiophene (s) 6.98, methylene-OTBS (t) 3.61, methylene-thiophene (t) 2.80, alkyl chain (m) 1.71. Alkyl chain (m) 1.40, alkyl chain (m) 0.93

Poly 3-hexylthiophene-b-poly 6-(thiophen-3-yl) hexan-1-ol. In a clean 50 mL single neck round bottom flask, 150 mg of P3OTBST (.103 mmol functional group) was dissolved in 20 mL of anhydrous THF under a N_2 atmosphere at 60ºC. The solution was stirred at 540 RPM while 0.11 mL of 1 M TBAF solution was added dropwise to the solution. (0.11 mmol in THF) The solution was stirred for ca 9 hours when product was concentrated under reduced pressure and predicated into methanol. Product was then washed with ca 250 mL of methanol and then dried under vacuum. (0.12909 g 86.06%)1H NMR (300.13 MHz, $CDCl_3$): δ (ppm)= 6.98 H- thiophene, 3.75 H-THF, 3.66 H-methylene-OH,2.80 H-methylene-thiophene, 1.85 H-THF, 1.710.83 alkyl chain of hexyl group

Poly 3-hexylthiophene-b-poly 6-(thiophen-3-yl) hexyl nicotinate. 65.1 mg of P3HT-b-P3OHT (0.0471 mmol -OH group) and 0.0230 g of 4-dimethylaminopyridine (0.1883 mmol) were heated at 91°C and stirred in 15 mL of anhydrous chlorobenzene under an argon atmosphere until they dissolved. 0.0171 g (0.0961 mmol) of Nicotinoyl chloride hydrochloride complex was added and the reaction mixture was heated and stirred for the next ca. 8 hours. The product was then concentrated and precipitated into methanol. The solvent was pumped off and solid polymer was recovered. Soxhlet extraction were performed with a series of solvents: methanol (3 hours), acetone (ca 5 hours), hexanes (overnight) and chloroform (ca 6 hours). The solution was concentrated and the product was recovered. (0.05901 g) 1H NMR (300.13 MHz, $CDCl_3$): δ (ppm) = 9.27 (d) H-pyridine, 8.75 (s) H- pyridine, 8.28 (s) H- pyridine 7.26 (s) D-chloroform, 6.98 (s) H-thiophene, 4.37 (t) H-methylene-nico 3.66 (t) H- methylene-OH, 2.80 (t) H-methylene-thiophene, 1.71-0.83 alkyl chain of hexyl group

Chapter 3

The inclusion of semiconductor nanoparticles into an organic photovoltaic to serve as a complementary absorber

3.1 Introduction

One of the many hurdles that needs to be overcome before OPVs become a viable technology revolves around the fact that the constituting materials' absorbance has poor overlap with the solar spectrum. There have been three approaches that have been developed to overcome this limitation. The first being through the modification of donor material to increase the absorption. However, this could add various degrees to the production of the final solar cell. Where the complex synthesis schemes will lead to numerous purification steps giving rise to an organic device that is no longer cost competitive when compared to their inorganic counterparts. The modification of band gap may also lead to the use of a more exotic electron acceptor material, either increasing the cost of the given cell or adding additional complexity of synthesis. The second method involves the stacking of active layers into a tandem or a multilayered device architecture.

Although this method can use fairly common donor and acceptor materials, this methodology requires somewhat complex manufacturing procedures. Where with organic photovoltaics the promise was a device that could be easily mass produced but with the multilayered device this promise is not kept and thusly not viable for the overall goal. The third method is through the incorporation of a complementary absorber. Like the various donor materials in the multilayered architecture, these complementary absorbers are meant to absorb in areas of the solar spectrum where the primary donor does not. Unlike the multilayer device, the complementary absorber is included into the single active layer of a more traditional device. Unlike the first method, the complementary absorber usually takes the form of a common or cheaply produced material, like a dye or a quantum dot.

For the purpose of this paper, the complementary absorber will take the form of quantum dots. In brief, these small particles of semiconducting material have attracted a lot of attention in the past 10 years or so. What makes them interesting is that they have a tunable band gap, based off the size of the particle. The material loses its bulk behavior below a value known as the Bohr exciton radius. Under this number, the exciton with in the quantum dot becomes squeezed by an effect known as quantum confinement. This is what leads to the trend that as the size of the particle shrinks the absorption maxima undergoes a distinct blue shift. For the purposes of solar cell, the quantum dot can play several rolls. This is because the material possesses an electron affinity higher than those of a conjugated polymer and in general a higher intrinsic carrier mobility. Another advantage of quantum dots is that they have a high surface area which will provide a good nanoscale mixing with the polymeric domain. This material does process several disadvantages as well. The first being that neat nanoparticles undergo Ostwald ripening,

an amalgamation of smaller particles to form larger particles. Where this is driven by the instability of the outer core atoms on these particles. To stop this from occurring, these nanoparticles are capped by a ligand. These ligands usually take the form of long chained carboxylic acid or phosphine oxide, trioctylphosphine oxide (TOPO) being amongst the most common. Although this fixes the problems with Ostwald ripening, this introduces another problem. These long alkyl chain-based ligands act as insulators, insolating the charge transport between the quantum dot and its neighbors. To solve this problem, shorter chain ligands are used, strongly binding thiol groups with a carbon or two spacers attached to it.

3.2 Synthesis of quantum dots

One of the reasons that quantum dots have attracted so much attention in the past 10 years or so is the ease that they can be produced. The synthetic method has not changed much since it first discovery by Ekimov and Brus in 1986. This methodology begins with the heating of one of the precursor materials to a given temperature under an inert atmosphere, generally this precursor is dissolved in liquefied ligand. The second precursor is then injected into the solution and the reaction is allowed to run for a given time. When the given time is reached the reaction is rapidly cooled down, thus ending the growth of the nanocrystals. Purification occurs through the centrifugation of the material in a good/bad solvent mixture. So, in the sense of this project, two quantum dots were used: Cadmium Selenide (CdSe) and Lead Sulfide (PbS). Where the CdSe quantum dots were to act as the test system and the PbS quantum dots were to act as the IR sensitizing

complementary absorber. Both quantum dots followed the scheme above, only differing by the precursors and ligands used. CdSe quantum dots use cadmium oxide dissolved in trioctylphosphine oxide as precursor one and metallic selenium carried in octadecene serves as precursor two. PbS quantum dots use lead oxide dissolved in oleic acid with the sulfur source being elemental sulfur. Formation of quantum dots were confirmed through

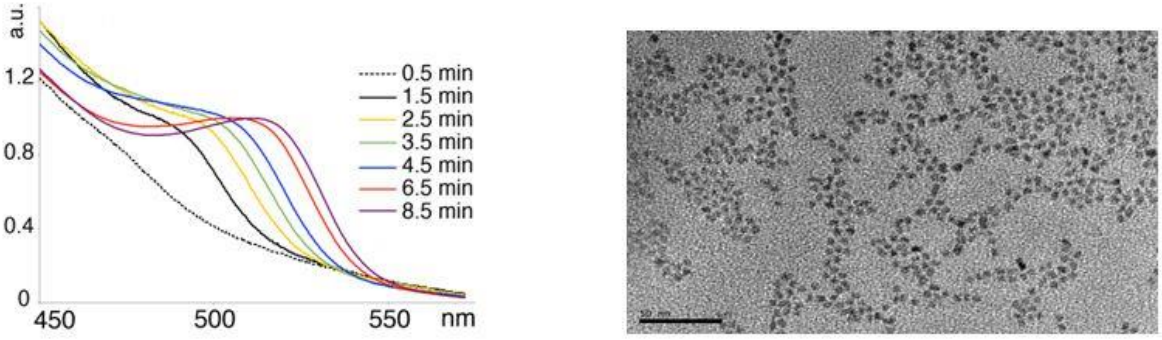

Figure 3.1 (right) Kinetics of CdSe quantum dot formation using UV-VIS spectra after the injection of the Se precursor. (left) TEM images of CdSe quantum dots after 8.5 min of reaction. Scale bar 50 nm. Courtesy: Lingyao Meng

a UV-VIS kinetic plot and TEM imagining (Fig 3.1). Purification for both species used the centrifugation method, where the quantum dot solution was first precipitated into methanol. This solution was then centrifuged at 20,000 RPM for 10 min, then the now clear methanol was decanted off. The quantum dots were then redissolved into a hexanes: methanol mixture, just enough to fully dissolve the quantum dots but not enough so they couldn't be centrifuged down. The clear solvent was then decanted off and this process was repeated three times. This solution was then dried under high vacuum overnight and stored in an inert atmosphere.

3.3 Ligand: selection, synthesis and exchange

Since the native ligand set was not indicative for the charge transport, a new ligand set needed to be found. Traditionally, the ligand that would be used would be pyridine, as ligand exchange could be achieved with ease. However, pyridine was not chosen for this project. This was because pyridine is an extremely weak coordinating ligand to the surface of the quantum dots, where this ligand forms a dative or coordination type ligand to metal interaction. This interaction is so weak that quantum dots with pyridine ligands have been used to model ligandless quantum dots in studies that have probed the effects of ligands on the electronics of the quantum dot. Pyridine ligand sets have also been known to come off the surface when either under high vacuum or an elevated temperature. So, it was also feared that this ligand would come off either during storage of the bulk material or during the creation of the device. Since the partial loss of the ligand shell would be detrimental to stability of the quantum dot as well possibly the device itself, a stronger ligand was needed. The class of molecules that were chosen were the sulfur containing thiols and dithiocarbamates, the only difference between the two being the dithiocarbamates bidentate nature makes them a stronger binder than the thiol.

Two ligands were chosen for initial study: ammonium phenyl dithiocarbamate and triethylammonium 2-pyridine dithiocarbamate. Their selection was mostly driven by the available starting material within the lab, although it was hoped that 4- pyridine dithiocarbamate would be the final version used in devices. These two would serve mostly as proof of concept ligands as they possessed the needed moieties for the complementary bonding with the block copolymer, where both of the ligands would allow for pi-pi type

interactions between the two species. The pyridine-based ligand would also allow for hydrogen bond with hydroxyl group of **P3**. Their synthesis is summarized in scheme 3.1. The phenyl dithiocarbamate is created from a based mediated reaction aniline and carbon disulfide. The initial tries at making this molecule proved more difficult as the published method used sodium hydroxide dissolved in water. Although a reaction did occur, as the

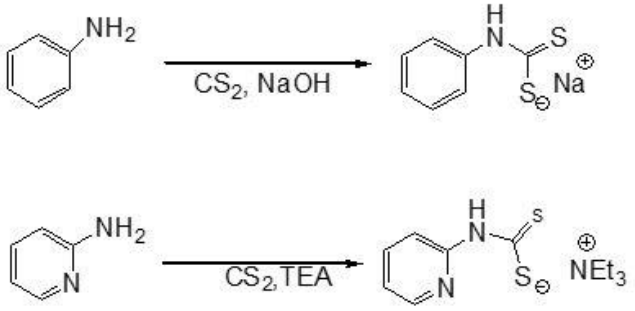

Scheme 3.1 Synthesis scheme of the two ligands (top) Ammonium phenylthiocarbamide (bottom) Triethylammonium 2-pyridine dithiocarbamate

mixture turned a bright hunter orange color, the required precipitation was not present. Although several modifications were made to the reactions scheme, the sodium-based reaction never resulted in the product. The reaction using lab grade ammonium hydroxide in water gave the required precipitation, which was purified through the filtration and further washes with water. The pyridine-based ligand was a little more difficult to make. The method used with the phenyl ligand did not work, under either bases, solvent mixtures or temperature. The needed modification was to change both the base and the solvent to an amine, triethyl amine to be more specific. As the carbon disulfide was added dropwise to the solution of triethyl amine with the 2-aminopyridine. Over the course of the reaction the solution turned a crystalline solid, requiring the switch of mixing from a stir bar to mechanical stirring. The ^{1}H NMR showed that some unreacted 2-aminopyridine in the

resulting yellow solid, this was removed through soxhlation with THF. A third ligand was also chosen to serve as a replacement. This ligand being 4-mercaptophenol. In case that that the first two ligands did not complex with the block copolymer, this ligand would introduce a stronger single point hydrogen bonding interaction between the ligand's para-positioned hydroxyl group and block copolymer's pendent pyridine group. It should be noted that a fourth ligand was bought to complex with the poly electrolyte, sodium mercaptoethanesulfonate (MES). A small amount of both the CdSe and PbS quantum dot had their ligands exchanged but since the corresponding polymer was insoluble this portion of the project was pretty much abandoned.

The ligand exchange took two forms and was dependent on how many solvents were used. The single layer or solvent method involved the quantum dot suspended and the ligand dissolved into a solvent. Over a given amount of time, the ligand shell will slowly exchange. As this exchange occurs, the quantum dot will gain solubility in the given

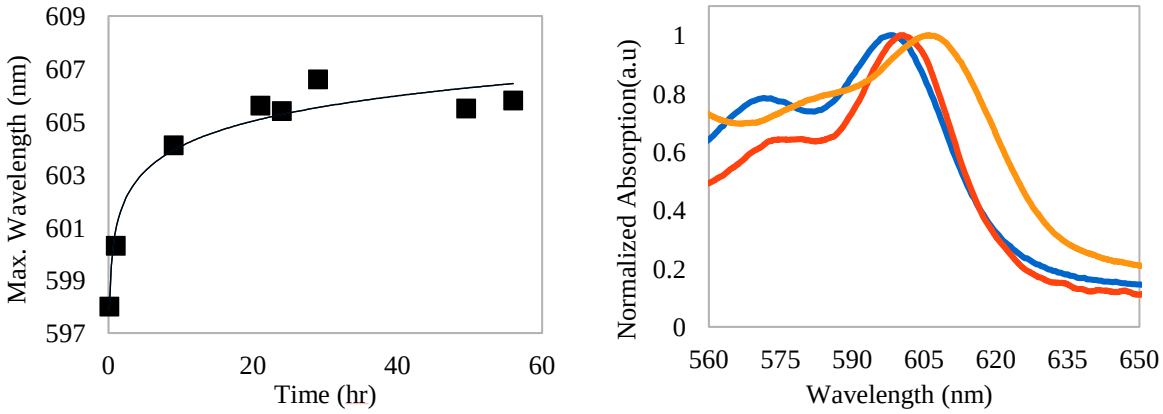

Figure 3.2 (right) Kinetics of ligands exchange as shown the exponential shifting of the peak initially at 598 nm (left) UV-VIS traces of CdSe quantum dots as a function of time after the addition of phenylthiocarbamide salt (where blue is t=0, red is 1 hr and orange is 56 hours.

solvent. The suspension of quantum dot will eventually break up during this process, until the ligand shell is mostly exchanged. The ligand shell will never completely exchange as the equilibrium forces that drive this process prevents it. The double layer or two solvent method involves the use of a good solvent for the quantum dot, hexanes, and a good solvent

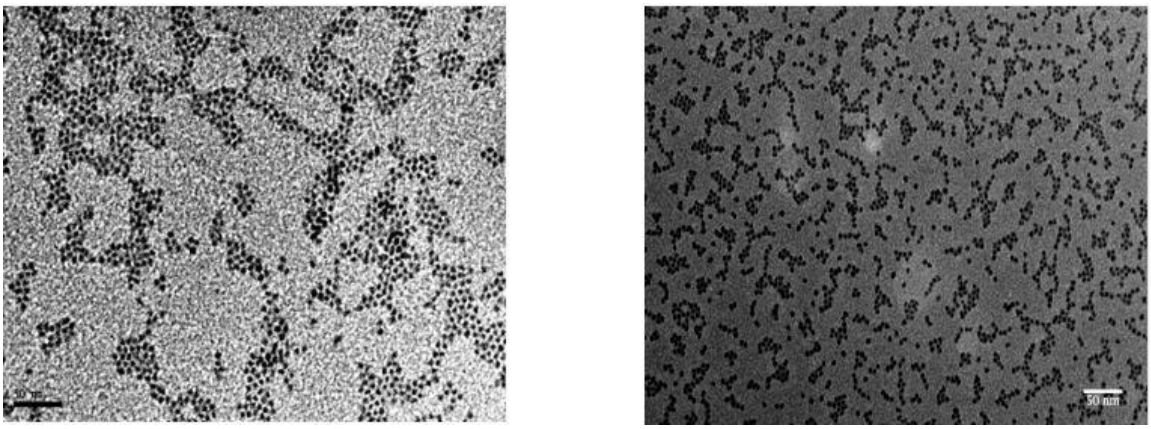

Figure 3.3 TEM images of quantum dots before (left) and after exchange (right). Scale bars are 50 nm.

for the ligand, dichloromethane in the case of the dithiocarbamate and methanol for the MES. The polarity of the solvents prevents them from mixing, forming a bi-layer. As the ligand exchange continues, the quantum dots will migrate to the ligand's good solvent. The process is completed when all the quantum dots migrate to the other solvent. The purification method is the same for the both methods, a continuous cycle of centrifugation with a mixed solvent of good and bad solvents. The phenyl dithiocarbamate ligand exchange initially followed the one solvent method as first published by the Wiess group.[169] The absorption spectra were monitored throughout this procedure. As the ligand shell is replaced, it was reported that the absorption maximum will undergo a red shift with a slight broadening. Where the red shift will be a result of the extension of the conjugation into the aromatic ligand. This red shift will take the form of an exponential function, where there is a rapid exchange of ligands at the beginning of the reaction then the rate slows as

the reaction reaches equilibrium. As we can see in figure 3.2, the exchange does take the form of an exponential. TEM images, figure 3.3, show that the size of the quantum dot does not change significantly as the initial size was 3.368 nm ± 0.2894 nm and the size after exchange was 3.0338 nm ± 0.14770 nm. This can discount Oswald ripening as the cause of the observed red shift, as the size of the particle actually decreased which would have produced a blue shift. Besides from the first ligand exchange process, all other ligand exchanges followed the two-solvent method. Figure 3.4 shows a two solvent exchange method, where in this case the cation of the bromocresol salt was changed from sodium to tetrabutylammonium. It can be clearly seen that the dye molecules have migrated from their usually good solvent DMOS (top layer) to the chloroform bottom layer.

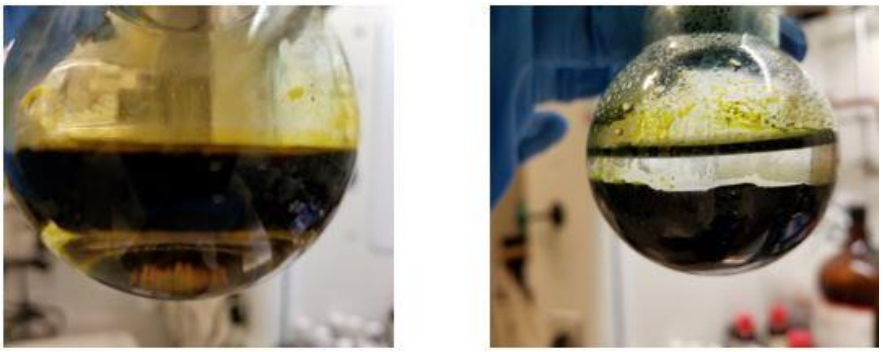

Figure 3.4 Example of the two solvent exchange method using sodium bromocresol dye where the sodium is being exchanged with TBA. Left is before exchange where the dye is in the DMSO layer and right is after exchange where the dye migrated to the chloroform layer

3.3.1 Infrared investigation of ligand shell replacement

For the MES capped PbS quantum dot, the ligand shell replacement was confirmed through the use of infrared spectroscopy. The corresponding spectra are in Figure 3.6. For

the spectra of the TOPO capped quantum dots, the most dominating feature is the doublet peak around 3000 cm^{-1} corresponding to the $–CH_2$- stretching modes. There is another

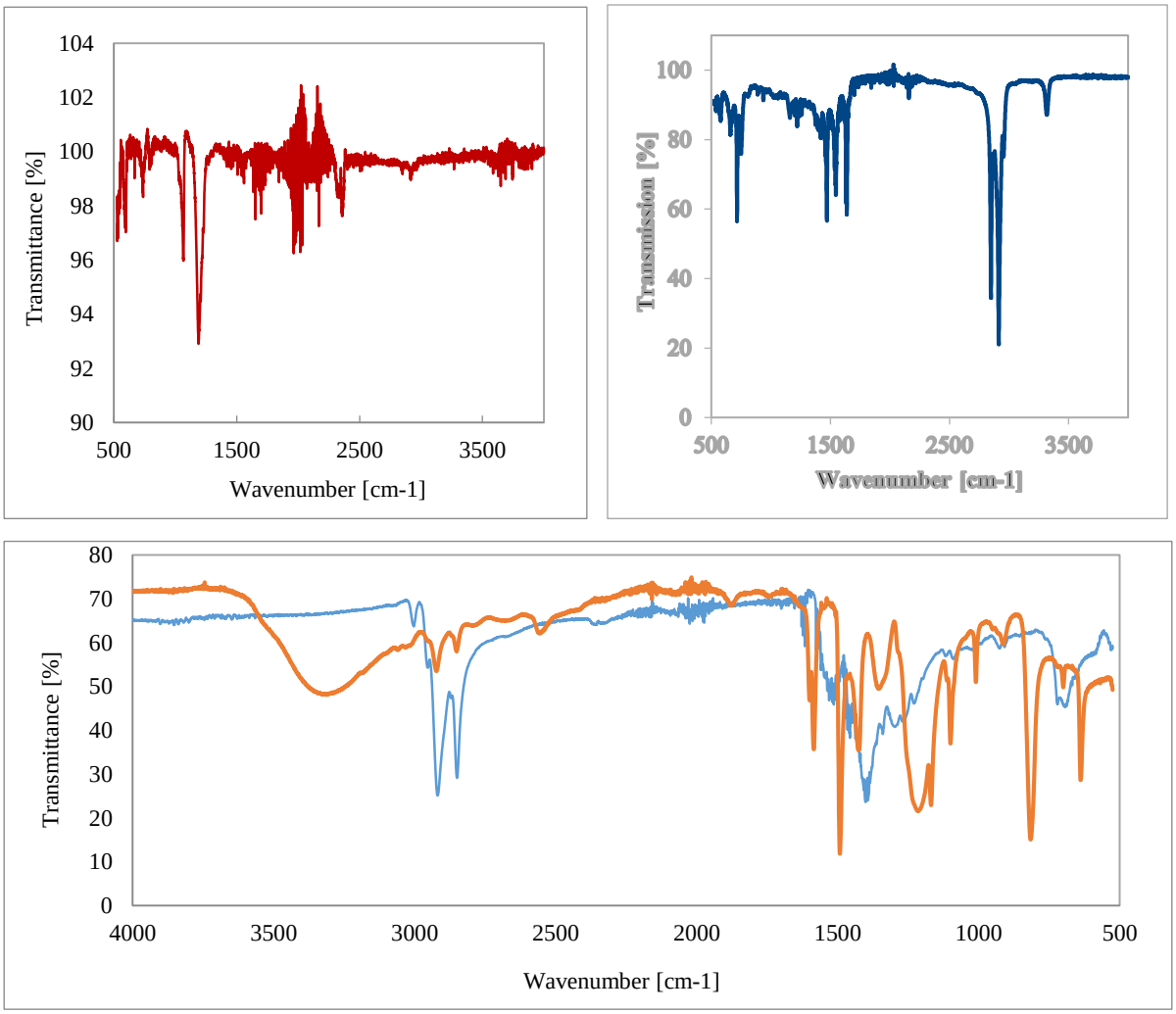

Figure 3.5 (top right) ATR IR spectrum of TOPO capped CdSe QD (top left) ATR IR spectrum of MES capped CdSe QD. Spectrums split for clarity. (bottom) ATR IR spectrum of before (blue) and after (orange) exchange of TOPO capped CdSe Qd with 4-mercaptophenol.

cluster of peaks around 1500 cm^{-1} which corresponds to C-H bending mode from the alkane portion of the ligand. When the purified MES capped ligands are subjected to the same investigation, we can see that most of the signal from the TOPO disappear. Being replaced by profound feature around 1100 cm^{-1} which corresponds to the $–SO_3$ stretching mode from

the sulfate group. It should also be noted that the reason behind the residual TOPO signal is from the fact that no ligand exchange process is 100% accomplishable.

The 4-mercaptophenol ligand exchange was also confirmed through the use of IR spectroscopy, seen in Figure 3.5. When the post exchange IR is examined we notice that like before we a have a small residue of TOPO signals still present as no ligand exchange is 100% effective. It can be seen that several peaks do appear and that those peaks can be contributed to new ligand. The most noticeable peak is the broad peak around 3500 cm^{-1} which is indicative of the O-H stretching mode from alcohol group. There is a smaller group of peaks that are imbedded in this broad peak, around 3000 cm^{-1} and they might be contributed to aromatic proton stretches. The peaks at 1580 $cm^{-1,}$ 1490 cm^{-1} and 1430 cm^{-1} can be contributed to the aromatic carbon stretches. The 1100 cm^{-1} might belong to the C-O stretching mode with the 909 cm^{-1} and 815 cm^{-1} peaks belonging to the bending mode of the C-H on a para-substituted aromatic ring.

3.4 Incorporation of quantum dots into polymeric blends

The blending of quantum dots into the polymeric blends is relatively straight forward as the new ligand shell gives the quantum dot solubility in both chloroform/chlorobenzene and acetone. For testing purposes, the non-exchanged quantum dots need to be blended into the nanofiber solution. However, the native TOPO ligand lacks solubility in either the chloroform/chlorobenzene or acetone. This required the modification of the solvent mixture with an alkane solvent. The most common solvent used

in this case would be hexanes, but its low boiling point would make it impractical for the use in the blend. The solvent that was selected was dodecane, as it possesses a high boiling point and more importantly it was available on hand. The next concern was whether the addition of dodecane would upset the formation of the nanofibers. As we can see in figure

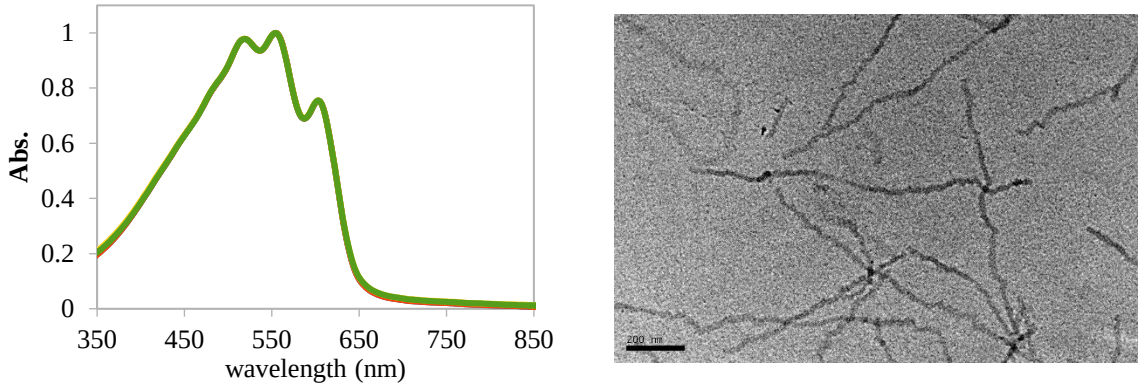

Figure 3.6 (left) UV-VIS spectra of nanofibers (4:1 CB:ace) after the addition of dodecane at t=0 (blue) t=10 min (orange) and t=25 min (green). (right) TEM images of nanofiber in ternary solvent mixture t=25 min. Scale bar is 100 nm.

3.6, the absorption spectra of the nanofibers did not significantly change due to the addition of dodecane into the solvent blend. Also seen in figure 3.6, the TEM images created from this mixture shows that the nanofiber does form, and they are approximately the same size as the chlorobenzene: acetone nanofibers. The order of addition does not matter, as one can add it during or after the addition of acetone. The weight ratio of quantum dot was chosen to be 1 in comparison to the weight of polymer, although this would be considered a high loading of quantum dots compared to other published studies. The TOPO liganded quantum dots where first dissolved into heated dodecane before addition to the nanofiber solvent mixture. The time of three hours after the addition of acetone was chosen for the adding of the quantum dots, the nanofiber solution would be allowed to further set up for the 9 hours required. The absorption spectrum is relatively unchanged compared to neat nanofibers, this can be explained through the broad nature of the absorption profile of the

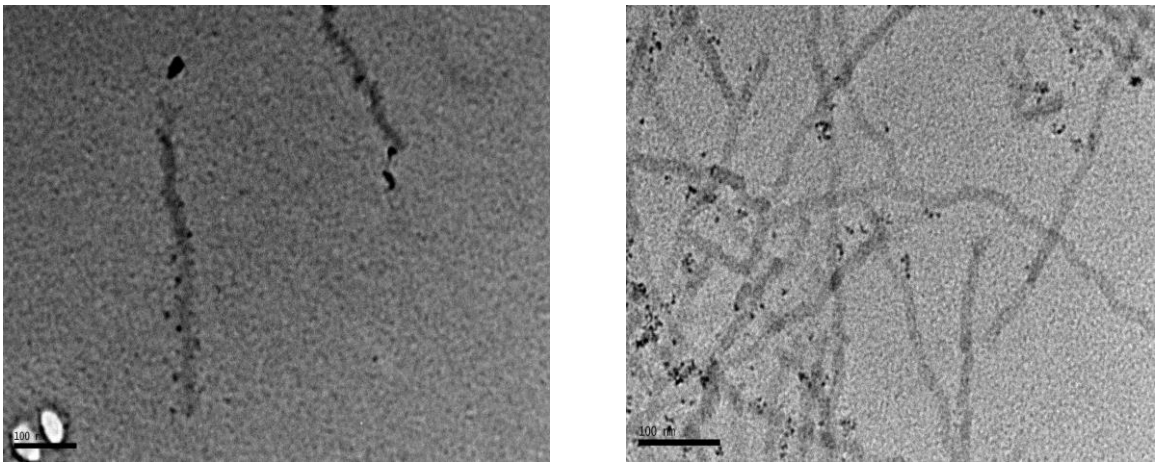

Figure 3.7 (left) TOPO capped QD coordinated to P3HT nanofiber (1:1 polymer: QD wt :wt) in ternary solvent mixture. Scale bar 50 nm. (right) TOPO capped QD coordinated to **P4** nanofiber (1:1 polymer: QD wt:wt) in ternary solvent mixture. Scale bar 100 nm.

quantum dot as well as the fact that all spectra are normalized. It should be noted that there is some scatter effect evident in the baseline, a non-zero value indicative of incoming light being scattered off the inorganic particle. The TEM images shown in figure 3.7 show the results of adding quantum dots to both the unmodified P3HT and the block copolymer **P4**. It can be clearly seen that in both cases that the quantum dots line up with the nanofibers, which was somewhat surprising in the case of normal P3HT as well as **P4**. In both cases there should be no interaction between the species, although one could expect in the case of **P4** the pyridine pendent group could displace a TOPO molecule. This case would be highly unlikely as the equilibrium would favor the bound TOPO state. The interaction between these two species can be explained through the shared hydrophobic nature, where the core of the nanofiber and the ligand shell are highly hydrophobic. When the ligand shell is changed to the phenyl dithiocarbamate (PTC), the dodecane co-solvent is not needed and removed from the mixture. The quantum dots are dissolved in heated chlorobenzene along with the polymer, this is done to ensure the full dispersion of the quantum dot aggregates.

It should be noted that the quantum dots do not fully show up in the absorption spectra as in the case of the PTC capped quantum dots. Again, the base line of the tail shows some of the expected scattering effect. The TEM images of 3.8 shows that there is no interaction of between the P3HT and the quantum dots as the quantum dots are seemingly randomly placed throughout the picture. However, with the case of **P4**, there are clear interactions between particle and polymer nanofiber. There are several nanofibers that are clearly decorated with quantum dots. In the case of P3HT and the PTC capped quantum dots, the explanation is simple-there is no or too little of a hydrophobic interaction between dot and

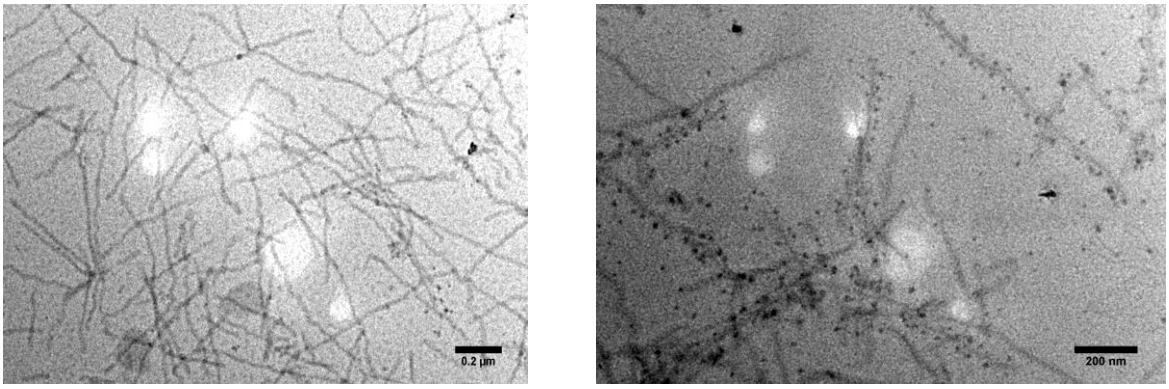

Figure 3.8 (left) P3HT nanofibers with PTC capped CdSe QD (1:1 polymer: QD wt: wt) scale bar: 0.2 µm (right) **P4** nanofibers with PTC capped CdSe QD (1:1 polymer: QD wt: wt) scale bar: 200 nm

polymer to bring them together in any meaningful way. For the case of the PTC, the picture may be a little more complex of what the nature of the interaction is. It is believed that it can either be through a pi-pi interaction between the phenyl and pyridine aromatic systems or a hydrogen bonding interaction between the lone pairs on the pyridine and the somewhat acidic hydrogen attached to the nitrogen originating from the amine group. Whatever the true cause of this interaction, the interaction is still there, and it coordinates to only the **P4** system.

TEM of **P4**:4-mercaptophenol capped quantum dots also shows some type of interaction between the quantum dot and the polymeric nanofiber. The loading of quantum dots decorating the nanofiber seems to be less than the loading of some polymeric system with the PTC ligand. Where the loading of the polymeric functional group is about 7.50%

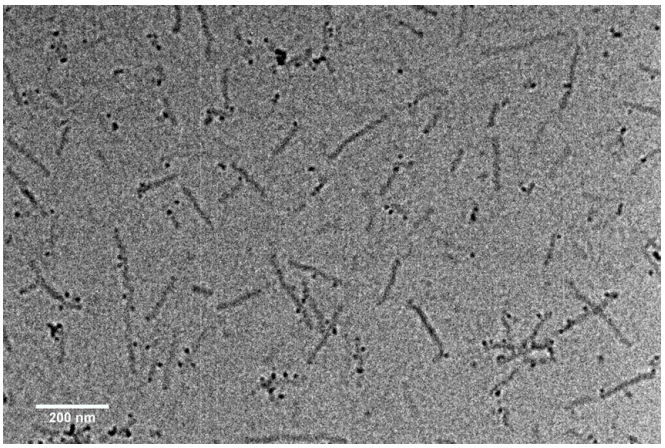

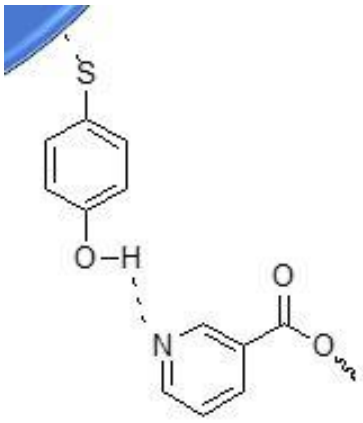

Figure 3.9 (left) **P4** nanofibers with 4-mercaptophenol capped CdSe quantum dots (1:1 polymer: QD wt: wt) (right) illustration showing the possible coordination between 4-mercaptophenol ligand and **P4.**

and the loading of the quantum dot in the solution was equal weight to that of the polymer. The difference between the PTC ligand and the 4-mercaptophenol ligand could also shine light on why there are so many uncoordinated quantum dots in the latter's case. Where in theory the PTC ligand could possible coordinate with the pi system of the nanofiber, located along the edge nanofiber. Where in the case of 4-mercaptophenol the only place were it could attach is the pendant pyridine group, the polar hydroxyl group would repel the non-polar nanofiber and serve as a barrier between the pi system on the ligand and the pi system on the nanofiber.

3.5 Quenching

To prove that there is a form of electronic communication between the quantum dot and the polymer, a fluorescence quenching experiment was carried out. In brief, a dilute

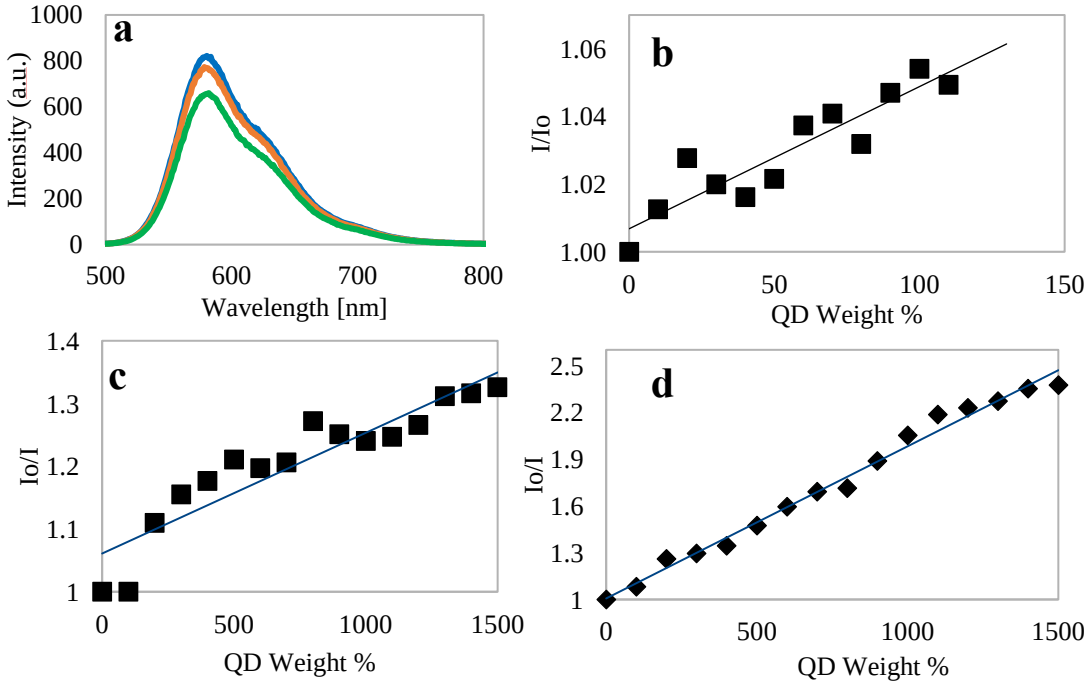

Figure 3.10 (a) Fluorescence trace of **P4** nanofiber solutions at different quantum dot wt %: 0% (blue) 100% (orange) and 1500% (green). Stern-Volmer plot of (b) P3HT nf vs TOPO CdSe QD (c) P3HT nf vs PTC CdSe QD (d) **P4** nf vs PTC CdSe

solution of nanofiber (in the same solvent mixture) was titrated with a concentrated solution of quantum dots. The dilute solution, concentration of 10^{-5} M, was used to eliminate any self-quenching.

Figure 3.10 (a) shows the fluorescence plots of **P4** and P3HT as a function of weight percentage of quantum dots with TOPO ligands. Figure 3.11 (b-d) shows the Stern-Volmer plots and shows that there is very weak quenching of the P3HT and **P4** by the quantum dot.

This is unsurprising because of the nature of TOPO ligand, where it electronically isolates the quantum dot from the rest of the system. When the same experiment is carried out with the PTC capped quantum dots, something different is observed. Figure 3.11 (c &d) shows the fluorescence plots of both polymeric systems when certain weights of quantum dots are added. More importantly the Stern-Volmer plot shows a 20-fold increase in quenching from the P3HT case to the **P4** system. This indicates that there is more communication between the **P4** system than the P3HT system. This can be explained by the non-covalent interaction binding the quantum dot more closely to the **P4** system allowing for better charge-transport between the two species. Although it should be noted that the quenching constants, slope of the line generated, are very small compared to electron donor materials such as PCBM.

3.6 Performance of solar devices with ternary blends

The active layer of these devices is constituted from equal weights of polymer, PCBM and quantum dots. Devices that use TOPO capped quantum dots performance are summarized in table 3.1. For devices that constitute P3HT nanofiber and TOPO capped quantum dots shows a marked increase in PCE, Jsc and Voc over those devices cast without the quantum dots, with PCEs approaching the non-nanofiber case. The enhancement to Jsc might be a result of the added charges given off by the quantum dots, although unlikely due to of the insulating nature of ligand shell. Manufacturing differences could account for the differences but again is unlikely because great care was taken to reproduce the method

Table 3.1 Summary of the performance of the solar devices consisting polymer: QD: PCBM 1:1:1 wt: wt: wt. N.f. denotes devices that use nanofibers. TOPO QD used a ternary solvent system of 4:1:0.5 CB: ace: dodecane.

Composition	PCE [%]	Jsc [mA]	Voc [mV]	FF	Series Resistance	Shunt Resistance
$P3HT_{n.f.}$:QD(TOPO):PCBM	4.85 (±0.92)	11.61 (±2.016)	0.600 (±0.012)	0.695 (±0.006)	1.420 (±0.240)	1369.24 (±403.82)
P4$_{nf}$: QD (TOPO):PCBM	1.25 (±0.22)	4.152 (±0.080)	0.630 (±0.016)	0.479 (±0.017)	5.928 (±3.340)	658.410 (±156.80)
$P3HT_{nf}$:QD(PTC):PCBM	0.53 (±0.21)	5.64 (±1.543)	0.640 (±0.024)	0.270 (±0.025)	1.420 (±1.261)	1369.21 (±136.88)
P4:QD(PTC):PCBM	0.78 (±0.08)	4.23 (±0.614)	0.490 (±0.010)	0.38 (±0.012)	5.830 (±1.550)	286.590 (±120.18)
P4$_{nf}$:QD(PTC):PCBM	0.42 (±0.06)	3.26 (±1.148)	0.340 (±0.949)	0.41 (±0.011)	27.17 (±4.500)	204.03 (±77.487)

almost exactly. The more likely cause of this increase is due to the scattering effect of the added quantum dot, which is known to occur with the casting solution based off the UV-VIS spectra, Figure 3.11. The scattering effect has been well known to help increase the performance of the organic solar cell, by in a sense giving photons a second chance to be absorbed. Since the active layer is thin to accommodate effective charge transport, not all photons will be absorbed in the active layer-even in regions where the polymer or acceptor absorb. Photons that are not absorbed will encounter these hard-inorganic particles and be scattered back into the active layer, allowing for their absorption by the donor material. Although the rise in Voc is more complex, as there are many factors that contribute to the Voc, a possible reason is that the quantum dots coating the nanofibers act as an insulator. Think of it as putting an insulator between the two metal plates of a capacitor, increasing

the amount of voltage needed to overcome this increase in dielectric constant. It should be noted that in some publications, the increase in these parameters are the results of better

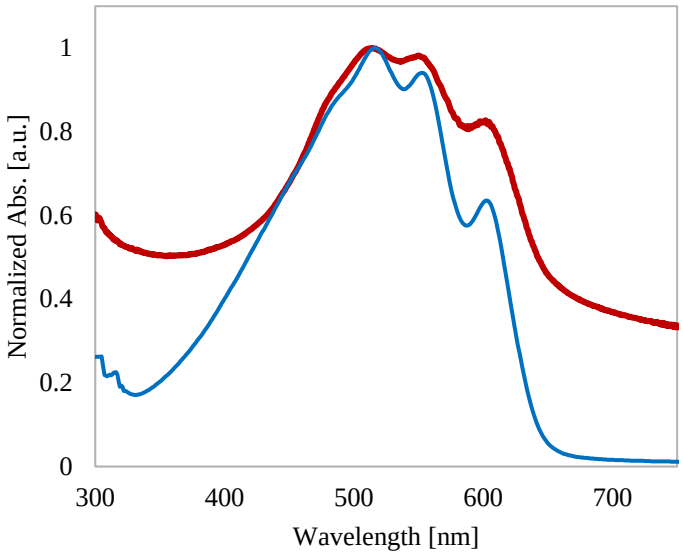

Figure 3.11 UV-VIS spectra of **P4** nanofibers without (blue) and with (red) TOPO capped CdSe QD

charge separation and transport through the active layer. However, this can be ruled out in this case because of the insulating nature of the TOPO ligand.

In the case of systems that employ **P4** as the donor material and staying with the TOPO capped quantum dots, the values of the ternary blend are not as promising. There is a marked decrease in the performance of these devices as both PCE and Jsc values decrease. As it has been previous stated, the Jsc value is partially dependent on the morphology of the active layer. Such a decrease in the value can only mean that the morphology of the **P4** thin film is further disrupted by the inclusion of the quantum dot or the solvent used to add the quantum dots. It is possible that the inclusion of either the non-polar solvent or quantum dot (through the ligand shell) further upsets the crystalline domain of the polar cable. Which can be evident in the shorter nature of the nanofiber, although the width of the

nanofiber is unchanged where the length is orders smaller than those made in chlorobenzene: acetone mixture. This shorter length can retard the charge transport capability of the donor phase thusly causing the degradation in Jsc that can be seen.

For the cases of the quantum dots using the PTC ligand, the quality of the device is extremely poor. These values are summarized in table 3.1. Where all of the parameters of the solar cell are significantly lower than their parent devices. A typical JV curve for these devices can be seen in figure 3.12. There is a large "s-kink" present in the curve, outside of the range where the data saves. This "s-kink "is evidence that there is one charge species

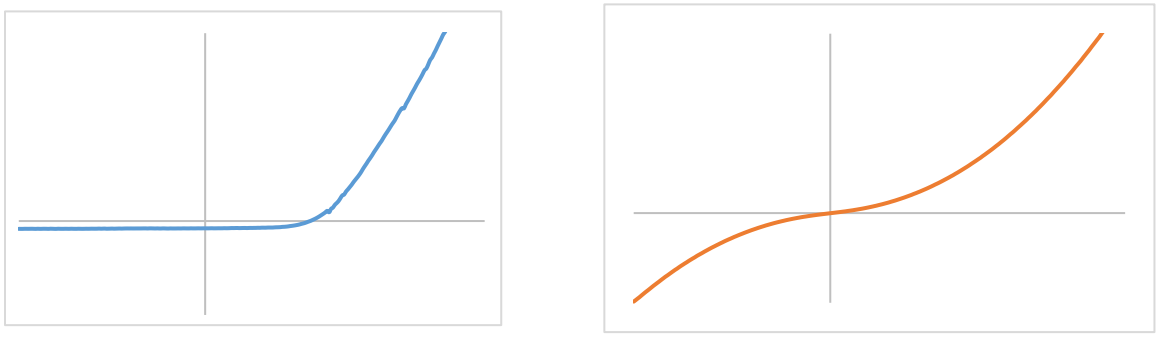

Figure 3.12 J-V curves of non-PTC QD containing devices (blue) and devices that included PTC capped QD (orange). Numbers removed for clarity.

in excess. If the paper published by the Weiss group[169,172] is referenced, then it can be seen that the ligand/quantum dot introduces a trap state into the active layer. Figure 3 13 (a) shows the planned cascade scheme for charge separation and transport and Figure 3.13 (b) shows the proposed cascade scheme. This trap site is generated from the high HOMO of the bound ligand. The before mentioned red-shift seen in the absorption spectra represents the migration of the excitonic hole from the quantum dot core into the ligand shell. With the hole trapped in the ligand shell, when the cascade process occurs the excitonic electron from the donor falls into that trap. With the electron captured by the trap site, the hole that

is still on the donor is free to migrate to its corresponding electrode. This could be a possibility of why the "s-kink" appears. Another sign that points at the trap site is the

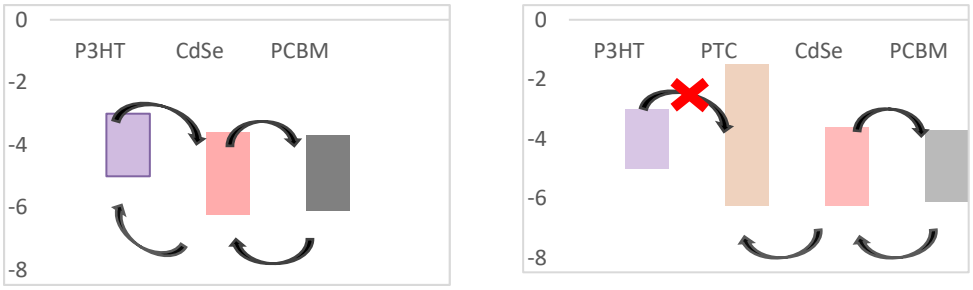

Figure 3.13 Illustration of (right) the planned cascade mechanism of the ternary system (left) the cascade mechanism with the PTC charge trap included.

drastically lower Voc for these devices. Where this is a large problem for the project is that it has been reported that most quantum dot/ligand systems exhibit this trap state nature. Although there have been several strategies proposed to alleviate this problem, these will be discussed in the future work section.

3.7 Conclusion

Overall, the inclusion of quantum dots into the active layer can be considered a benefit and/or detrimental to the performance of the solar cell. As one can see in the case of P3HT and the TOPO capped quantum dot, the scattering effect can be a boon to the PCE of the given device. There have been numerous recent papers that have reported that by adding inorganic nanoparticles to the active layer have increased the PCE of their devices. However, the inclusion of these nanoparticles into the active layer can cause detrimental effects to the device performance. If the conclusion in the **P4** and TOPO capped quantum

dot is to be believed, these particles can further disrupt the morphology. Of course, this is a case by case situation as the ligand shell will affect different systems differently. Another thought is that these nanoparticles take valuable space within the active layer. As we only have a small space that the active layer can exist within, any space that the nanoparticle occupies is lost to the other components. In this case, the benefit of these nanoparticles would only be seen if the benefits of the scattering overcome the loss of absorption and charge transport channels. As a few years ago, the inclusion of nanoparticles for scattering purpose have been seen as a viable method to increase the performance of polymer based organic photovoltaics. There was a push before this to incorporate nanoparticles into the active layer to directly participate in the generation of excitonic species. However, it appears that the insurmountable challenge of the charge trapping nature of the particle/ligand shell seems to have stopped all research efforts into these hybrid devices. The working mechanism of the charge trap is still under debate but does not change the fact that as soon as the ligand is changed from the long chain carboxylic acid this trapping nature arises. The prevailing theory revolves around surface defects on the quantum dot and that these trap sites are isolated by the isolating nature of carboxylic acid ligand. So, by trying to increase the communication of the system, the cascade mechanism, the device performance is killed off. If the Wiess paper's computational measurement are to be believed, the hole trap that is generated by the interaction of the PTC ligand and defect on the surface of the quantum dot kills off the performance of the device. As seen in table 3.2, it can be clearly seen that this drop off in performance can be attributed to the quantum dot's inclusion. There has been work done to try and eliminate these trap sites, modification to the ligand to introduce electron donating or withdrawing groups. Again, from the Wiess

group, the para-positioned electron withdrawing modified PTC ligand shows computationally to lower the HOMO level of the quantum dot/ligand complex.[173] But at this time, it is not known that these techniques still are not enough to overcome the inherent nature of the quantum dots.

3.8 Future Work

For the case of PbS, the findings of the CdSe quantum dots pretty much canceled anymore work with the dithiocarbamates.[170] As it is believed that any benefits that are gained through the increase in absorption would be diminished by the present of the trap sites. PbS quantum dots were exchanged to MES ligands, in hopes that the cationic polyelectrolyte would be available for testing purposes. However, solid methylated polyelectrolyte is not soluble in any common laboratory solvents, their mixtures nor the previous under elevated temperature or sonication. There is a window when the polymer may be worked with, about 2 hours after the addition of the methylation agent. The polymer

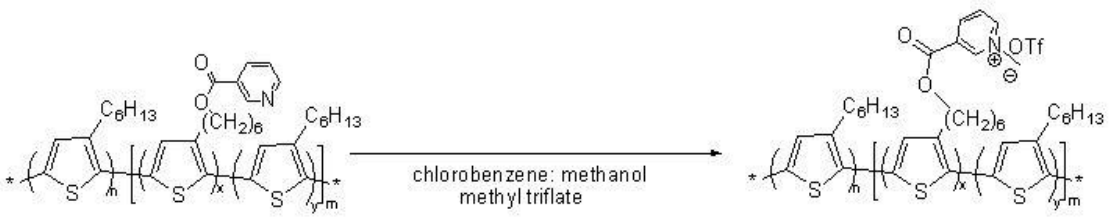

Scheme 3.2 Synthesis scheme showing the methylation reaction that produces the cationic polyelectrolyte.

can only be used when in its original reaction solvent and kept at an elevated temperature. After 2 hours, the polymer begins to self-aggregate and suffers from the same problem

from the solid polymer. This pretty much makes quantifying the methylation process impossible to determine, where the NMR is difficult to obtain. As even during the two-hour window the polymer is still aggregated to such a degree that the peaks are hard to resolve. It seems that even in the early stages of the methylation, the side chain probably folds into itself or creates a localized micelle with other cationic side chains. IR does not

Figure 3.14 (left) possible cationic polyelectrolyte in methanol (purple) and DMSO (blue). 100:1 dilution from heated chlorobenzene into pure solvent. (right) same methanol solution next to a "solution" of P3HT in methanol. 100:1 dilution from heated chlorobenzene into pure solvent.

give high enough resolution to see any useful information as the concentration of functionalized side groups on the polymer are small. Figure 3.14 shows that the cationic polyelectrolyte mixture can be diluted into polar solvents such as methanol and DMSO. It should be noted that normal P3HT and **P4** systems cannot be diluted in any concentration into such polar solvents, but this is secondary evidence that the polymer changed to the polyelectrolyte. Although still lacking primary evidence, it was decided to add MES capped PbS quantum dots to a batch of polymer that was undergoing methylation. When the TEM pictures of this system are investigated, it can be seen that the nanoblobs that the polymers form is outlined by quantum dots. As we have noted previously, the ligand shell of the PbS has been mostly replaced by the MES ligand. This allows for the hydrophobic-hydrophobic interaction between the polymer and TOPO ligand to be discounted as the

factor that is bringing the quantum dot and polymer together. Again, this is secondary evidence to the formation of a cationic species on the side chain and the NMR is needed.

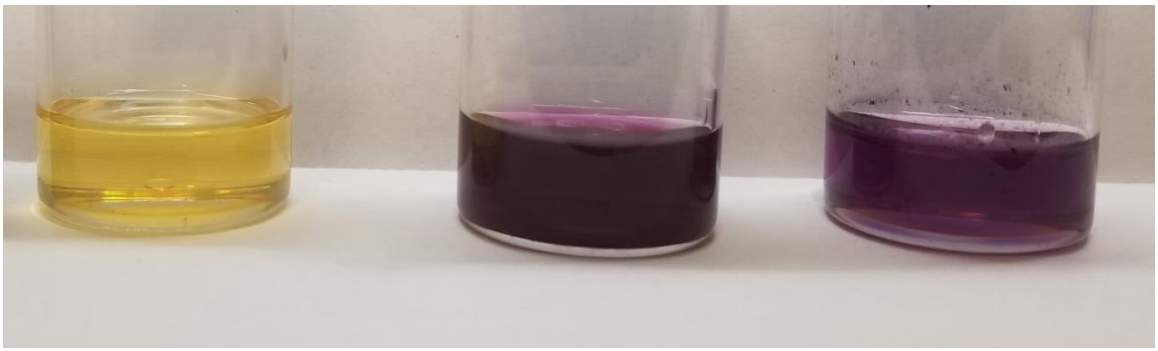

Figure 3.15 Dilutions of **P8** into CB (left), methanol (middle) and DMSO (right). 200:1 dilutions of heated CB into pure solvent.

Work was started on other cationic polymers, but these polymers were surprisingly difficult to obtain. The hydroxyl group on **P3** was nearly impossible to convert to a bromo group, even though the reaction is well documented. The reaction that was tried was even shown to work on the very polymeric system employed in this study. The reason for this failure is not known, as there could be any number of factors that could have resulted in the negative result. The reaction scheme was changed to side chain hydroxyl group directly to the required amine. The intermediate tosylate polymer was obtained and purified through soxhelt but the subsequential reaction to form the azide functionalized polymer did not succeed. This reaction was undertaken under numerous conditions. For this portion of the project to continue, the cationic co-block is needed. It may require the creation of **M3**, as the terminal bromide group is already built in and terminal bromine group reaction should

make it safe for the GRIM process. But it is not known if the resulting cationic ammonium polymer or its analogs would have long term solubility.

A side project was started with the reaction of **P3** with 1, 3 sultone to create **P8**. The reaction of this is summarized in scheme 3.4. As seen in figure 3.16, this polymer shows good solubility in THF and chloroform with dilutions into methanol and DMSO possible. NMR spectra (Figure 3.17) was able to be achieved with this polymer, as the tetrabuytlammoinum cation seems to allow for a good solubility in chloroform. The

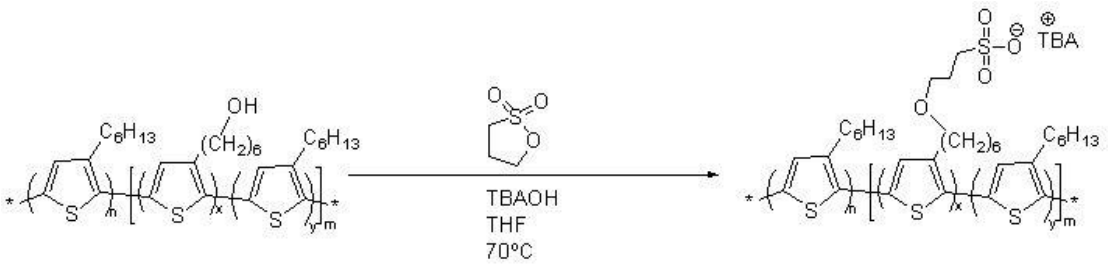

Scheme 3.3 Synthesis showing the modification of **P3** to **P8**.

limitation of this portion of the project comes to finding a corresponding cationic species to coordinate to this polymer. Although the lab had a finite supply of **JZ1**, for such trials it was deemed too valuable (in the authors mind) and hard to reproduce to use.

So, for the future of the project a suitable species is needed. It is thought by the author that the direction should focus on ionic dye molecules. Since they do not have, at least to the knowledge of the author, suffer from the trap state defect of the quantum dots, they should be an acceptable alternative. Since the largest problem with dye based ternary blends is the dye's tendency to phase separate from the other domains, introducing an interaction that binds them together should be beneficial to the device. The dye can come in either a cationic or anionic variety and within each of those categories there is a full

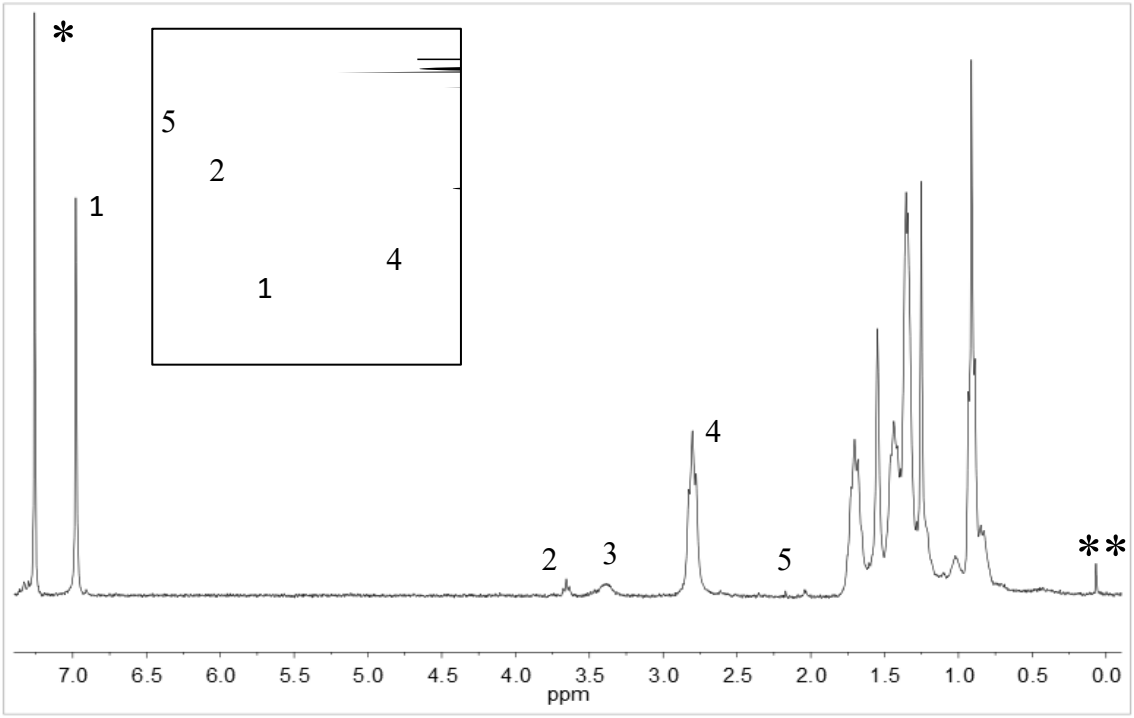

Figure 3.16 ^{1}H NMR of **P8**. Peak labeled 1 corresponds to the proton on the thiophene ring, 2 corresponds to the ether methylene protons, 3 corresponds to the methylene protons in the TBA cation, 4 corresponds to the methylene closest to the thiophene ring, 5 corresponds to the ethyl group closest to the sulfate group. All other signals are located in the alkyl region. * denotes $CDCl_3$. ** denotes grease.

spectrum of absorption profiles. Amongst the various dyes, there exists a class that can form highly ordered nanostructures based on self-aggregation driven by strong pi-pi interactions between dye molecules. In theory these nanostructures could be used to help direct the orientation of a polyelectrolyte when cast into a film. For example, the use of copper phthalocyanine-3, 4′, 4″, 4‴-tetrasulfonic acid tetrasodium could be used to coordinate the cationic polyelectrolyte along the nanocable that the dye will form. With this strategy, we could achieve a level of control over the morphology with systems that cannot form high ordered nanostructures.

Although the polyelectrolytes have the promise of eliminating the need for the use of non-green solvents, the largest unanswered question still remains. That being based

around the nature of charged species at the end of the side chain. Evidence suggests that the ionic pendent group will act as a charge trap not unlike the surface defect on a quantum dot. Although this evidence is somewhat rare, the strongest evidence to this detrimental effect of the polar group may be found in the fact that most sources focus on the solvochromatic effect of such polymers and omit any solar cell testing.

As a donor material these suggested polyelectrolyte systems may not be the best answer. However, there are still usages that can be explored using such systems. Most of the previous research effort has fallen into either their application as interlayers in active layers, organic field effect transistors or as polymer light emitting diodes. It should be noted that the latter two examples use more complex systems than just polythiophene based polymers. The cationic polyelectrolyte has been used as an electron transport layer, studies from the early 2010's claim that the addition of this layer increases both the Voc and the PCE of the device.[175] In another example, cationic polythiophene was mixed with PEDOT: PSS.[174] The authors claimed that the mixed interlayer had performance comparable to the devices with just PEDOT: PSS and other interfacial layer while exhibiting a stability of over 500 hours. It should be noted that in all these previous examples were pure polyelectrolyte systems.

As a summary of the future work, the use of quantum dot needs to be abandoned as the nature of trap state is too large to overcome. The future may be in the use of organic dye that can be coordinated to the polymer through some type of interaction. This introduced interaction can either be by a traditional non-covalent bonding mode or through the use of electrostatic interactions. Since these dye molecules have large pi electron

systems, pi-pi interactions may be a simple way to go, as the pendent moiety would simply insert itself into the pi system of the dyes. Hydrogen bonding moieties can be installed on both polymer and dye to introduce a stronger bonding mode. However, the presence of the pi system on the dye may lead to the insertion into the polymer film causing a disruption of the thin film morphology. If electrostatic methods are the chosen method, then commercially available cationic or anionic dyes can be paired with a modified block copolymer system. With the block copolymer system that is used, they can be formed into nanofibers-some examples point these fibers surviving the methylation process. The inclusion of the ionic dye can still keep with scheme of the core shell structure first proposed in chapter 1. Of the commercially available dyes, band gaps should be chosen to keep with the idea of the cascade charge transport process. Even without the nanofibers, sources have stated that polyelectrolyte block copolymers favor a lamella phase separation. The use of this self-assembly can be possibly used to help engineer the morphology of the active layer, another goal that was outlined in the beginning of this project. If the use of these materials is detrimental to the performance of the OPV as the sole donor material, these materials can be further used as either additives or as interfacial layers. However, since the time of P3HT based donor materials has largely passed the chosen donor material may need to evolve into a push-pull type polymer.

3.9 Experimental Section

3.9.1 Materials and general methods

All reagents and solvents were used as received from either Sigma Adrich, Alfa Aeisa or TGI unless otherwise noted. Cadmium Selenide quantum dots were purchased from Ocean Nanotech and was produced in house according to reported literature procedure. Sodium mercaptoethanesulfonate and 4-mercaptophenol were purchased and used without further purification. Dry Tetrahydrofuran was distilled over sodium using benzophenone as an indicator and was collected in a flame-dried, air free storage flask. Other solvents were dried by first exposing it to CaH and then through the application of a freeze/pump/throw cycle. Hexanes and dodcane were dried via bubbling a dry stream of nitrogen through the solvent overnight. All NMR spectra were recorded on one of two Bruker Avance III 300 MHz using standard proton experimental protocols, unless otherwise noted. All NMR spectra are referenced internally to the solvent signals or referenced by an internal standard such as Trimethylsilane (TMS). Size exclusion chromatography was performed on a Waters 1515 series equipped with a 2414 refractive index detector and 2707 auto sampler. The mobile phase was chloroform with 0.5% (v/v) triethylamine passing through two styragel columns (Polymer Laboratories, 5 m Mix-C) at a flow of 1 mL/min, kept in a column heater at 35^{o}C. SEC trials were calibrated by external polystyrene standards (Varian). Ultraviolet-visible (UV-VIS) absorption was recorded on a Shimadzu UV-2401 PX spectrometer over a range of 300-900 nm using quartz cuvettes. Infrared spectra were generated by a Bruker Alpha-P spectrometer, using a powder sample in ATR mode. TEM imaging was performed with a JEOL 2010 microscope with a lanthanum hexaboride beam source and Gatan camera while in bright field mode. Samples were prepared by drop casting a diluted sample onto a carbon coated copper grid.

3.9.2 Solar Cell preparation and testing

Blend solutions were prepared by dissolving predetermined weight ratios of polymer, quantum dot and PCBM in chlorobenzene and heating it for 1 hr at 90^{o}C in a nitrogen glovebox. The solution was then taken off the heat and stirred for 1 hr, when a predetermined amount of "bad" solvent (usually acetone) was added dropwise via a micropipette. This solution was stirred at 400 RPM for 9 hr. ITO-coated glass substrates (China Shenzhen Southern Glass Display Ltd, 8/) were cut into 1 in^2 squares and then underwent a cleaning procedure: 15 min ultrasonic sequentially in detergent, DI water, acetone and isopropyl alcohol, finally undergoing an UV Ozone (Novascan PSD series) treatment for 45 min. These sides were then stored in nitrogen glovebox until MoO_3 coating. 10 nm of MoO_3 was deposited using an Angstrom Engineering Amond deposition system with a vacuum level of <7x10^{-8} Torr. The blend solution was spin coated on to the MoO_3 surface at "500" RPM for 30 sec, ramp for 3 seconds and dwell for 27 seconds. Aluminum electrodes were then added to the device via thermal evaporation through patterned masks. Some devices were then annealed through the application of heat (150^{o}C) for a set amount of time. Current-voltage measurements were taken by a Keithley 2400 source while the device was under irradiation (100 mW/cm^2) generated by a Xe arc lamp-based Newport 67005 150 W solar stimulator equipped with an AM1.5 filter. The light intensity was calibrated on wavelength 576 nm by a Newport thermopile detector (model 818-010-12) equipped with a Newport 1916-C Optical Power Meter.

3.9.3 General method for nanofiber preparation

In a dry scintillation vial 5 mg of polymer and a magnetic stir bar were added. The vial was transferred to a nitrogen glovebox. This polymer was dissolved in 0.4 mL

chlorobenzene and was heated at 90^{o} C for 1 hour while undergoing stirring at 400 RPM. The solution was allowed to cool down to room temperature and allowed to stir for another 1 hour. At this time, 0.1 mL of acetone was added dropwise via a microsyringe. The solution was allowed to age for an amount of time, 9 hours seems like the minimum time for good nanofiber formation to about 72 hours when the nanofibers start to aggregate. The color of the solution is also a good indicator of the progress of nanofiber formation. The solution needed to be violet and any hints at a red color shows that the process is yet to be completed. Nanofibers with quantum dots were created in one of two ways: (A) if the ligand required the use of dodecane then the solution was added after the formation of nanofibers and allowed to mix for up to 3 hours; (B) the ligand was soluble in chlorobenzene then the solid quantum dot was added to the solid polymer then co dissolved in chlorobenzene. The further steps of nanofiber formation were unchanged. The ternary blend followed the same procedure as outlined above. With the PCBM being added at the same time as the polymer.

3.9.4 Synthetic detail

CdSe Quantum Dots CdSe quantum dots were synthesized by using modified procedures from previous reports. [176] A typical synthetic procedure for 3.35 nm CdSe quantum dots was as follows: selenium precursor was prepared by mixing 0.518 g (6.56 mmol) selenium powder and 2 mL tributylphosphine (TBP, 1.62 g, 8.01 mmol) in a scintillation vial for 30 min. Cadmium precursor was prepared by loading 0.042 g CdO (0.33 mmol), 0.386 g stearic acid (SA, 1.36 mmol) 3.88 g hexadecylamine (16.07 mmol) and 3.88 g trioctylphosphine oxide (TOPO, 10.04 mmol) into a 50 mL flask. The initial reddish-brown

solution was heated with stirring to 150^{o}C and kept under N2 flow until the color of the solution changed to transparent. Then, the mixture was heated to 320^{o}C. At this temperature, the Se precursor was quickly injected into the reaction flask. After the injection, the temperature dropped to 290 ^{o}C and the reaction was kept for 2 min. After the reaction, the sample was naturally cooled down to room temperature. The product was re-dispersed in chloroform. Then it was precipitated by acetone followed by centrifugation. The product was washed for three times and dried under vacuum for overnight and re-dispersed in hexane.

PbS quantum dot A typical synthetic procedure for PbS quantum dots was as follows: Sulphur precursor was prepared by mixing 42 um g (6.56 mmol) bis(trimethylsilyl)sulfide (TMS) and 2 mL octadecene (ODE, 1.62 g, 8.01 mmol) in a scintillation vial for 30 min. Cadmium precursor was prepared by loading 0.093 g PbO (0.33 mmol), 4 mL oleic acid (OA, 1.36 mmol) into a 25 mL flask. The initial reddish-brown solution was heated with stirring to 100 ◦C and kept under N2 flow until the color of the solution changed to transparent. At this temperature, the Se precursor was quickly injected into the reaction flask. After the injection, the temperature kept at 100 ^{o}C and the reaction was kept for 2 min. After the reaction, the sample was naturally cooled down to room temperature. The product was re-dispersed in chloroform. Then it was precipitated by acetone followed by centrifugation. The product was washed for three times and dried under vacuum for overnight and re-dispersed in hexane.

Ammonium Phenyl Dithiocarbamate[177]30 mL of concentrated ammonium hydroxide (0.435 mol) and a stir bar were added to a clean 50 mL two necked round bottom flask.

While under flowing nitrogen and stirring at 1260 RPM; 5 mL of carbon disulfide (0.055 mol) was added dropwise, after which ca. 10 mL of ethanol was added. This resulted in the solution turning an opaque rose color. The solution was immersed into an ice bath and 5 mL of aniline (0.083 mol) was added dropwise to the solution over ca. 5 minutes. The solution was allowed to react for 45minutes when it was removed from the ice bath. The solution was vacuum filtered and the resulting solid was washed with chloroform. Additional solid formed in the filtrate after some time and the process was repeated until no more solid formed. The pale yellow/white solid was then vacuum dried and stored in the refrigerator. 1H NMR (300.13 MHz, D_2O): δ (ppm) = 7.485-7.319 (m)- phenyl ring, 7.286 7.260 (m)- amine proton, 4.789 (s)- D_2O

Triethylammonium Pyridin-2-yl dithiocarbamate (T2PyTC) [178] In a clean 100 mL flask, with a flowing air condenser attached, 30 mL of triethyl amine (0.215 mol) and 20.34 grams of 2-Aminopyridine (0.216 mol) were heated until the solid fully dissolved. While stirring, 14 mL of carbon disulfide (0.238 mol) was added dropwise over 5 minutes. This solution thickened to form a bright yellow solid over the next hour and a half, causing the method of stirring to be changed from magnetic to mechanical. The bright yellow solid was recovered, purified via soxhlet -diethyl ether- and finally dried overnight under high vacuum. 1H NMR (300.13 MHz, D_2O): δ (ppm) = 9.82 (s)- amine, 8.96 (pyridine, 8.26: pyridine:7.64, 7.26-chloroform-d, 6.92: T2PyTC, 6.64: T2PyTC, 3.26: T2PyTC (cation),1.40 T2PyTC (cation), 4.789 (s)- D_2O.

Ligand exchange (one solvent) In a clean 250 mL darkened round bottom flask 2.50 grams of TOPO capped CdSe quantum dots were suspended in 125 mL of

dichloromethane. To this mixture a clean magnetic stir bar was added and the mixture was stirred at a rate of no less than 750 RPM on a standard for ca. 30 min. To this mixture 5.00 g of APTC ligand solid was added slowly. This solution was allowed to mix for 82 hours or until the red shift in the absorption stopped. The solution was then concentrated and precipitated into methanol. The quantum dots were then washed in a mixture of methanol and hexanes, starting with a majority methanol and slowly switching to a majority hexanes system. Each time the suspension of quantum dots was concentrated through the use of centrifugation. This process was repeated until the solvent was completely clear. The resulting quantum dots were dried overnight and then stored in a nitrogen glovebox.

Ligand exchange (two solvent) In a clean 250 mL darkened round bottom flask 2.50 g of TOPO capped CdSe quantum dots was dissolved in 100 mL of hexanes. To this solution 100 mL of dichloromethane with 5.00 g APTC ligand dissolved in it was added. To the resulting bilayer a clean magnetic stir bar was added, and the solution was stirred at 780 RPM for 48 hours. The completeness of the ligand replacement was monitored by the migration of the CdSe quantum dots from hexanes layer to the dichloromethane layer. When this migration is complete, the hexanes is carefully decanted off and the resulting dichloromethane solution is concentrated and precipitated into methanol. The quantum dots were concentrated through the use of centrifugation. The quantum dots were then resuspended in a mixture of methanol and hexanes, being re- concentrated through the use of centrifugation. This process was repeated several times or until the solvent was clear.

References

(1) International Energy Outlook 2017 - Energy Information. https://www.eia.gov/outlooks/ieo/pdf/0484(2017).pdf (accessed Feb 24, 2019)

(2) U.S. Energy Information Administration, Annual Energy Review, 2016, page 78.

(3) Bundgaard, E.; Hagemann, O.; Manceau, M.; Jørgensen, M.; Krebs, F. C. *Macro molecules.* **2010**, *43*, 8115.

(4) Karl, T.; Trenberth, K. *Science*. **2003**, *302*, 1719.

(5) Vidic,R.; Brantley,J.; Vandenbossche,J.; et al. *Science*.**2013**, *340*, 1235009.

(6) Energy Independence. America's Solar Energy Potential. http://www.americanenergyindependence.com/solarenergy.aspx (accessed Mar 24, 2019).

(7) Song, Z.; Watthage, S. C.; Phillips, A. B.; Heben, M. J. J. *Photonics Energy.* **2016**, *6*, 22001.

(8) Brenner, T. M.; Egger, D. A.; Kronik, L.; Hodes, G.; Cahen, D. *Nat. Rev. Mate*r. **2016**, *1*, 15007.

(9) Grätzel, M. J.; Photobiol. C. *Photochem*. *Rev*. **2003**, *4*, 145.

(10) Hagfeldt, A.; Boschloo, G.; Sun, L.; Kloo, L.; Pettersson, H. *Chem. Rev*. **2010**, *110*, 6595.

(11) Lin, Y.; Li, Y.; Zhan, X. *Chem. Soc. Rev*. **2012**, *41*, 4245.

(12) Mishra, A.; Bäuerle, P. *Angew. Chem., Int. Ed*. **2012**, *51*, 2020.

(13) Günes, S.; Neugebauer, H.; Sariciftci, N. S. *Chem. Rev.* **2007**, *107*, 1324.

(14) Cheng, Y.; Yang. S.; Hsu, C. *Chem Rev.* **2009**, *109*, 5689-5923.

(15) Energy Sage: History of Solar Energy. News.energysage.com/the-history-and-invention-of-solar-panel-technology/ (accessed Feb 28, 2019)

(16) Tang, C. W. *Appl. Phys. Lett*. **1986**, *48*, 183.

(17) Yu, G.; Gao, J.; Hummelen, J. C.; Wudl, F.; Heeger, A. J. *Science*. **1995**, *270*, 1789.

(18) Hummelen, J. C.; Knight, B. W.; LePeq, F.; Wudl, F.; Yao, J.; Wilkins, C. L. J. *Org. Chem*. **1995**, *60*, 532.

(19) Shaheen, S. E.; Radspinner, R.; Peyghambarian, N.; Jabbour, G. E. *Appl. Phys. Lett*. **2001**, *79*, 2996.

(20) Reyes-Reyes, M.; Kim, K.; Carroll, D. L. *Appl. Phys. Lett.* **2005**, *87*, 083506.

(21) Kim, J. Y.; Kim, S. H.; Lee, H. H.; Lee, K.; Ma, W.; Gong, X.; Heeger, A. J. *Adv. Mater*. **2006**, *18*, 572.

(22) Dang, M. T.; Hirsch, L.; Wantz, G. *Adv. Mater*. **2011**, *23*, 3597.

(23) Dennler, G.; Scharber, M. C.; Ameri, T.; Denk, P.; Forberich, K.; Waldauf, C.; Brabec, C. J. *Adv. Mater.* **2008**, *20*, 579–583.

(24) Y. Zhong, M. T. Trinh, R. Chen, W. Wang, P. P. Khlyabich, B. Kumar, Q. Xu, C

.-Y. Nam, M. Y. Sfeir, C. Black, M. L. Steigerwald, Y.-L. Loo, S. Xiao, F. Ng, X .-Y. Zhu and C. Nuckolls, *J. Am. Chem. Soc*., **2014**, *136*, 15215.

(25) Y. Zong, B. Kumar, S. Oh, M. T. Trinh, Y. Wu, K. Elbert, P. Li, X. Zhu, S. Xiao , F. Ng, M. L. Steigerwald and C. Nuckolls, *J. Am. Chem. Soc.* **2014**, *136*, 8122.

(26) Y. Zhong, M. T. Trinh, R. Chen, G. E. Purdum, P. P. Khlyabich, M. Sezen, S. O h, H. Zhu, B. Fowler, B. Zhang, W. Wang, C.-Y. Nam, M. Y. Sfeir, C. T. Black, M. L. Steigerwald, Y.-L. Loo, F. Ng, X.-Y. Zhu and C. Nuckolls, *Nat. Commun*., **2015**, *6*, 8242.

(27) W. Chen, X. Yang, G. Long, X. Wan, Y. Chen and Q. Zhang, *J. Mater. Chem. C* , **2015**, **3**, 4698.

(28) S.-Y. Liu, C.-H. Wu, C.-Z. Li, S.-Q. Liu, K.-H. Wei, H.-Z. Chen and A. K.-Y. Jen, *Adv. Sci*. **2015**, *2*, 1500014.

(29) Y. Liu, J. Y. L. Lai, S. Chen, Y. Li, K. Jiang, J. Zhao, Z. Li, H. Hu, T. Ma, H. Li n, J. Liu, J. Zhang, F. Huang, D. Yu and H. Yan, *J. Mater. Chem. A*, **2015**, *3*, 136 32.

(30) Lin, Y.; Wang, Y.; Wang, J.; Hou, J.; Li, Y.; Zhu, D.; Zhan, X.; *Adv. Mater*. **2014**, *26*, 5137.

(31) Liu, Y.; Mu, C.; Jiang, K.; Zhao, J.; Li, Y.; Zhang, L.; Li, Z.; Lai, J. Y. L.; Hu, H .; Ma, T.; Hu,R; Yu,D.; Huang, X,; Tang B.Z. and Yan, H. *Adv. Mater*. **2015**, *27*, 1015.

(32) Zhang, X.; Zhan, C.; and Yao, J. *Chem. Mater*. **2015**, *27*, 166.

(33) Fan, H. and Zhu, X. *Sci. China: Chem*. **2015**, *58*, 922.

(34) Li, Y. F., *Acc. Chem. Res*. **2012**, *45*, 723.

(35) Yusoff, A. R. b. M., Kim, D., Kim, H. P., Shneider, F. K., da Silva, W. J., Jang, *J., Energy Environ. Sci.* **2015**, *8*, 303.

(36) Topham, P. D.; Parnell, A. J.; Hiorns, R. C. *J. Polym. Sci., Part B: Polym. Phys.* **2011**, *49*, 1131.

(37) Blom, P. W. M.; Mihailetchi, V. D.; Koster, L. J. A.; Markov, D. E. *Adv. Mater*. **2007**, *19*, 1551.

(38) Kirova, N. *Polym. Int.* **2008**, *57*, 678.

(39) Clarke, T. M. and Durrant, J. R. *Chem. Rev*. **2010**, *110*, 6736.

(40) Beljonne, D; Curutchet, C; Scholes, GD; Silbey, RJ. "Beyond Forster Resonance Energy Transfer in Biological and Nanoscale Systems," *JOURNAL OF PHYSIC AL CHEMISTRY B.*, **2009**, *113*, 6583.

(41) Knoester, J., & Agranovich, V. M. Frenkel and charge transfer excitons in orga nic solids. *In Host Publication;* Elsevier: Amsterdam, 2003. p 1-96.

(42) Kuhn, O.; Lochbrunner, S. Quantum Dynamics and Spectroscopy of Excitons in Molecular Aggregate. In *Semiconductors and Semimetals;* Elsevier: Amsterdam, 2011; Vol. 85, Pages 47-81.

(43) Nelson, J. *Materials Today*. **2011**, *14*, 462-470.

(44) Pal, S.K.; Kesti, T.; Maiti, M.; Zhang, F.; Inganäs, O.; Hellström, s.; Andersson, M.R.; Oswald, F.; Langa, F.; Österman, T.; Pascher, T.; Yartsev, A.; Sundström, V**.** *J. Am. Chem. Soc*.**, 2010,** *132*, 12440-12451.

(45) Credgington, D.; Jamieson, F.; Walker, B.; Nguyen, T-Q. Durrant, *J. Advanced materials.* **2012**, *24*, 2135-2141.

(46) Gorenflot J.; Heiber, M.; Baumann, A.; Lorrmann, J.; Gunz, M.; Kämpgen, A.; Dyakonov, V.; Deibel, C. *Journal of Applied Physics*, **2014** *14*, 144502.

(47) Griffin Canning, Alan K. Thomas, David H. Dunlap, and John K. Grey, *ACS App l. Mater. Interfaces.* **2018**, *10*,19853-19862

(48) Liu A.; Zhao S.; Rim S.; Wu J.; Könemann, M.; Erk P.; Peumans, P. *Adv. Mater* . **2008**, *20*,1065.

(49) Sommer, M.; Huetter, S.; Thelakkat, M. *J. Mater. Chem.* **2010**, *20*, 10788.

(50) Leyrer, J., Rubilar, M., Morales, E. et al. *Journal of Elec Materi*. **2018**, *47*, 6136.

(51) Zhan, X.; Zhu, D. *Polym. Chem.* **2010**, *1*, 409.

(52) Kalowekamo, J.; Baker, E. *Sol. Energy.* **2009**, *83*, 1224.

(53) Hedley, G.J.; Ruseckas, A.; Samuel. D.W. *Chem. Rev.* 2017, **117**, *2*, 796-837

(54) Qi, B.; Wang, J. J. *Mater. Chem.* **2012**, *22*, 24315.

(55) Qi, B.; Wang, J. *Phys. Chem. Chem. Phys.* **2013**, *15*, 8972.

(56) Guo, J.; Ohkita, H.; Benten, H.; Ito, S. *J. Am. Chem. Soc.* **2010**, *132*, 6154.

(57) El Chaara, L.; lamonta, L.A.; El Zein, N. *Renewable and Sustainable Energy Re views* **2011**, *15* 2165-2175.

(58) Razykov, T.M.; Ferekides, C.S.; Morel, D.; Stefanakos, E.; UllalL H.S.; Upadhy aya, H.M. *Solar Energy* Volume 85, Issue 8, August 2011, Pages 1580-1608.

(59) Reese, M. O.; White, M. S.; Rumbles, G.; Ginley, D. S.; Shaheen, S. E. *Appl. Ph ys. Lett.* **2008**, *92*, 053307.

(60) Subbiah, J.; Sarasqueta, G.; So, F.; Ding, H.; Gao, Y. *Appl. Phys. Lett.* **2009**, *95* , 093304.

(61) Van Reenen, S.; Kouijzer, S.; Janssen, R. A.; Wienk, M. M.; Kemerink, M. *Adv* . *Mater. Interfaces* **2014**, *1*, 1400189.

(62) Yuan, Y. B.; Reec, T. J.; Sharma, P.; Poddar, S.; Ducharme, S.; Gruverman, A.; Yang, Y.; Huang, J. S.; *Nat. Mater.* **2011**, *10*, 296.

(63) Yip, H. L.; Jen, A. K. Y. *Energy Environ. Sci.* **2012**, *5*, 5994.

(64) Bilby, D.; Frieberg, B.; Kramadhati, S.; Green, P.; Kim, J.; *ACS Appl. Mater. Int erfaces* **2014**, *6*, 14964.

(65) Manders, J. R.; Tsang, S. W.; Hartel, M. J.; Lai, T. H.; Chen, S.; Amb, C. M.; R eynolds, J. R.; So, F. *Adv. Funct. Mater*. **2011**, *23*, 2993.

(66) Jørgensen, M.; Norrman, K.; Gevorgyan, S. A.; Tromholt, T.; Andreasen, B.; Kr ebs, F. C. *Adv. Mater*. **2012**, *24*, 580.

(67) Yin, Z. G.; Zheng, Q. D.; Chen, S.-C.; Cai, D. D. *ACS Appl. Mater. Interfaces*

2013, *5*, 9015.

(68) White, M. S.; Olson, D. C.; Shaheen, S. E.; Kopidakis, N.; Ginley, D. S. *Appl. P hys. Lett.* **2006**, *89*, 143517.

(69) Waldauf, C.; Morana, M.; Denk, P.; Schilinsky, P.; Coakley, K.; Choulis, S. A.; Brabec, C. J. *Appl. Phys. Lett.* **2006**, *89*, 233517.

(70) Siddiki, M. K.; Venkatesan, S.; Qiao, Q. *Phys. Chem. Chem. Phys.* **2012**, *14*, 46 82.

(71) Trost, S.; Zilberberg, K.; Behrendt, A.; Riedl, T.; *J. Mater. Chem.* **2012**, *22*, 162 24.

(72) Huang, J.; Yin, Z. G.; Zheng, Q. D. *Energy Environ. Sci.* **2011**, *4*, 3861.

(73) Yip, H. L.; Jen, A. K. Y. *Energy Environ. Sci.* **2012**, *5*, 5994.

(74) Jasieniak, J. J., Seifter, J.; Jo, J.; Mates, T.; Heeger, A. J. *Adv. Funct. Mater.* **201 2**, *22*, 2594.

(75) Xie, F. X.; Choy, W. C. H.; Wang, C. D.; Li, X. C.; Zhang, S. Q.; Hou, J. H. *Adv . Mater.* **2013**, *25*, 2051.

(76) Zilberberg, K.; Trost, S.; Meyer, J.; Kahn, A.; Behrendt, A.; Lutzenkirchen-Hec ht, D.; Frahm, R.; Riedl, T. *Adv. Funct. Mater.* **2011**, *21*, 4776.

(77) Kim, H. P.; Yusoff, A. R. bin M.; Kim, H. M.; Lee, H. J.; Seo, G. J.; Jang, J. *Nanoscale Res. Lett.* **2014**, *9*, 150.

(78) Chen, C. P.; Chen, Y. D.; Chuang, S. C. *Adv. Mater.* **2011**, *23*, 3859.

(79) Bao, X. C.; Zhu, Q. Q.; Wang, T.; Guo, J.; Yang, C. P.; Yu, D. H.; Wang, N.; C hen, W. C.; Yang, R. Q.; *ACS Appl. Mater. Interfaces* **2015**, *7*, 7613.

(80) Liao, H.-C.; Ho, C.-C.; Chang, C.-Y.; Jao, M.-H.; Darling, S. B.; Su, W.-F. *Mate r. Today* **2013**, *16*, 326–336.

(81) Dang, M. T.; Hirsch, L.; Wantz, G. *Adv. Mater.* **2011**, *23*, 3597.

(82) He, W.; Jiang, Y.; Qin, Y. *Polym. Chem.* **2014**, *5*, 1298–1304.

(83) Kim, Y.; Choulis, S. A.; Nelson, J.; Bradley, D. D. C.; Cook, S.; Durrant, J. R. A ppl. Phys. Lett. 2005, 86, 63502. Yao, Y.; Hou, J.; Xu, Z.; Li, G.; Yang, Y. *Adv. Funct. Mater.* **2008**, *18*, 1783.

(84) He, W.; Livshits, M. Y.; Dickie, D. A.; Yang, J.; Quinnett, R.; Rack, J. J.; Wu, Q .; Qin, Y. *Chem. Sci.* **2016**, *7*, 5798–5804.

(85) Peet, J.; Solci, C.; Coffin, R.C.; Nguyen, T.Q.; Mikhailovsky, A.; Moses, D.; Ba zan, G.C. Method for increasing the photoconductive response in conjugated pol ymer/fullerene composites. *Appl. Phys. Lett.* **2006**, *40*, 13353.

(86) Salim, T.; Wong, L.H.; Brauer, B.; Kukreja, R.; Foo, Y.L.; Bao, Z.N.; Lam, Y.M . Solvent additives and their effects on blend morphologies of bulk heterojunctio ns. *J. Mater. Chem.* **2011**, *21*, 242–250.

(87) Lee, J.K.; Ma, W.L.; Brabec, C.J.; Yuen, J.; Moon, J.S.; Kim, J.Y.; Lee, K.; Baz an, G.C.; Hegger, A.J. Processing additives for improved efficiency from bulk he

terojunction solar cells. *J. Am. Chem. Soc.* **2008**, *130*, 3619–3623.

(88) Szarko, J.M.; Guo, J.; Liang, Y.; Lee, B.; Rolczynski, B.S.; Strzalka, J.; Xu, T.; Loser, S.; Marks, T.J.; Yu, L.; et al. When function follows form: effects of dono r copolymer side chains on film morphology and BHJ solar cell performance. *Ad v. Mater.* **2010**, *22*, 5468–5472.

(89) Li, T.; Hu, W.; Zhu, D. Contents. Adv. Mater. **2010**, *22*, 135–138.

(90) Yang, J.S.; Oh, S.H.; Kim, D.L.; Kim, S.J.; Kim, H.J. Hole transport enhancing e ffects of polar solvents on poly(3,4-ethylenedioxythiophene): poly(styrene sulfon ic acid) for organic solar cells. *ACS Appl. Mater. Interfaces* **2012**, *4*, 5394–5398.

(91) Li, G.; Yao, Y.; Yang, H.; Shrotriya, V.; Yang, G.; Yang, Y. Solvent annealing e ffect in polymer solar cells based on Poly(3-hexylthiophene) and methanofullere nes. Adv. Funct. Mater. **2007**, *17*, 1636–1644.

(92) Wang, D.H.; Pron, A.; Leclerc, M.; Heeger, A.J. Additive-Free bulk-heterojuctio n solar cells with enhanced power conversion efficiency, comprising a newly des igned selenophene-thienopyrrolodione copolymer. Adv. Funct. Mater. **2013**, *23*, 1297–1304.

(93) Cook, S.; Furube, A.; Katoh, R. *Energy Environ. Sci.* **2008**,*1* 294–299.

(94) Chang, J.; Sun, B.; Breiby, D.W.; Nielsen, M.M.; Solling, T.I.; Giles, M.; McCu lloch, I.; Sirringhaus, H. *Chem. Mater.* 2004, *16* 4772–4776.

(95) Bavel, S.S.; Sourty, E.; With, G.; Loos, J. *Nano Lett.* **2009,** *9*, 507–513.

(96) Salammal, S.T.; Mikayelyan, E.; Grigorian, S.; Pietsch, U.; Brinkmann, M. *Mac romolecules* **2012**,*45* 5575–5585.

(97) Oliver, A.; Steffi, S.; Gerhard, G. *Appl. Phys. Lett.* **2005**, *86* 2011201–2011203.

(98) Verploegen, E.; Mondal, R.; Bettinger, C.J.; Sok, S.; Toney, M.F.; Bao, Z.; *Adv. Funct. Mater.* **2010** *20* 3519–3529.

(99) Siddharht, J.; Pingel, P.; Grigorian, S.; Panzner, T.; Pietsch, U.; Neher, D.; Forst er, M.; Scherf, U. *Macromolecules* **2009** *42*. 4651–4660.

(100) Hoppe, H.; Sariciftci, N. S. *J. Mater. Chem.* **2006**, *16*, 45.

(101) Tang, H. W.; Lu, G. H.; Li, L. G.; Li, J.; Wang, Y. Z.; Yang, X. N. *J. Mater. Chem.* **2010**, *20*, 683.

(102) Savenije, T. J.; Kroeze, J. E.; Yang, X. N.; Loos, J. *Adv. Funct. Mater.* **2005**, *15* , 1260.

(103) Ramos, A. M.; Rispens, M. T.; van Duren, J. K. J.; Hummelen, J. C.; Janssen, R . A. J. *J. Am. Chem. Soc.* **2001**, *123*, 6714.

(104) Miyanishi, S.; Zhang, Y.; Tajima, K.; Hashimoto, K. *Chem. Commun.* **2010**, *46* , 6723.

(105) Miyanishi, S.; Zhang, Y.; Hashimoto, K.; Tajima, K. *Macromolecules* **2012**, *45* , 6424.

(106) Boudouris, B. W.; Frisbie, C. D.; Hillmyer, M. A. *Macromolecules***2007**, 41, *67*

(107) Zhang, C.; Matos, T.; Li, R.; Sun, S.-S.; Lewis, J. E.; Zhang, J.; Jiang, X. *Polym.*

Chem. **2010**, *1*, 663−669.

(108) Greene, L.; Law, M.; Yuhas, B.; et al. Journal of Physical Chemistry C, **2007**. *50*, 18451.

(109) Mariani,G.; Laghumavarapu, R.; Tremolet De Villers, B.; et al. *Applied Physics Journals.* **2010**. *97*, 3.

(110) Aryal, M.; Trivedi, K.; Hu, W. *ACS Nano.* **2009**, *3*, 3085.

(111) Meuler, A. J.; Hillmyer, M. A.; Bates, F. S. *Macromolecules* **2009**, *42*, 7221.

(112) Sary, N.; Richard, F.; Brochon, C.; Leclerc, N.; Lévêque, P.; Audinot, J.-N.; Berson, S.; Heiser, T.; Hadziioannou, G.; Mezzenga, R. *Adv. Mater.* **2010**, *22*, 763.

(113) Lynd, N. A.; Meuler, A. J.; Hillmyer, M. A. Prog. *Polym. Sci.* **2008**, *33*, 875.

(114) V. D. Mitchell and D. J. Jones, Russian Chemical Reviews., **2012**, *00*, 1-3.

(115) M. He; F. Qiu; Z. Lin, J. Mater. Chem., **2011**, *21*, 17039-17048.

(116) P. D. Topham; A. J. Parnell; R. C. Hiorns, J. Polym. Sci., Part B: Polym. Phys., **2011**, *49*, 1131-1156.

(117) C.-C. Ho; Y.-H. Lee; C.-A. Dai; R. A. Segalman; W.-F. Su, Macromolecules, **2009**, *42*, 4208-4219.

(118) R. A. Segalman; B. McCulloch; S. Kirmayer; J. J. Urban, Macromolecules, **2009**, *42*, 9205-9216.

(119) Kim, K.; Carroll, D. L. Appl. Phys. Lett. **2005**, *87*, 203113.

(120) Naidu, B. V. K.; Park, J. S.; Kim, S. C.; Park, S.-M.; Lee, E.-J.; Yoon, K.-J.; Joon Lee, S.; Wook Lee, J.; Gal, Y.-S.; Jin, S.-H. Sol. Energy Mater. Sol. Cells **2008**, *92*, 397.

(121) Miyakoshi, R.; Yokoyama, A.; Yokozawa, T. J. Am. Chem. Soc. **2005**, *127*, 17542.

(122) Yokoyama, A.; Miyakoshi, R.; Yokozawa, T. Macromolecules **2004**, *37*, 1169.

(123) Bao, Z.; Chan, W.; Yu, L. Chem. Mater., **1993**, *5* , 2–3.

(124) Kaneyoshi, H.; Matyjaszewski, K. *Macromolecules*, **2005**, *38* , 8163–8169.

(125) Yokozawa, T.; Suzuki, R.; Nojima. M.; Ohta Y.; Yokoyama A. *Macromol. Rapid Commun.* **2011**, *32*, 801–806.

(126) Kiriy, A,; Senkovskyy, V.; Sommer, M. *Macromol. Rapid Commun.***2011**, *32***,** 1503-1517.

(127) Loo, Y.-L.; Register. R. A.; A. J. Ryan, *Macromolecules*, **2002**, *35*, 2365-2374.

(128) He, W.-N.; Xu, J.-T.; *Prog. Polym. Sci.*, 2012, *37*, 1350-1400.

(129) Yu. X.; Yang, H.; Wu, S.; Geng, Y.; Han, Y. *Macromolecules*, **2012**, *45*, 266-274.

(130) Zhou, E.; Tan, Z.A.; Yang, Y.; Huo, L.; Zou, Y.; Yang, C.; Li, Y. Synthesis, hole mobility, and photovoltaic properties of cross-linked polythiophenes with vinylene-terthiophene-vinylene as conjugated bridge. *Macromolecules* **2007**, *40*, 1831–1837.

(131) Bilge, A.; Zen, A.; Forster, M.; Li, H.; Galbrecht, F.; Nehls, B.S.; Farrell, T.; Neher, D.; Scherf, U. Swivel-cruciform oligothiophene dimers. *J. Mater. Chem.* **2006**, *16*, 3177–3182.

(132) Feser, S.; Meerholz, K. *Chem. Mater.* **2011,** *23*, 5001.

(133) B.J. Kim, et al. *Adv. Funct. Mater.* **2009,** *19*, 2273.

(134) K. Lu, et al. *Macromolecules*, **2009,** *42***,** 3222.

(135) Miyanishi, S.; Tajima, K.; Hashimoto, K. *Macromolecules* **2009** *42*, 1610.

(136) Nam, C.-Y. et al. *Macromolecules* **2012** *45*, 2338.

(137) Hammer, B.A.G., et al. *ACS Appl. Mater.* Interfaces **2014** *6*, 7705.

(138) Cho, W.; Kim, Y.; Song, D., et al. *J. Mater. Chem.* A, **2014**. *2*, 17746.

(139) Yue, G.; Wu, J.; Xiao, Y., et al. *Chinese Science Bulletin.* **2011**. *3*, 325.

(140) Tembo, M.; Munyati, M.; Hatwaambo, S.; Maaza,M. *Afr. J. Pure Appl. Chem.* 2015. *9*, 50.

(141) Kumar, R.; Grancini,G.; Peterozza, A. *Optics Express.* 2013. *21*, A469.

(142) Greaney, M.; Das, S.; Webber, D. et al. *ACS Nano.* 2012. *6*, 4222.

(143) Lek, J.; Xing, G.; Sum, T., et al. *ACS Applied Materials and Interfaces.* **2014**. *6*, 894.

(144) Wang, J.; Guo, C.; Yu. Y., et al. *RSC Adv.* **2015**, *5*, 17905.

(145) Truong, N.; Kim, W.; Farva, U.; et al. *Solar Energy Materials and Solar Cells.* **2011**. *95*, 3009.

(146) Facchetti, A. *Materials Today.* **2013**. *16*, 123.

(147) Liu, Y.; Larsen-Olsen, T.; Zhao, X., et al. *Solar Energy Materials and Solar Cells.* **2013**. *112*, 157.

(148) Iwan, A.; Chuchmala,A. *Progress in Polymer Science.* **2012**. *37*,1805.

(149) Lu, L.; Xu, T.; Chen, W., et al. *Nature Photonics.* **2014**,*1*.

(150) Albero, J.; Zhou, Y.; Eck, M.; Rauscher, F.; Niyamakom, P.; Dumsch, I.; Allard, S.; Scherf, U.; Kruger, M.; Palomares, *E. Chem. Sci.* **2011**, *2*, 2396−2401.

(151) Lu, L.; Xu, T.; Chen, W., et al. *Nature Photonics.* **2014**, *8*, 716-722.

(152) Ameri, T.; Khoram, P.; Min, J., et al. *Advanced Materials.* **2013**. *25*, 4245.

(153) Machui, F.; Abbott, S.; Waller, D.; Koppe, M.; Brabec, C. J. Determination of Solubility Parameters for Organic Semiconductor Formulations. *Macromol. Chem. Phys.*, **2011** *212*: 2159-2165.

(154) Koppe, M.; Egelhaaf, H. J.; Dennler, G.; Scharber, M. C.; Brabec, C. J.; Schilinsky, P.; Hoth, C. N. *Adv. Funct. Mater.* **2010**, *20*, 338.

(155) Khlyabich, P.P.; Burkhart, B.; Thompson B.C. *J. Am. Chem. Soc.* **2011**, *133*, 14534-14537.

(156) Li, N.; Machui, F.; Waller, D.; Koppe, M.; Brabec, C. J. *Sol. Energ. Mat. Sol.* C. **2011**, *95*, 3465.

(157) Hu, Z.; Tang, S.; Ahlvers, A.; Khondaker, S. I.; Gesquiere, A. J.; *Appl. Phys. Lett.* **2012**, *101*, 053308.

(158) Huang, J.-H.; Velusamy, M.; Ho, K.-C.; Lin, J.-T.; Chu, C.-W.; *J. Mater. Chem.* **2010**, *20*, 2820.

(159) Cha, H.; Chung, D. S.; Bae, S. Y.; Lee, M.-J.; An, T. K.; Hwang, J.; Kim, K. H.; Kim, Y.-H.; Choi, D. H.; Park, C. E. *Adv. Funct. Mater.* **2012**, DOI: 10.1002/adfm.201201913.

(160) Collier, C. P.; Vossmeyer, T.; Heath, J. R. *Annual Review of Physical Chemistry*, **1998**, *49*, 371.

(161) Reimann, S. M.; Manninen, M. *Reviews of Modern Physics*, **2002**, *74*(4), 1283.

(162) Mulpur, P.; Rattan, T.; Kamisetti, *V. Journal of Nanoscience*, **2013**.

(163) Karl, T.; Trenberth, K. *Scieince*. **2003**, *302*, 1719.

(164) Zilner, E.; Fengler, S., et al. *Journal of Physical Chemistry C.* **2012**, *116*, 16747.

(165) Zhang, Q.; Cirpan, A.; Russell, T. P.; Emrick, T. *Macromolecules.* **2009**, *42*,

1079.

(166) Li, F.; Yager, K. G.; Dawson, N. M.; Jiang, Y.-B.; Malloy, K. J.; Qin, Y. *Polym. Chem.* **2015**, *6*, 721-731.

(167) Li, Z.; Zhang, Y.; Tsang, S.-W.; Du, X.; Zhou, J.; Tao, Y.; Ding, J. *J. Phys. Chem. C 2011 115*,18002 .

(168) Frederick, M. T.; Weiss, E. A.; *ACS Nano,* **2010**, *4*, 3195–3200.

(169) Pradhan, S.; Stavrinadis, A.; Gupta, S.; Bi, Y.; Di Stasio, F.; Konstantatos, G. *Small* **2017**, *13*, 1700598.

(170) Tan, Y.; Jin, S.; Hamers R.J. *ACS Appl. Mater. Interfaces*, **2013**, *5*, 12975–12983.

(171) Patra, S.; Samanta A. *J. Phys. Chem. C.* **2014**, *118*, 18187-18196.

(172) Aruda, K.; Amin, V.; Thompson, C.; Lau, B.; Nepomnyashchii, A.; Weiss, E.A. *Langmuir* **2016**, 32, *14*, 3354-3364.

(173) Rider, D.A.; Worfolk, B.J.; Harris, K.D; Lalany, A.; Shahbazi, K.; Fleischauer M.D. *et al. Advanced Functional Materials* **2010**, *20*, 2404.

(174) H, Hu.; Wu, F.; Li, C., et.al *Macromolecules*, **2015**, *48*, 5578–5586.

(175) Li, F.; Yager, K.; Dawson, N. et al. *Chemistry of Materials*, **2014**. *26*, 3747.

(176) Frederick, M.; Weiss, E. *ACS Nano.* **2009**, *4*, 60208.

(177) Brand, W.; Drabb, T. (American Cyanamid Company). Procedure for the prepration of aromatic 2-imino-1-3-dithietanes. *US Patent* 3,470,207, Feb 11 1974.